isvr Institute of Sound and Vibration Research

Active Isolation of a Flexible Equipment Structure on a Rigid Base

X. Huang, S.J. Elliott and M.J. Brennan

ISVR Technical Memorandum 866

July 2001

University of Southampton

SCIENTIFIC PUBLICATIONS BY THE ISVR

Technical Reports are published to promote timely dissemination of research results by ISVR personnel. This medium permits more detailed presentation than is usually acceptable for scientific journals. Responsibility for both the content and any opinions expressed rests entirely with the author(s).

Technical Memoranda are produced to enable the early or preliminary release of information by ISVR personnel where such release is deemed to the appropriate. Information contained in these memoranda may be incomplete, or form part of a continuing programme; this should be borne in mind when using or quoting from these documents.

Contract Reports are produced to record the results of scientific work carried out for sponsors, under contract. The ISVR treats these reports as confidential to sponsors and does not make them available for general circulation. Individual sponsors may, however, authorize subsequent release of the material.

UNIVERSITY OF SOUTHAMPTON

INSTITUTE OF SOUND AND VIBRATION RESEARCH

SIGNAL PROCESSING & CONTROL GROUP

Active Isolation of a Flexible Equipment Structure on a Rigid Base

by

X Huang, S J Elliott and M J Brennan

ISVR Technical Memorandum N° 866

July 2001

Authorised for issue by
Prof S J Elliott
Group Chairman

Abstract

This report investigates the dynamic characteristics and control mechanisms associated with an active vibration isolation system of a flexible equipment structure attached by four mounts to a rigid base. Four electromagnetic control actuators are installed in parallel with each of four mounts, and stingers are used to connect the actuators, flexible equipment plate and mounts together. The control strategy applied is decentralised velocity feedback control, where each of the four actuators is operated independently by feeding back the absolute velocity response of the flexible equipment at the same location. Although one end of each actuator is collocated with a sensor location, the control system is not collocation control because of the flexibility of the equipment structure. Isolation of low frequency vibration is considered where the mounts can be modelled as lumped parameter springs and dampers, but the flexible modes of the equipment must also be considered. The dynamic characteristics and control mechanisms of the mounted flexible equipment structure on a rigid base as well as on a flexible base have been analysis theoretically by means of the impedance method. As an initial study, only the results of the mounted equipment structure on a rigid base are presented and discussed in this report. It has been shown analytically that the system is unconditionally stable, and so perfect vibration isolation is theoretically achievable. Various single channel control and multichannel control systems have been implemented experimentally, and the results are discussed in comparison with the theory. The measured system response and closed loop attenuation are very similar to the predicted results. Good stability properties are found in the experiments and attenuation of vibration levels of up to 30 dB at all resonance frequencies can be achieved with a gain margin of over 14 dB for various implementations of control systems. Control performance has been assessed both theoretically and experimentally in terms of absolute velocity response as well as the kinetic energy of the mounted flexible equipment. Global reductions in vibration level have been achieved at all resonance frequencies of analysis. If very high feedback gains are used in the experiments, however, instability is encountered at about 1 Hz due to some undesirable phase shifts in the electrical equipment used.

1. Introduction

Isolating a piece of delicate equipment from the vibration of a base structure is of practical importance in various engineering fields. Examples are the instrument boxes in aeroplane and telescopes in satellites. Passive mounts are widely used to support the equipment and protect it from severe base vibration. However, conventional passive mounts have an inherent trade-off between low and high frequency isolation performances depending on the dissipating elements used [1]. Low mount damping brings poor performance at low frequencies, while high mount damping brings poor performance at high frequencies. Although the use of an active control system can overcome these limitations and allows high levels of vibration isolation, generally the best isolation performance is achieved at all frequencies of interest when an active system is used in combination with a passive mount.

When an active isolator is designed, two configurations are possible, i.e., the secondary actuator can be placed in series or in parallel with the passive mount. Beard et al [2] investigated the first configuration by coupling a piezoelectric actuator in series with a passive mount. However, the effectiveness of such a mounting design was shown to be dependent heavily upon the high stiffness of the actuators. Due to a very small deflection capacity, the use of such actuation is limited for the isolation of very small amplitude motion of base structure. In many situations, the base vibration is of the order of millimetres. As a result, an actuator with a long throw, such as electromagnetic shaker, is required. An experimental study on the active vibration isolation of a rigid equipment structure, where two electromagnetic shakers were installed in parallel with two passive mounts, was reported by Serrand and Elliott [3].

An active isolator can be achieved by feedback control strategies, among which velocity feedback control is one of the most popular. The absolute velocities of a plant structure measured by identical sensors are directly fed back to the actuators, which is easy to implement in practice. In particular, when one end of the actuator is collocated with the sensor and the other reacts off an inertial ground, the multichannel control system is proven to be asymptotically stable [4,5]. Using velocity feedback control, Kim et al [6] investigated a general four-mount active vibration isolation system for a three-dimensional rigid equipment structure. It was shown experimentally that a decentralised feedback multichannel control configuration was able to reduce the equipment vibration at all frequencies of interest.

This research is an extension of the work [6] investigating the four-mount active vibration isolation for a three-dimensional flexible equipment structure. Using a similar experimental configuration to reference [6], electromagnetic actuators were installed in parallel inside the mounts, connecting the flexible equipment and the mounts to an active isolation system. Particular emphasis is placed on the isolation of low frequency vibration (0~200Hz), assuming the mounts to be springs and dampers. The objective of this research is to investigate the performance and stability issues associated with this four-mount vibration isolation system for a flexible equipment structure using the decentralised velocity feedback control. The initial results of the active vibration isolation system on a rigid base are described in this report. The dynamic characteristics of the multiple mounted flexible equipment structure are analysed using the impedance method. In addition, plant responses of the coupled system on a rigid base have been measured in the experiment and compared with those from simulation. The Nyquist criterion is employed to analyse the stability of

the active isolation system. Performances of the single channel and multichannel velocity feedback control are presented and discussed.

2. Theoretical analysis of the mounted equipment

2.1 Impedance representation of a single mount system

Considering the connection of the equipment, mount and the actuator, Kim et al [6] presented a simple model for the active vibration isolation of a single mount system using the impedance method. The model can be extended to study a single mount active isolation of a flexible equipment. Figure 1(a) shows a one-dimensional mounted equipment structure, where the flexible equipment is supported by a passive mount consisting of a spring k_m and a damper c_m. The actuator, which generates a control force, f_c, is installed to connect the equipment and the mount into a whole isolation system. The whole system on a rigid base can be represented in terms of impedance as shown in Figure 1(b), where Z_a, Z_e, and Z_m denote the impedances of the actuator, flexible equipment and mount, respectively. On a rigid base, f_c is the primary excitation force as well as the secondary force, inducing a velocity v_e in the flexible equipment. Compared to the electromagnetic shaker and the equipment, the mount is assumed to be massless. For the convenience of the theoretical analysis, no time delay is assumed in the electric controller.

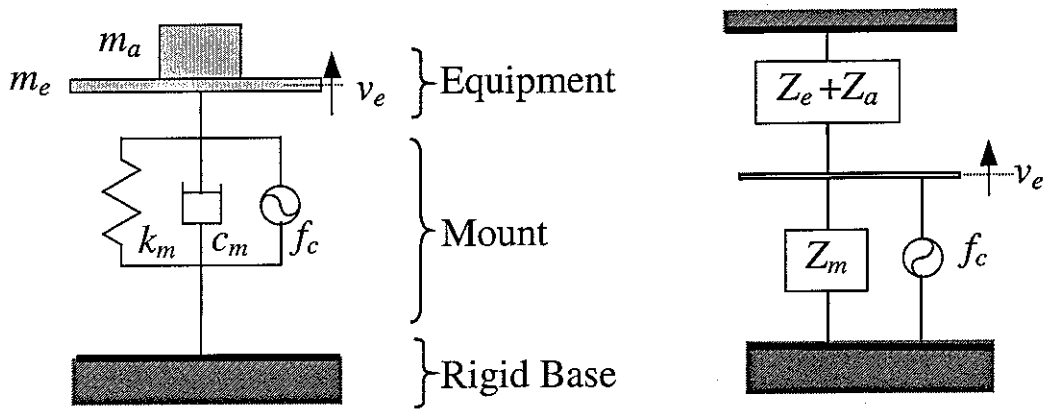

(a) one d.o.f system (b) impedance representation

Figure 1 Single mounted flexible equipment on a rigid base

Let the force acting through the mount be f_m, the flexible equipment response can be written as,

$$(Z_e + Z_a)v_e = f_c - f_m \tag{1}$$

$$f_m = Z_m v_e \tag{2}$$

where, $Z_e = Y_e^{-1}$, $Z_a = j\omega m_a$ and $Z_m = c_m + k_m / j\omega$. It is noted that in this one-dimensional analysis, the moment of inertia of the actuator could not be taken into account. In addition, the impedance of the flexible equipment is obtained by inverting the corresponding mobility Y_e, and the actuator is assumed to have the same velocity as the flexible equipment for the connection used in this research. By combining equation (1) and (2), the single mount system on a rigid base can be described by,

$$(Z_e + Z_a + Z_m)v_e = f_c \tag{3}$$

The model can be further extended for a generalized case, i.e. a single mount active vibration isolation system on a flexible base. The base structure is excited by a primary force f_p, and vibrated with a base velocity v_b, as shown in Figure 2. Using the same method, the base response is described by,

$$Z_b v_b = f_p - f_m - f_c \tag{4}$$

$$f_m = Z_m (v_b - v_e) \tag{5}$$

It is noted that for the case of a flexible base, the force f_c generated by the actuator is no longer a primary force. Thus the flexible equipment response is expressed by,

$$(Z_e + Z_a)v_e = f_c + f_m \tag{6}$$

Combining equation (4), (5) and (6), the dynamic behaviour of an active isolation of a flexible equipment on a flexible base can be described in matrix form,

$$\begin{bmatrix} Z_e + Z_a + Z_m & -Z_m \\ -Z_m & Z_b + Z_m \end{bmatrix} \begin{Bmatrix} v_e \\ v_b \end{Bmatrix} = \begin{Bmatrix} f_c \\ f_p - f_c \end{Bmatrix} \tag{7}$$

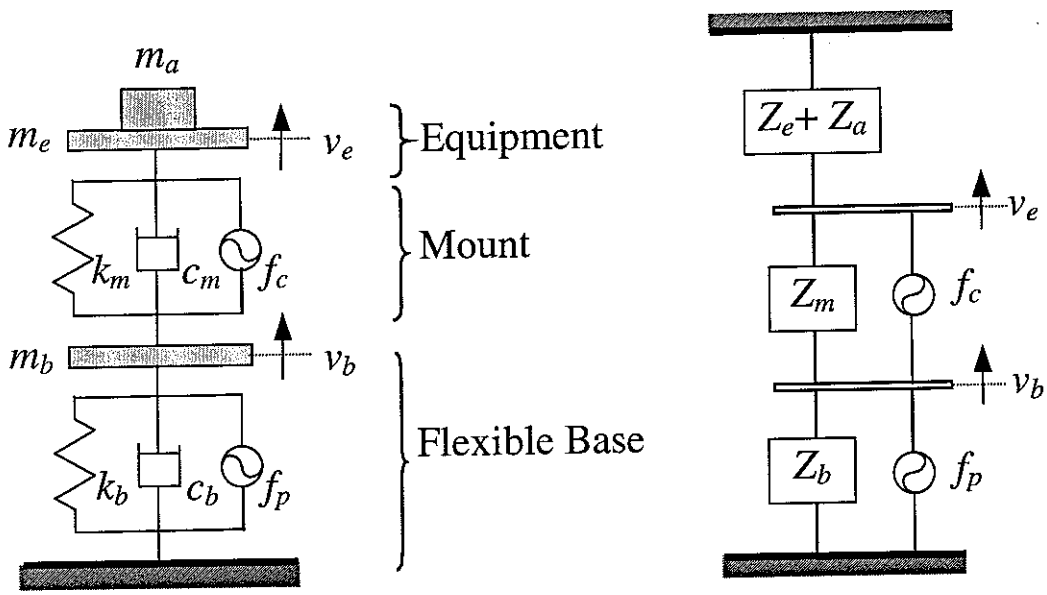

(a) Physical representation (b) Impedance representation

Figure 2 Single-mount vibration isolation system on a flexible base

Because the passive system is stable, the velocity responses can be obtained by inverting the impedance matrix in equation (7). In this research, the control system employs the direct velocity feedback control strategy that uses the measured velocity signal v_e from the equipment to activate the actuator with a constant gain of $-H$. At

low frequencies, the control force generated from the actuator is approximately proportional to the input velocity signal, i.e., $f_c = -Hv_e$. Thus, equation (7) becomes

$$\begin{bmatrix} Z_e + Z_a + Z_m + H & -Z_m \\ -(Z_m + H) & Z_b + Z_m \end{bmatrix} \begin{Bmatrix} v_e \\ v_b \end{Bmatrix} = \begin{Bmatrix} 0 \\ f_p \end{Bmatrix} \tag{8}$$

2.2 Impedance representation of a multiple-mount system

The impedance representation of a single mounted flexible equipment structure can be generalised for the more general case where the flexible equipment structure is supported by a set of mounts. As an extension to Figure 1, the multiple-mount vibration isolation system on a rigid base is represented in terms of impedance as shown in Figure 3(a). The number of mounts under consideration is M, and the total number of modes in the flexible equipment is N. Again no mass effects are considered in the mounts. Since M mounts are used, the end velocities of all mounts are denoted as M length vectors $\mathbf{v}_e$ to the flexible equipment. M actuators are used to connect the mounts and the flexible equipment, providing M length of primary force vector $\mathbf{f}_c$. Assuming a force vector $\mathbf{f}_m$ acting through the mounts, the dynamic behaviour of a multiple mounted flexible equipment structure on a rigid base can be written as,

$$(\mathbf{Z}_e + \mathbf{Z}_a)\mathbf{v}_e = \mathbf{f}_c - \mathbf{f}_m \tag{9}$$

$$\mathbf{f}_m = \mathbf{Z}_m \mathbf{v}_e \tag{10}$$

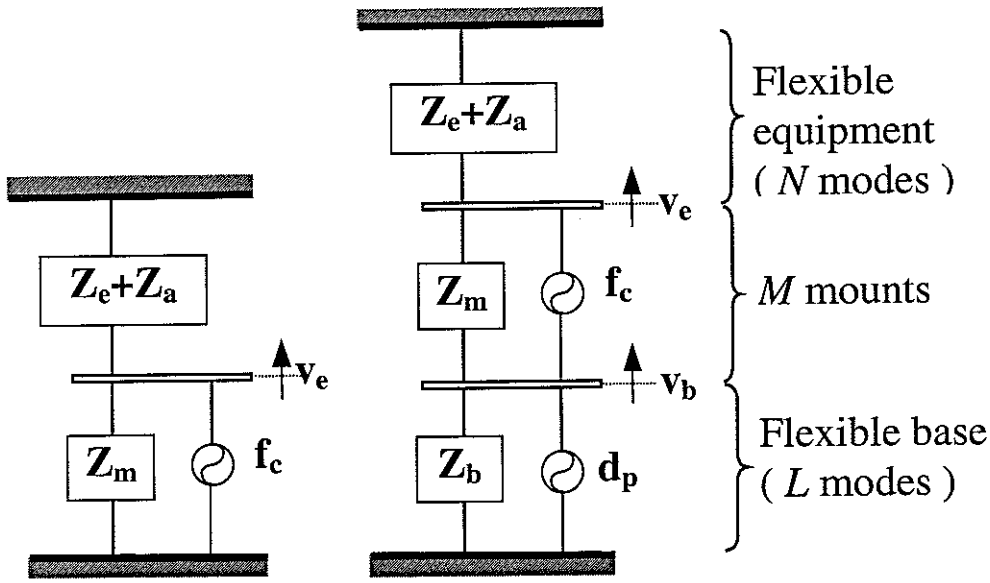

(a) Rigid Base (b) Flexible Base

Figure 3. Impedance representation of a multiple mount vibration isolation system

where, $\mathbf{Z}_a$, $\mathbf{Z}_e$ and $\mathbf{Z}_m$ denote the impedance matrix of the actuators, flexible equipment and mounts, respectively. In particular, $\mathbf{Z}_e = \mathbf{Y}_e^{-1}$, provided the mobility matrix $\mathbf{Y}_e$ of the flexible equipment is invertible. The mobility matrix is invertible if the elements of the vector $\mathbf{v}_e$ are linearly independent. Impedance matrixes $\mathbf{Z}_a$ and $\mathbf{Z}_m$

are ($M\times M$) diagonal matrixes, whose diagonal terms are the impedances due to the mass of each actuator, the stiffness and damping of the corresponding mount, respectively. As an extension to equation (3), the multiple-mount flexible equipment structure on a rigid base can be represented by,

$$(\mathbf{Z}_e + \mathbf{Z}_a + \mathbf{Z}_m)\mathbf{v}_e = \mathbf{f}_c \tag{11}$$

Considering the multiple-mount vibration isolation system on a flexible base as shown in Figure 3(b), the dynamic behaviour of the flexible base is strongly coupled with the mounted flexible equipment. Assuming that the flexible base is excited by a primary force vector $\mathbf{f}_p$, the base response can be written as,

$$\mathbf{Z}_b\mathbf{v}_b = \mathbf{d}_p - \mathbf{f}_m - \mathbf{f}_c \tag{12}$$

where, $\mathbf{d}_p = \mathbf{Z}_b\mathbf{Y}_{bp}\mathbf{f}_p$, in which $\mathbf{Y}_{bp}$ are the mobility matrix of the uncoupled flexible base due to the primary force vector $\mathbf{f}_p$. By extending equation (5) and (6), the dynamic behaviour of the multiple-mount active vibration isolation of a flexible equipment on a flexible base can be described in matrix form,

$$\begin{bmatrix} \mathbf{Z}_e + \mathbf{Z}_a + \mathbf{Z}_m & -\mathbf{Z}_m \\ -\mathbf{Z}_m & \mathbf{Z}_b + \mathbf{Z}_m \end{bmatrix} \begin{Bmatrix} \mathbf{v}_e \\ \mathbf{v}_b \end{Bmatrix} = \begin{Bmatrix} \mathbf{f}_c \\ \mathbf{d}_p - \mathbf{f}_c \end{Bmatrix} \tag{13}$$

Equation (13) is a compact description of the whole mounted flexible equipment-base coupled system in terms of impedance at the mount positions. It is a simple extension to equation (7) for the single mounted system. If the control strategy can be implemented to achieve $\mathbf{f}_c = -\mathbf{Z}_m\mathbf{v}_b$ in equation (13), perfect vibration isolation from the flexible base can be achieved. In this case, the mounted flexible equipment structure and the flexible base are uncoupled. The flexible base would behave as if there was no mounted flexible equipment structure attached, and the mounted flexible equipment structure would behave as if it was placed virtually on a rigid base. It is noted that the impedance matrix $\mathbf{Z}_m$ can be constructed from the impedance of each mount, while the impedance matrixes $\mathbf{Z}_e$ and $\mathbf{Z}_b$ are determined from their corresponding mobility matrixes $\mathbf{Y}_e$ and $\mathbf{Y}_b$, providing they are invertible. Mobility matrix $\mathbf{Y}_e$ is generally invertible if the total number of the flexible equipment modes N is not less than the number of mounts, M, i.e. $N \geq M$. The same applies to $\mathbf{Y}_b$, so that the condition is $L \geq M$ where L is the total number of base modes considered. In this case, the velocity responses in $\{\mathbf{v}_e \quad \mathbf{v}_b\}^T$ are linearly independent and the complete impedance matrix of the coupled system of ($2M\times 2M$) size is invertible.

Again by adopting direct velocity feedback control, the control force vector $\mathbf{f}_c$ generated by the multiple actuators is,

$$\mathbf{f}_c = -\mathbf{H}\mathbf{v}_e \tag{14}$$

It is noted that, each of the actuators is operated independently by feeding back the equipment absolute velocity with the same gain at each mount location. This is termed as decentralised control, where the control gain matrix is diagonal. Substituting equation (14) into (11), the response of the multiple-mount flexible equipment structure on a rigid base is given by,

$$(\mathbf{Z}_e + \mathbf{Z}_a + \mathbf{Z}_m + \mathbf{H})\mathbf{v}_e = \mathbf{f}_p \tag{15}$$

It is noted that for a rigid base, one of the actuators generates a primary force as well as a secondary force. Detailed implementations of the single channel and multichannel velocity feedback control of the mounted flexible equipment structure on a rigid base are described in section 4.3 and thus omitted here for brevity.

The system response of the multiple-mount flexible equipment structure on a flexible base is obtained similarly by substituting equation (14) to (13),

$$\begin{bmatrix} \mathbf{Z}_e + \mathbf{Z}_a + \mathbf{Z}_m + \mathbf{H} & -\mathbf{Z}_m \\ -(\mathbf{H} + \mathbf{Z}_m) & \mathbf{Z}_b + \mathbf{Z}_m \end{bmatrix} \begin{Bmatrix} \mathbf{v}_e \\ \mathbf{v}_b \end{Bmatrix} = \begin{Bmatrix} \mathbf{0} \\ \mathbf{d}_p \end{Bmatrix} \quad \cdot(16)$$

Conventionally, control performance is discussed in terms of transmissibility, which is defined by v_e/v_b for a single mount active isolation system. Because of the special installation of the control actuator in this research, the dynamic behaviour of the mounted flexible equipment structure is strongly coupled with the dynamics of the flexible base as can be seen from equation (7) and (13). In this case, v_b changes after attachment as well as a change of the control gain, therefore, the transmissibility does not represent the absolute vibration response of the flexible equipment. Thus, the absolute velocity of the mounted flexible equipment structure is more preferable as a control performance measure for mounted active isolation system. Pan et al [9] studied the dynamics of an active isolator by considering the power transmission, which extended the modelling of the passive mount system in terms of power to the modelling of the active isolation system. Power is not only considered as a good parameter for describing vibration, but also power minimization has been applied as a new control strategy for the active vibration isolation system. Kim et al [6] employed the kinetic energy of a rigid equipment to investigate the control performance of a multiple-mount active isolation system. Using the same idea, the kinetic energy of the *flexible* equipment will be employed as the control performance measure in addition to the absolute velocity in this study.

If the active controlled multiple-mount flexible equipment-base system is stable, the velocities at both ends of the mounts can be obtained by taking the inverse of the total system impedance matrix. However, because the number of flexible modes of the equipment is greater than that of the mounts generally, i.e. $M < N$, the kinetic energy of the equipment can not be obtained directly from equation (15) or (16), which only gives velocity responses at the mount locations. Thus it is necessary to consider the dynamics of the active vibration isolation system in modal co-ordinates. Assuming that the equipment, a flexible rectangular plate, is described by the physical co-ordinate system $\mathbf{r}$, the kinetic energy is given by,

$$E_k^e = \frac{\rho_e t}{2} \int_{S_e} |v_e(\mathbf{r}, \omega)|^2 dS \quad (17)$$

where, $v_e(\mathbf{r}, \omega)$ is the velocity at the position $\mathbf{r}$, and ρ_e, t, and S_e are the material density, thickness and area of the plate, respectively. The vibration response in the flexible equipment can be represented by a summation of N modes, which is expressed by a product of a shape function and an amplitude function [10],

$$\mathbf{v}_e(\mathbf{r}, \omega) = \sum_{n=1}^{N} \psi_n(\mathbf{y}) a_n(\omega) = \boldsymbol{\psi}^T \mathbf{a} \quad (18)$$

where ^{T} denotes the transpose, and the N length column vectors $\boldsymbol{\psi}$ and $\mathbf{a}$ consist of the arrays of the modal shape function $\psi_n(\mathbf{r})$ and the complex amplitude of the modal velocity $a_n(\omega)$ respectively. It is noted that the modal functions refer to those of the uncoupled equipment plate instead of the complete coupled system. If the modal shape function $\psi_n(\mathbf{r})$ is normalised according to $S_e = \int_{S_e} \psi_n^2(\mathbf{r}) dS$, the kinetic energy given in equation (17) can be rewritten as,

$$E_k^e = \frac{M_e}{2} \mathbf{a}^H \mathbf{a} \quad (19)$$

where, M_e is the total mass of the flexible plate, i.e. $M_e = \rho_e t S_e$, and the superscript $^{\mathrm{H}}$ denotes the Hermitian transpose. For the particular installation of the actuators that can be assumed as rigid masses, the kinetic energy stored in the actuators must be considered when discussing the control performance. Therefore, the kinetic energy of the mounted flexible equipment structure is,

$$E_k = \frac{M_e}{2}\mathbf{a}^{\mathrm{H}}\mathbf{a} + \frac{1}{2}\mathbf{A}^{\mathrm{H}}\mathbf{J}_{\mathrm{a}}\mathbf{A} \tag{20}$$

where, $\mathbf{A} = \begin{Bmatrix} \dot{w}_a & \dot{\theta}_a & \dot{\varphi}_a \end{Bmatrix}^T$ denoting the heave, pitch and roll velocities of the actuators, can be determined from the velocities of the flexible equipment at the mount positions. The inertia matrix of the actuators, $\mathbf{J}_{\mathrm{a}}$, is given by,

$$\mathbf{J}_{\mathrm{a}} = \begin{bmatrix} M_a & 0 & 0 \\ 0 & J_\theta & 0 \\ 0 & 0 & J_\phi \end{bmatrix} \tag{21}$$

where, M_a is the total mass of the actuators, I_θ and I_φ are the moment of inertia of the actuators in respect to the pitch and roll motions, respectively. In order to calculate the kinetic energy, the dynamic response of the multiple mounted active vibration isolation system described by equation (15) or (16), needs to transform from the physical co-ordinate to modal co-ordinate, by replacing the physical velocity response vector $\mathbf{v}$ with the modal velocity vector $\mathbf{a}$. According to equation (18), the equipment velocity response vector $\mathbf{v}_e$ at the mount positions can be expressed by,

$$\mathbf{v}_e = \Psi_{\mathrm{M}}^{\mathrm{T}}\mathbf{a} \tag{22}$$

where, matrix $\Psi_{\mathrm{M}}^{\mathrm{T}}$ is a transformation matrix which transforms the N length modal velocity vector $\mathbf{a}$ to the M length physical velocity vector $\mathbf{v}_e$. Since $\Psi_{\mathrm{M}}^{\mathrm{T}}$ is a $(M \times N)$ size matrix where $M < N$ (underdetermined), $\mathbf{a}$ can not be obtained directly from $\mathbf{v}_e$ [11] because $\Psi_{\mathrm{M}}^{\mathrm{T}}$ is not invertible even in the least square sense. This is the reason why a modal domain formulation is necessary. Substituting equation (22) into equations (15) and (16), the dynamics of the multiple mounted flexible equipment structure on a rigid base in modal co-ordinates is described by,

$$(\overline{\mathbf{Z}}_{\mathrm{e}} + \overline{\mathbf{Z}}_{\mathrm{a}} + \overline{\mathbf{Z}}_{\mathrm{m}} + \overline{\mathbf{H}})\,\mathbf{a} = \overline{\mathbf{f}}_{\mathrm{p}} \tag{23}$$

and on a flexible base,

$$\begin{bmatrix} \overline{\mathbf{Z}}_{\mathrm{e}} + \overline{\mathbf{Z}}_{\mathrm{a}} + \overline{\mathbf{Z}}_{\mathrm{m}} + \overline{\mathbf{H}} & -\Psi_{\mathrm{M}}\mathbf{Z}_{\mathrm{m}} \\ -(\mathbf{Z}_{\mathrm{m}} + \mathbf{H})\Psi_{\mathrm{M}}^{\mathrm{T}} & \mathbf{Z}_{\mathrm{b}} + \mathbf{Z}_{\mathrm{m}} \end{bmatrix} \begin{Bmatrix} \mathbf{a} \\ \mathbf{v}_{\mathrm{b}} \end{Bmatrix} = \begin{Bmatrix} \mathbf{0} \\ \mathbf{d}_{\mathrm{p}} \end{Bmatrix} \tag{24}$$

where the modal impedance matrices are given by,

$$\overline{\mathbf{Z}}_{\mathrm{e}} = \overline{\mathbf{Y}}_{\mathrm{e}}^{-1} \qquad \overline{\mathbf{Z}}_a = \Psi_{\mathrm{M}}\mathbf{Z}_a\Psi_{\mathrm{M}}^{\mathrm{T}} \qquad \overline{\mathbf{Z}}_{\mathrm{m}} = \Psi_{\mathrm{M}}\mathbf{Z}_{\mathrm{m}}\Psi_{\mathrm{M}}^{\mathrm{T}} \tag{25a,b,c}$$

$$\overline{\mathbf{H}} = \Psi_{\mathrm{M}}\mathbf{H}\Psi_{\mathrm{M}}^{\mathrm{T}} \qquad \overline{\mathbf{f}}_{\mathrm{p}} = \Psi_{\mathrm{M}}\mathbf{f}_{\mathrm{p}} \tag{26a,b}$$

It is noted that, $\overline{\mathbf{Z}}_{\mathrm{a}}$, $\overline{\mathbf{Z}}_{\mathrm{m}}$ and $\overline{\mathbf{H}}$ are obtained by transformations from physical co-ordinates into modal co-ordinates, while $\overline{\mathbf{Z}}_{\mathrm{e}}$ is directly obtained from the inverse of modal mobility matrix $\overline{\mathbf{Y}}_{\mathrm{e}}$ of the flexible equipment. This is because the matrix $\overline{\mathbf{Z}}_{\mathrm{e}}$ of rank N can not be obtained from $\Psi_{\mathrm{M}}\mathbf{Z}_{\mathrm{e}}\Psi_{\mathrm{M}}^{\mathrm{T}}$, whose rank is M, where $N > M$. It is noted that, $\overline{\mathbf{Z}}_{\mathrm{e}}$ is diagonal, while $\overline{\mathbf{Z}}_{\mathrm{m}}$ is generally non-diagonal but symmetric although $\mathbf{Z}_{\mathrm{m}}$ is diagonal. The non-diagonal terms act as coupling terms between the equipment modal responses. The general representations of equations (23) and (24)

are valid regardless of the difference of M and N. Since the modal velocity vector $\mathbf{a}$ can be obtained by inverting the modal impedance matrix in equations (23) and (24), the control performance of the multiple-mount active isolation system can be assessed in terms of kinetic energy determined by equation (20). The physical velocity vector $\mathbf{v}_e$ at the mount positions can also be obtained from equation (22).
In summary, a general theoretical analysis of a flexible equipment supported by a set of mounts on a rigid base as well as on a flexible base is presented in this section. It is very useful to fully understand the mechanisms of a simple case of a mounted flexible equipment on a rigid base before moving to a more complicated one on a flexible base. Therefore, a 3-dimensional flexible equipment structure with four mounts on a rigid base has been studied theoretically and experimentally, and discussed in the following sections.

2.3 Simulation of a four-mount active isolation system on a rigid base

In this section, simulations are performed for a flexible equipment structure on a rigid base with four passive mounts and electromagnetic actuators as shown in Figure 4. It is assumed that the flexible equipment is of uniform and all four mounts are massless and have the same mechanical properties. Particular interest is the low frequency range (0~200 Hz), where the mount can be modelled as a parallel connection of a spring and a damper. Relevant physical and geometry properties used in the simulation are tabulated in Table 1 and 2. The theoretical stiffness and damping properties of the mounts were chosen to best fit the measured natural frequency and bandwidth in the experiments.
For the convenience, the locations of the four mounts are denoted as nodes 1, 2, 3, 4 as shown in Figure 4. When the flexible equipment on a rigid base is excited by one of the actuators via a white noise signal, the plant response $\mathbf{G}$ at each mount location is calculated according to equation (11), which is expressed,

$$\mathbf{G} = (\mathbf{Z}_e + \mathbf{Z}_a + \mathbf{Z}_m)^{-1} \tag{27}$$

It is noted that, $(\ )^{-1}$ is the inverse of the impedance matrix of the mounted flexible equipment structure. In particular, G_{ij} is the velocity response at the ith mount location due to unit force excited at the jth mount location. The magnitude of each simulated plant response as well as its phase angle is shown in dashed lines in Figure 6 to Figure 21. Each peak in the plant response figures corresponds to a resonance frequency of either a rigid or a flexible mode. Each motion can be clearly distinguished by comparing the other plant responses and checking the corresponding phases at that particular frequency. Using the simple impedance modal outlined in the previous section, only the heave, the pitch and the roll rigid body modes of the mounted flexible equipment structure are considered. However, only one rigid body resonance is predicted from the simulation, as seen from the plant response G_{11} in Figure 6. This can be explained by looking at the natural frequencies of the mounted flexible equipment structure. The resonance frequencies of the three rigid body modes can be estimated by the following equations, which give 17.40, 17.78 and 17.43 Hz respectively,

$$f_h = \frac{1}{2\pi}\sqrt{\frac{4k_m}{(M_e + 4M_a)}},\ f_p = \frac{1}{2\pi}\sqrt{\frac{4k_m \times l_\theta^{\,2}}{I_\theta}},\ f_r = \frac{1}{2\pi}\sqrt{\frac{4k_m \times l_\phi^{\,2}}{I_\phi}} \quad \text{(28a, b, c)}$$

where, K_m is the spring stiffness of each mount, I_θ and I_ϕ are the moments of inertia of the mounted flexible equipment structure in respect to the Y and X axis as shown in Figure 4. The resonance frequencies of the three rigid body modes are so close that they are merged into one large peak instead of three small ones. This explanation is further substantiated from the experimental observations as seen from the experimental plant responses in solid lines from Figure 6 to Figure 21. The frequency of the first flexible mode of the mounted flexible equipment structure is predicted to be around 50.7 Hz, with the second around 132.1 Hz. The theoretical analysis has been validated through a detailed comparison with the measured plant responses of the mounted flexible equipment structure on a rigid base from the experiment, which is described in the following section. After the whole plant matrix **G** is obtained, stability of the active four-mount vibration isolation system can be assessed using the generalized Nyquist criterion [12].

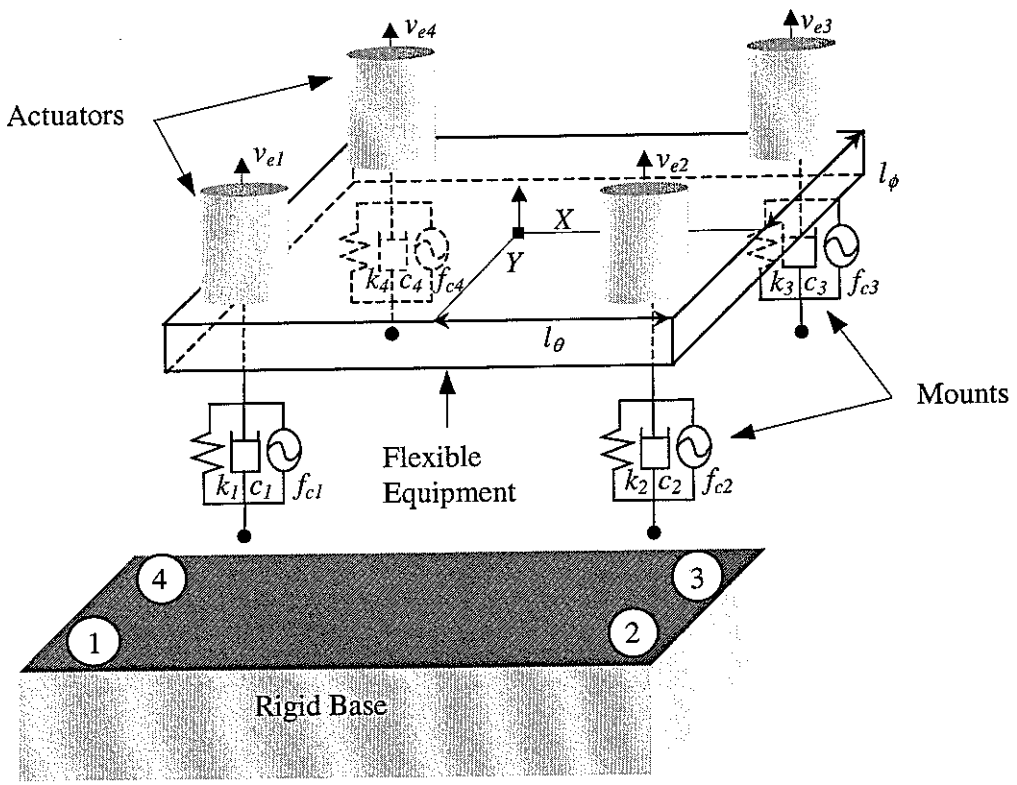

Figure 4. A four-mount flexible equipment structure on a rigid base

Table 1. Physical properties

Equipment Structure	Material of the flexible equipment plate	Aluminium
	Density of the flexible equipment plate	2700 kgm^{-3}
	M_e, Mass of the flexible equipment plate	0.3564 Kg
	Young's Modulus	7.1×10^{10} Nm^{-2}
	Poisson's Ratio	0.33
	Damping ratio	$\zeta_e = 0.01$
Mount	k_m, spring stiffness of each mount	1.2×10^4 N/m
	c_m, Damping of each mount	11.5 Ns/m
Actuator	M_a, Mass of each actuator	0.91 Kg

Table 2. Geometric data

($L_x \times L_x \times t$), Dimensions of the flexible equipment plate (mm)	$(300 \times 160 \times 3.54)$
Mount locations on the flexible equipment (mm)	$l_\theta = 117,\ l_\phi = 47$
Location of node 1	$(L_x/2 - l_\theta, L_y/2 - l_\phi)$
Location of node 2	$(L_x/2 + l_\theta, L_y/2 - l_\phi)$
Location of node 3	$(L_x/2 + l_\theta, L_y/2 + l_\phi)$
Location of node 4	$(L_x/2 - l_\theta, L_y/2 + l_\phi)$

3. Experimental study of a four-mount flexible equipment structure on a rigid base

3.1 Description of the experimental set-up

The four-mount active vibration isolation system has been built as shown in Figure 4. The mounted flexible equipment structure was installed on the top of a rigid base, i.e., a thick steel plate. It is noted that the mounted equipment structure refers to a combination of the flexible equipment, i.e., the aluminium plate of thickness 3.54 mm, four rubber mounts and four electromagnetic shakers, which acts as the actuators. To achieve the same parallel installation of actuators with the mounts as shown in Figure 4, the four actuators are fixed on the flexible equipment and are mounted on top of each mount position. The mount is made of natural rubber with a hollow cylinder shape, which is connected to the flexible equipment by a stinger between the actuator and a mount foot through the mount as shown in Figure 5. The physical and geometric properties of the experimental set-up, as well as the locations of the mounts, are the same as those in the simulation as shown in Tables 1 and 2.

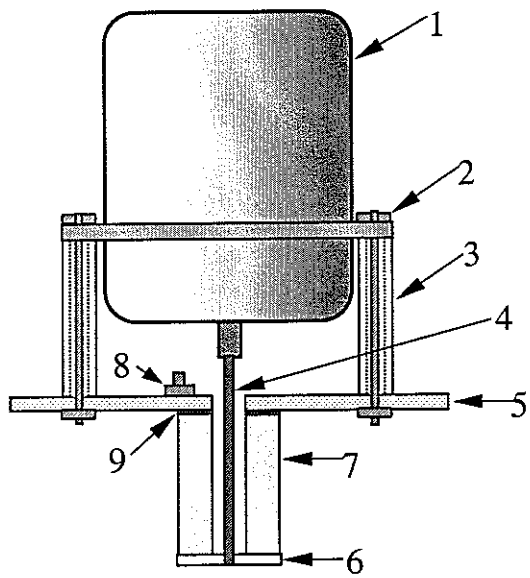

1 Electromagnetic Actuator
2 Bolt
3 Support (height = 40 mm)
4 Stinger
5 Flexible Equipment Structure (Al)
6 Adapter (Al)
7 Rubber Mount (height = 30 mm, outer dia. = 30mm, inner dia. = 10 mm)
8 Accelerometer
9 Steel Washer

Figure 5 Connection of the actuator, flexible equipment and the mount.

3.2 Experimental plant response of the four-mount active isolation system

When the mounted flexible equipment structure was excited by one of the actuators via a white noise signal generated from an FFT Analyzer (Advantest R9211C), the acceleration signal at each mount location was measured using an accelerometer (B&K type 4375). The acceleration signal was passed to a general signal conditioner (B&K type 2635) and converted to a velocity signal by an integrated module inside the signal conditioner. It is noted that the integrator is operated in conjunction with a highpass filter. In this study, the cutoff frequency of the highpass filter was set to be 1 Hz. Finally the velocity signal was inputted into the analyzer to measure the frequency response function. It is noted that there is a built-in filter in the analyzer to reduce aliasing. The plant responses of the mounted flexible equipment structure on a rigid base in the experiment are shown in solid lines in Figure 6 to Figure 21. As pointed out in the previous section, stability analysis of the active vibration isolation system can be evaluated after the plant responses of the mounted flexible equipment structure on a rigid base are obtained. Moreover, the theoretical model developed in section 2 has been validated by a comparison between the corresponding plant responses from the simulation and those from experiment. In order to match the first flexible resonance of the plant response measured from experiment, the thickness of the flexible equipment plate in the model is set to be 2.9 mm. This lowers the frequency of the first flexible mode in the model and is thought to compensate for the frequency lowering effect of the rotational moments of inertia of the shakers in the experimental arrangement, which were not accounted for in the model.

The first main peak noticeable in the experimental driving point plant responses is related to the rigid body modes of the mounted flexible equipment structure. This is in accordance with the prediction given in section 2.3 because the frequencies of the three rigid body modes are very close to each other. In particular, the measured natural frequencies of the rigid body modes (17.42, 17.98 and 17.45 Hz) are very close to those from simulation (17.40 Hz, 17.78 Hz and 17.42 Hz). It is noted that the corresponding experimental rigid body frequencies are obtained from the mode decompositions described in section 4.2. The following peaks correspond to the flexible modes, with the first one at about 50.5 Hz, the second at around 140.0 Hz and the third at around 189.6 Hz. The experimental plant measurements have some discrepancies at frequencies below 10 Hz compared with the simulations, which suffer from the poor coherence due to the low sensitivity of the actuators and the sensor used. Although the frequency of the first flexible mode is very close to that from simulation, the resonance of the second flexible mode occurs at 140.0 Hz in the experiment, instead of around 132.1 Hz as predicted from simulation. These are because that, the four mounts are assumed to be identical in the simulation, while in the experiment, they have small differences which may be traced back to the installation of the experimental set-up. There is a slightly discrepancy in each experimental driving point plant response, which is also due to the fact that the four mounts used in the experiment are not exactly the same.

4. Discussion of results

4.1 Comparison of plant responses from simulation and experiment

Matching the results of a theoretical model to measurements from experiment is a good way of evaluating the degree of confidence in using the theoretical model to predict the dynamics of the mounted flexible equipment structure, assuming all the parameters affecting the system are properly considered. In addition, it is a powerful tool for interpreting and understanding experimental results as it superposes a theoretical background to the phenomena observed from experiment. Therefore, the plant responses from simulation (dashed line) are compared with those measured from the experiment (solid line) as shown from Figure 6 to Figure 21 in order to validate the theoretical model developed in section 2. It is noted that, the plant response G_{ij} is the velocity response measured at the ith node when the mounted equipment structure on a rigid base is excited by unit force at the jth node.

Both simulation and experiment demonstrate that coupling in the mount nodes is significant at the natural frequencies of the rigid body modes, since the rigid body modes generate almost the same amplitude of vibration at the four nodes of the mounted flexible equipment structure with very similar phase shifts. The coupling is also significant at the resonance frequency around 50.6 Hz of the first flexible mode. It is found that the driving point plant responses from the simulation agree well with those from experiments, with the frequencies and mode shapes listed in Table 3. However, for the off-diagonal terms in the plant response matrix, there are some discrepancies noticed in the frequencies above 60 Hz between the simulation and experiment. The experimental plant responses clearly show a third flexible mode in the frequency band of analysis, compared to only two flexible modes predicted from simulation. As pointed out earlier, there are small differences in the four mounts used in the experiment, whereas four identical mounts with the same properties are assumed in the simulation. In summary, the plant responses from simulation are reasonably close to those from experiment, which demonstrates that, the dynamics of the four-mount flexible equipment structure can be understood using the theoretical model outlined in the previous section.

Table 3. Natural frequencies of the mounted flexible equipment structure

Simulation						Experiment					
Frequency (Hz)	Motion	Mode shape				Frequency (Hz)	Motion	Mode shape			
		1	2	3	4			1	2	3	4
17.40	Heave	+	+	+	+	17.42	Heave	+	+	+	+
17.78	Pitch	+	-	-	+	17.98	Pitch	+	-	-	+
17.42	Roll	+	+	-	-	17.45	Roll	+	+	-	-
50.6	Flexible (Torsion)	+	-	+	-	50.5	Flexible (Torsion)	+	-	+	-
132.1	Flexible (Heave)	+	+	+	+	140.0	Flexible (Pitch)	+	-	-	+
						189.6	Flexible (Torsion)	+	-	+	-

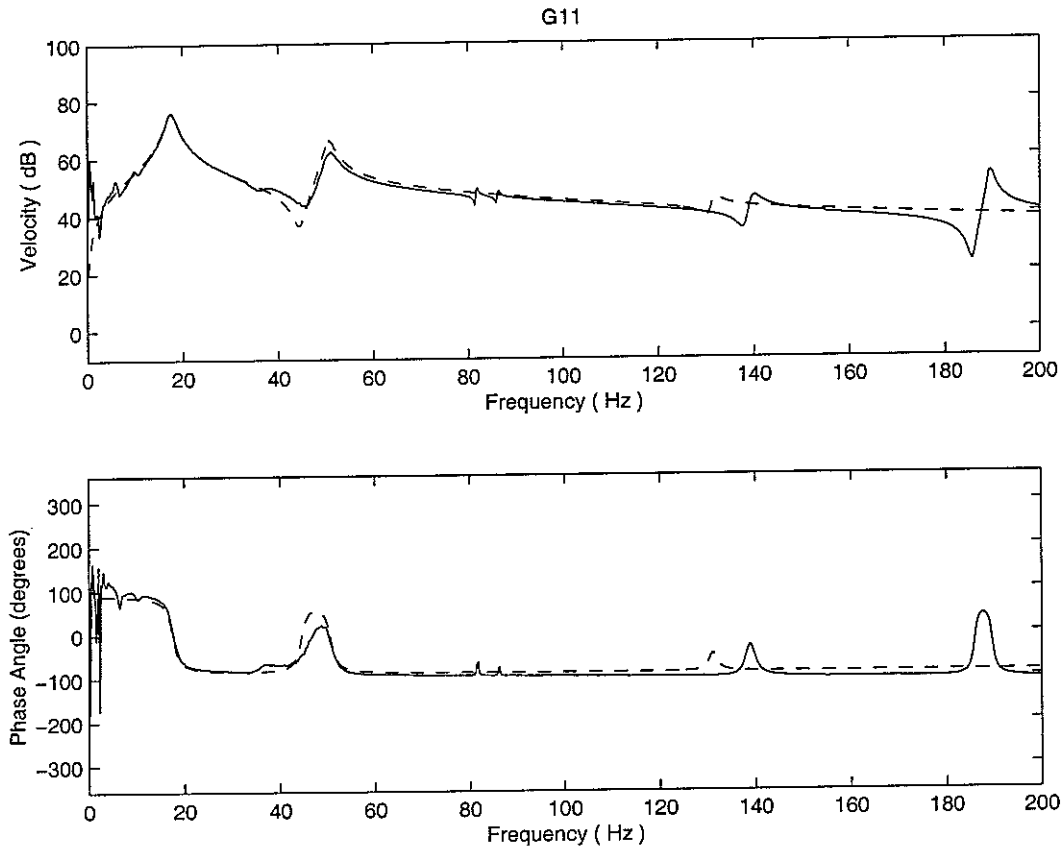

Figure 6 Comparison of plant response G_{11} from simulation (—) and experiment (—)

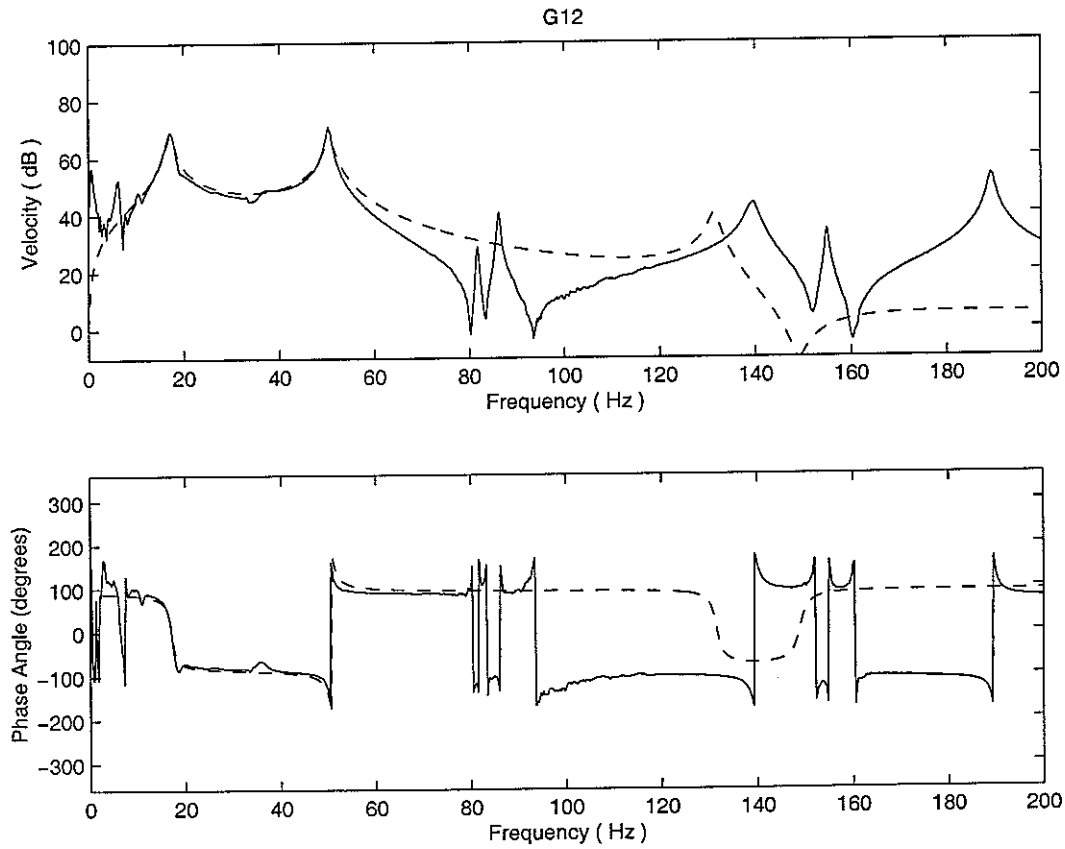

Figure 7 Comparison of plant response G_{12} from simulation (—) and experiment (—)

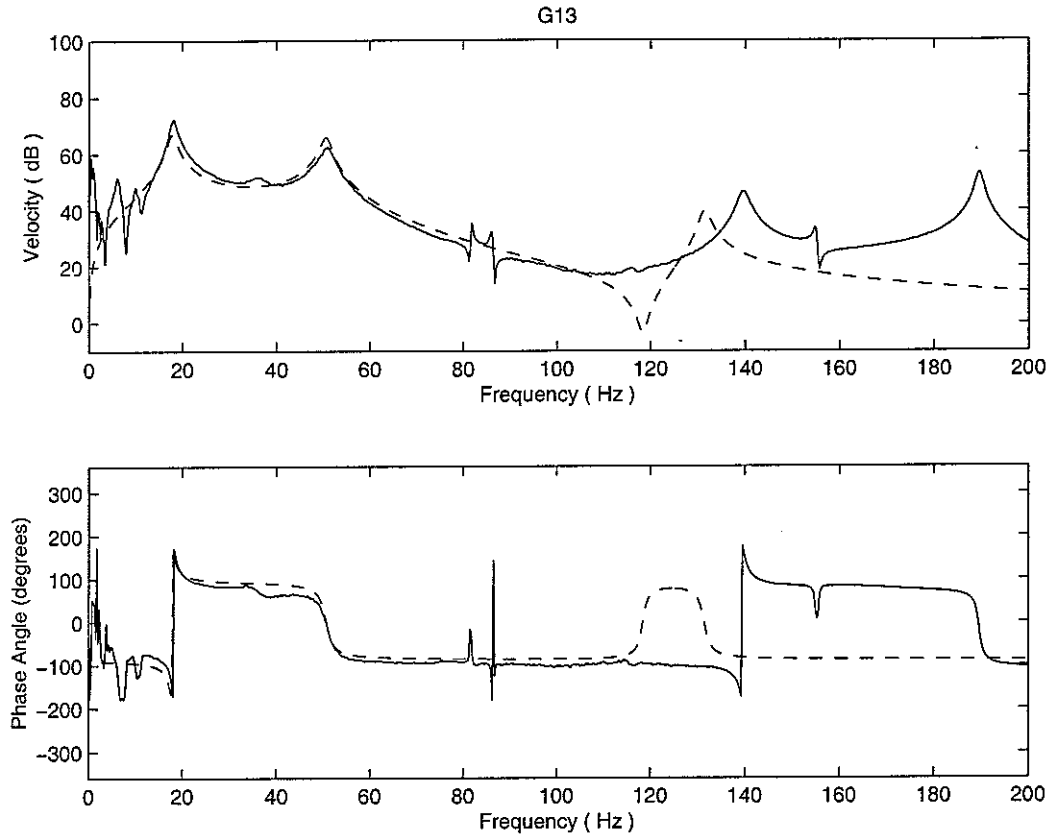

Figure 8 Comparison of plant response G_{13} from simulation (--) and experiment (—)

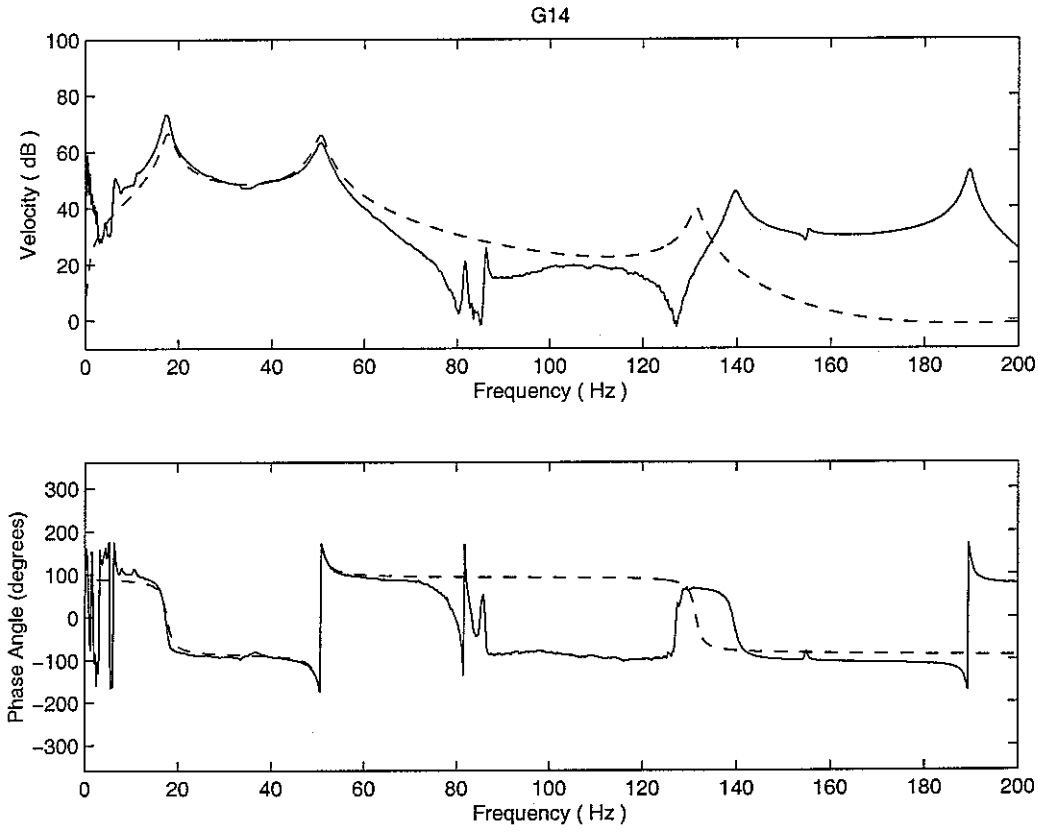

Figure 9 Comparison of plant response G_{14} from simulation (--) and experiment (—)

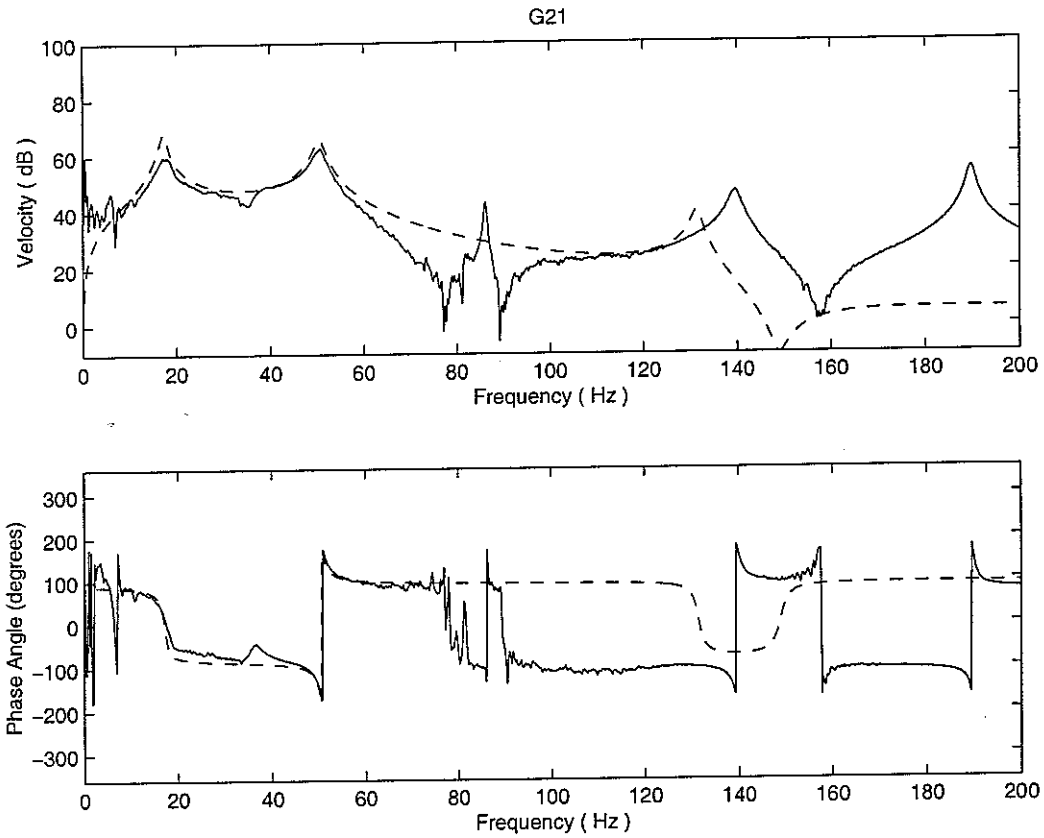

Figure 10 Comparison of plant response G_{21} from simulation (—) and experiment (—)

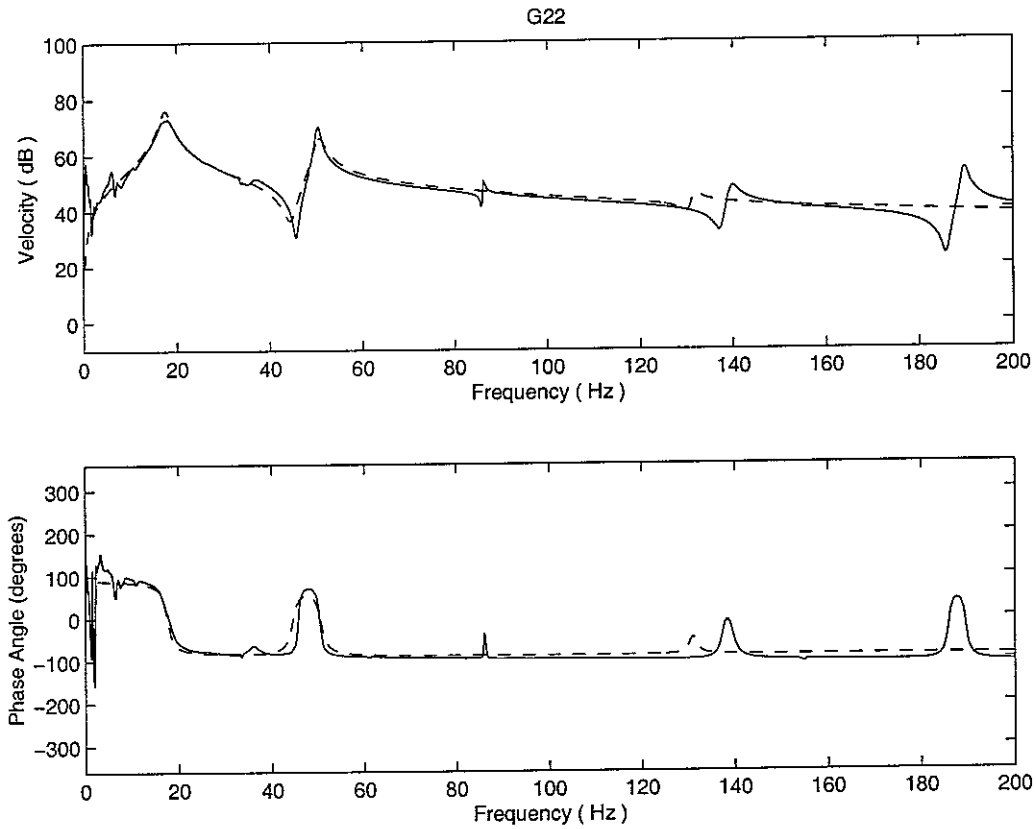

Figure 11 Comparison of plant response G_{22} from simulation (—) and experiment (—)

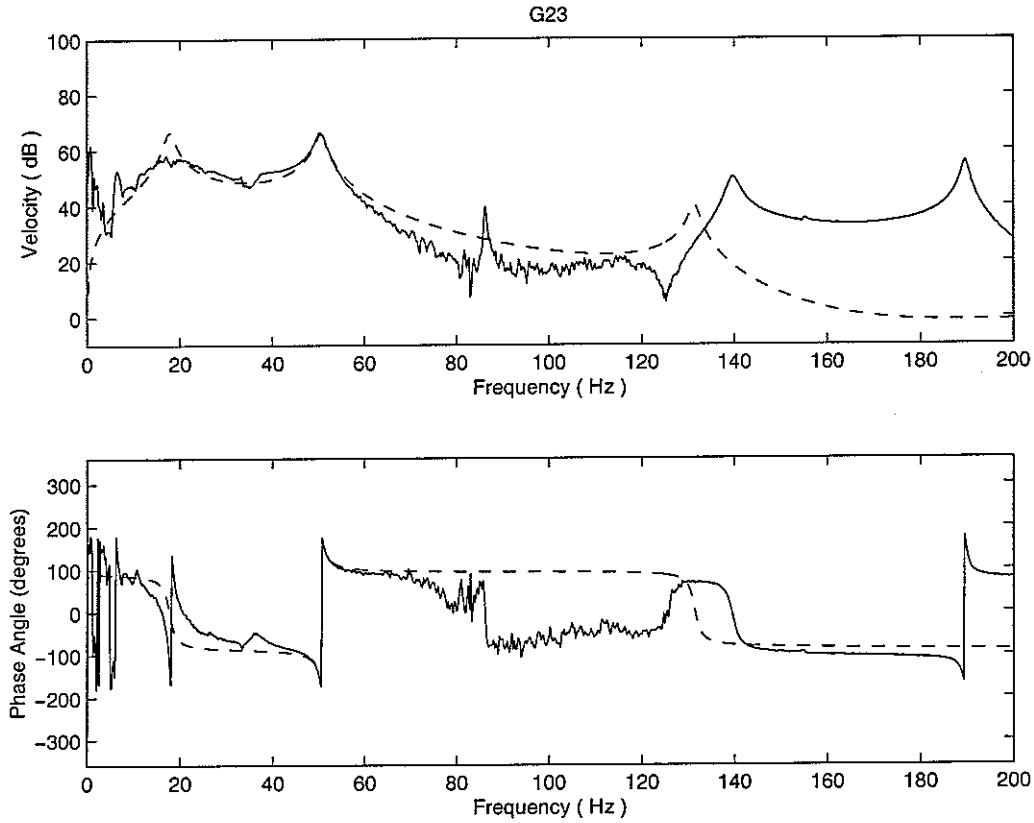

Figure 12 Comparison of plant response G_{23} from simulation (—) and experiment (—)

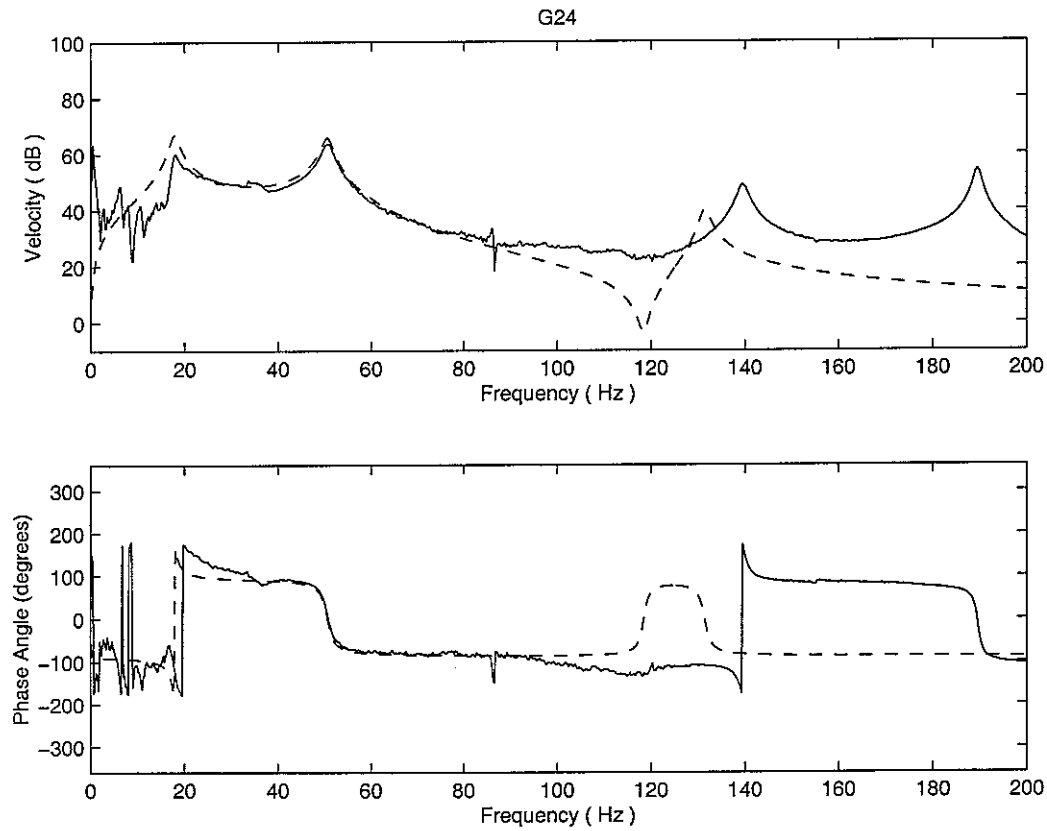

Figure 13 Comparison of plant response G_{24} from simulation (—) and experiment (—)

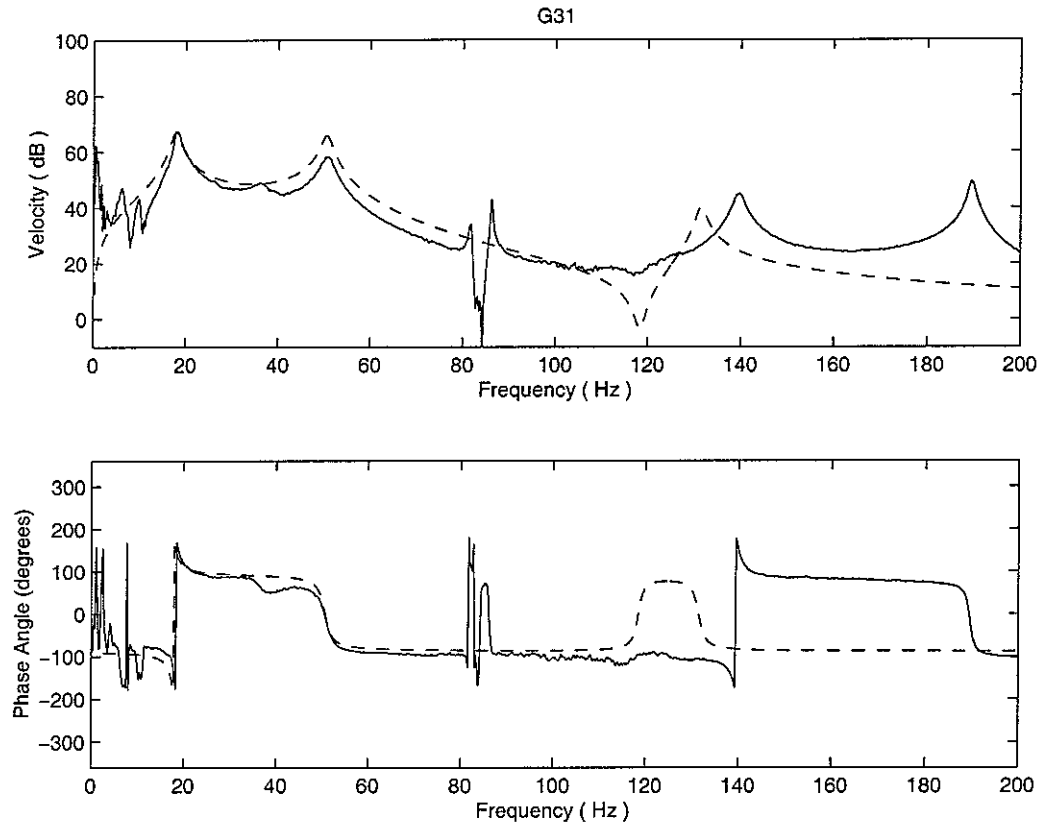

Figure 14 Comparison of plant response G_{31} from simulation (—) and experiment (—)

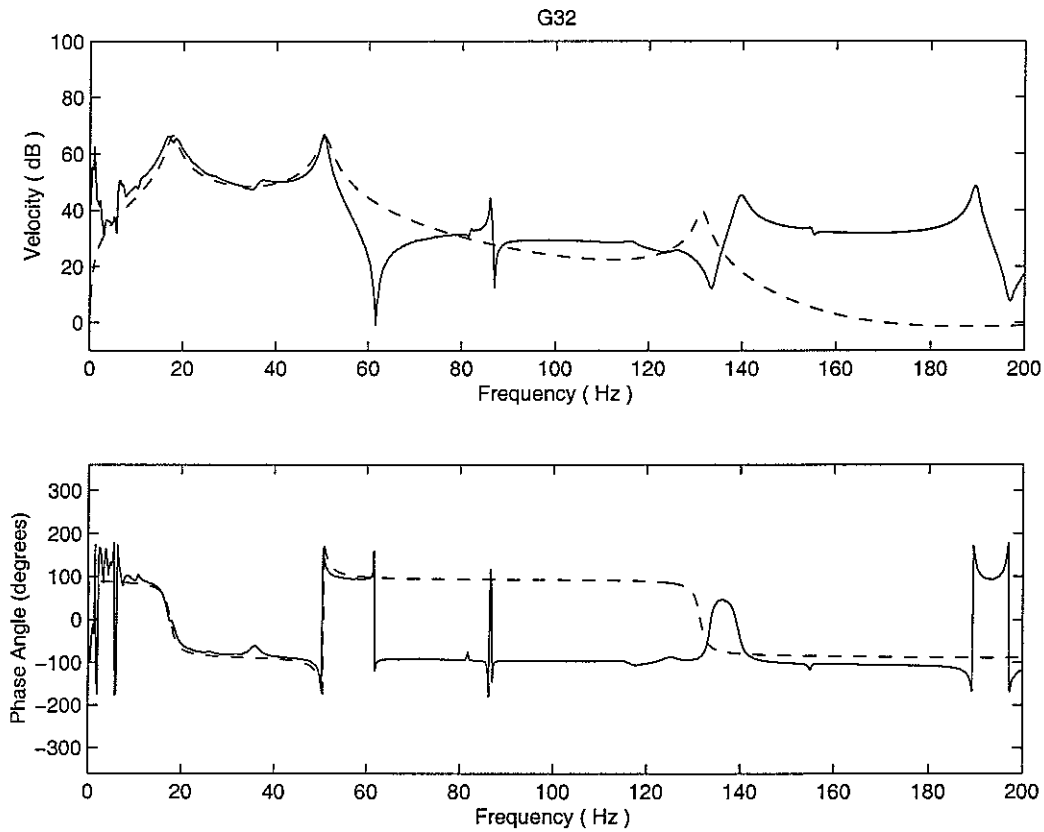

Figure 15 Comparison of plant response G_{32} from simulation (—) and experiment (—)

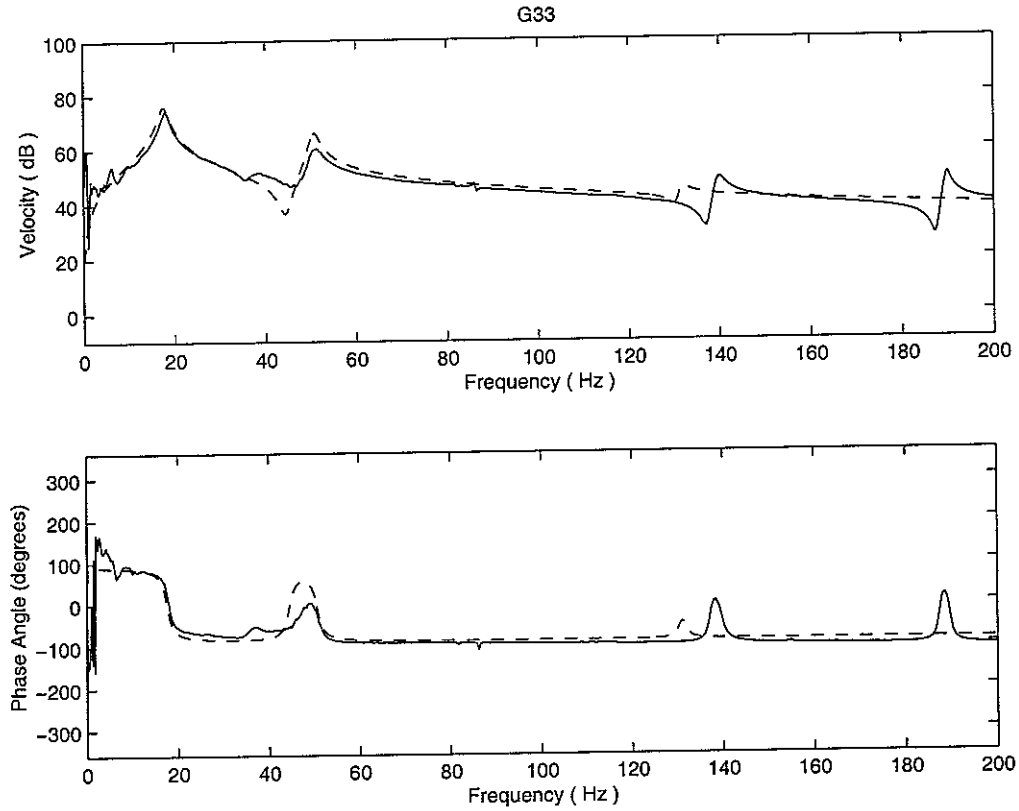

Figure 16 Comparison of plant response G_{33} from simulation (—) and experiment (—)

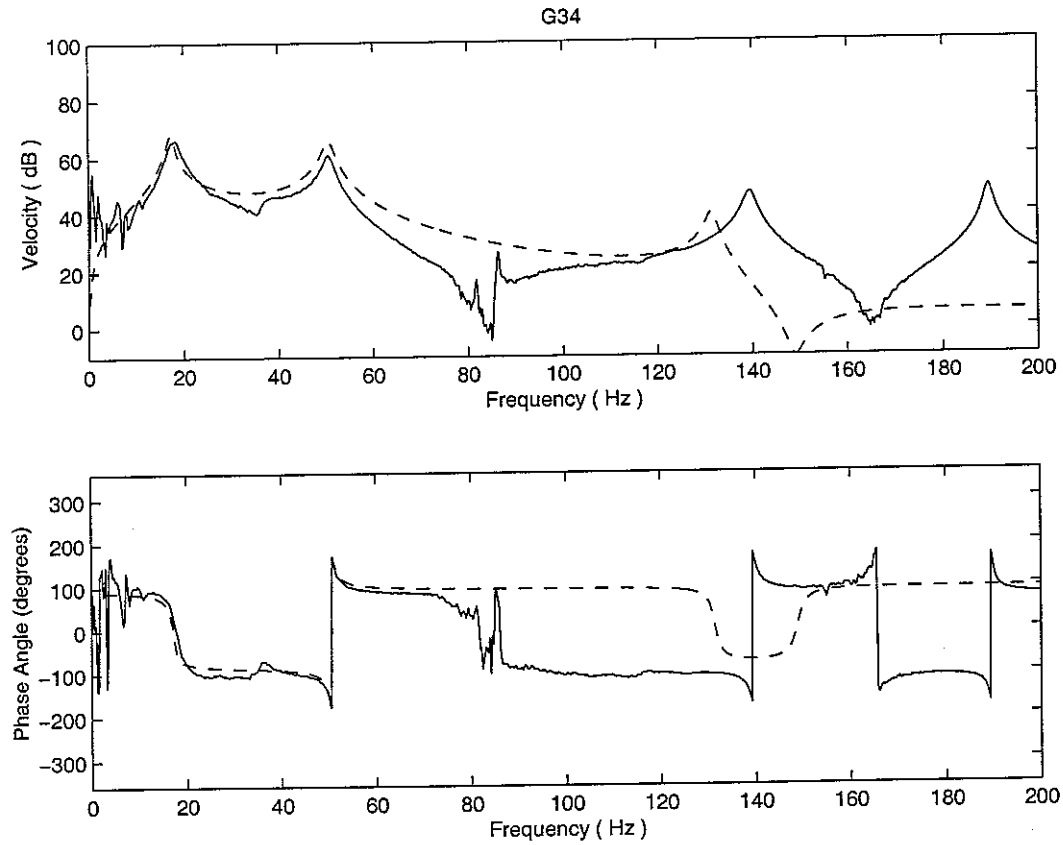

Figure 17 Comparison of plant response G_{34} from simulation (—) and experiment (—)

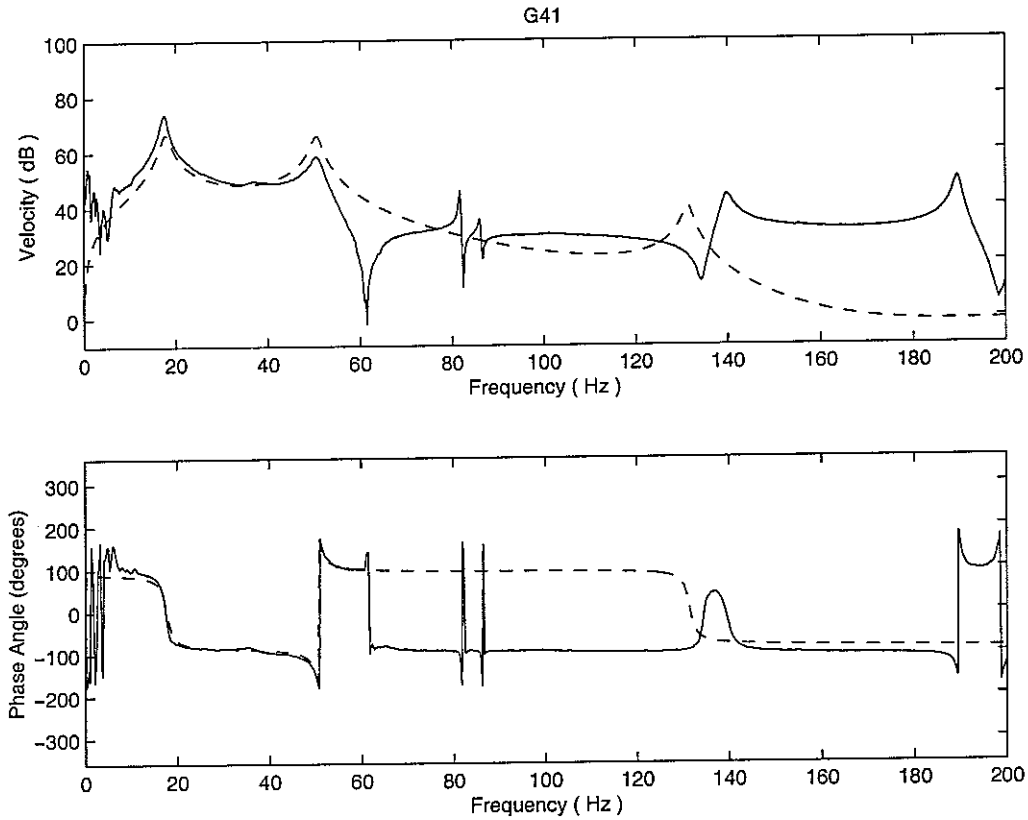

Figure 18 Comparison of plant response G_{41} from simulation (—) and experiment (—)

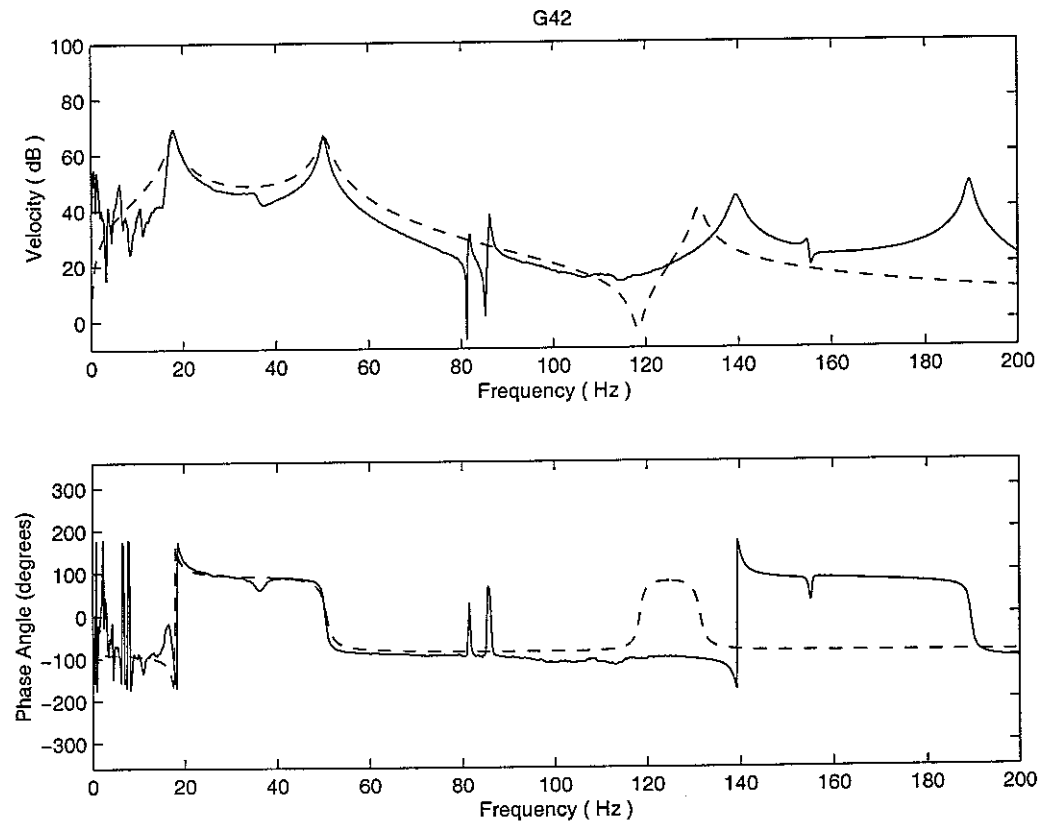

Figure 19 Comparison of plant response G_{42} from simulation (—) and experiment (—)

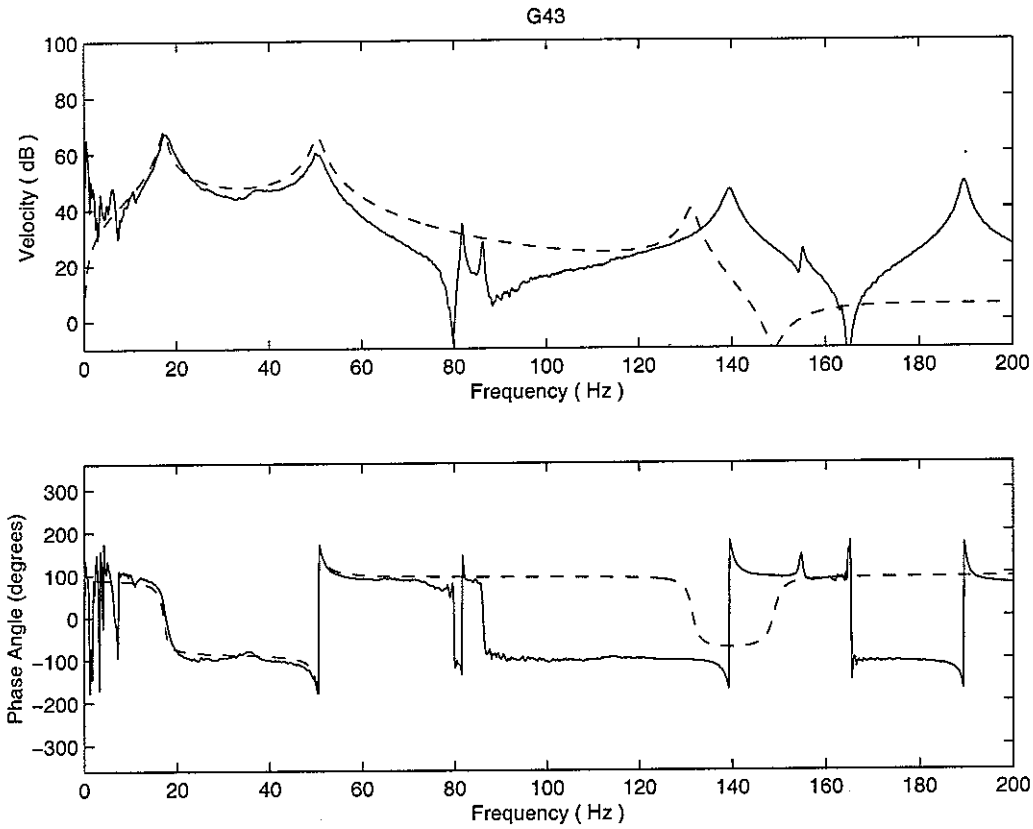

Figure 20 Comparison of plant response G_{43} from simulation (—) and experiment (—)

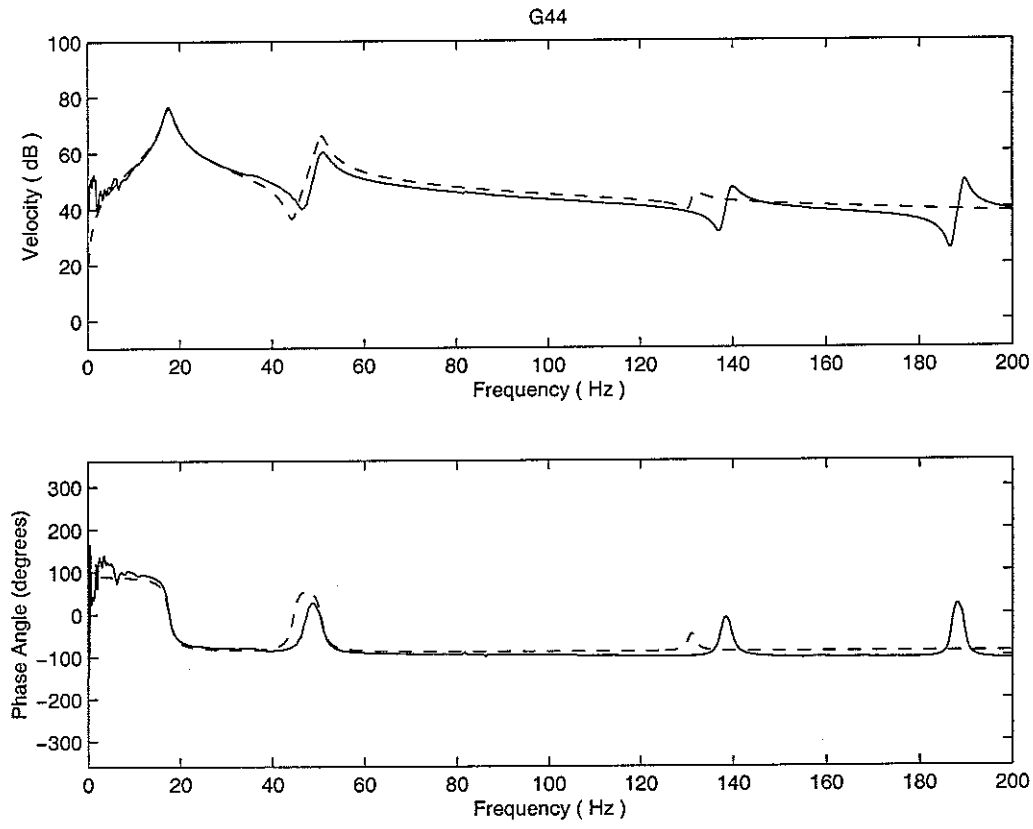

Figure 21 Comparison of plant response G_{44} from simulation (—) and experiment (—)

4.2 Stability assessment of the four-mount active vibration isolation system

Before any control strategy can be applied to an active vibration isolation system, it is very important to perform a stability analysis first. A general block as shown in Figure 22 can be used to represent the velocity feedback control of the four-mount flexible equipment structure, which is described by,

$$\mathbf{v}_e = \mathbf{G}(j\omega)\,\mathbf{f}_c \tag{29}$$

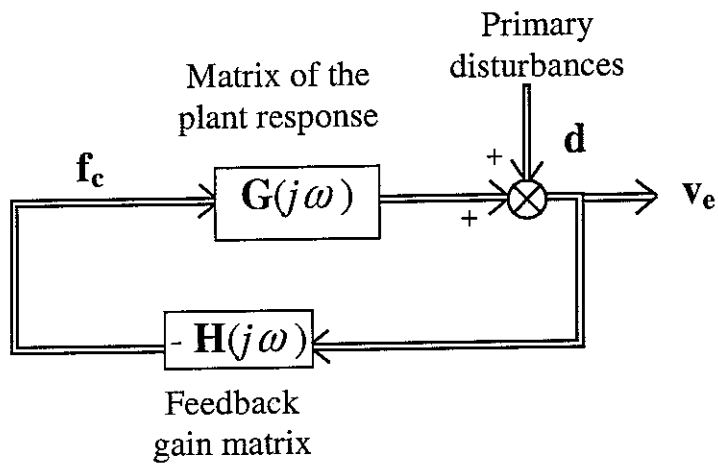

Figure 22 Equivalent electrical block diagram for a velocity feedback control system

Stability of a multichannel velocity feedback control system can be determined from the open loop frequency response function matrix, $\mathbf{L}(j\omega) = \mathbf{G}(j\omega)\mathbf{H}(j\omega)$, using the generalised Nyquist criterion [10], which states that the closed loop control system is stable provided none of the eigenvalue loci of $\mathbf{L}(j\omega)$ should encircle the $(-1, 0)$ point in the complex plane. When an identical constant control gain of H is used in each control channel, i.e, equi-decentralised control, the feedback gain matrix is simply given by,

$$\mathbf{H}(j\omega) = \mathbf{H} = \begin{bmatrix} H & 0 & 0 & 0 \\ 0 & H & 0 & 0 \\ 0 & 0 & H & 0 \\ 0 & 0 & 0 & H \end{bmatrix} \tag{30}$$

Therefore, $\mathbf{L}(j\omega)$ can be rewritten as

$$\mathbf{L}(j\omega) = H\,\mathbf{G}(j\omega) \tag{31}$$

The stability analysis of the four-mount flexible equipment structure is thus simplified to study the Nyquist plots of the eigenvalues of the plant response matrix $\mathbf{G}(j\omega)$. The four-mount active isolation system is stable if none of the eigenvalue loci of $\mathbf{G}(j\omega)$ encircles the (-1,0) point. If none of the eigenvalue loci crosses the negative real axis, the system is unconditional stable. For the special case of a single channel velocity feedback control using a constant gain at the ith mount position, the stability can be

assessed by examining the Nyquist plot of the corresponding diagonal velocity response term, $G_{ii}(j\omega)$.

The relationship between the plant response $\mathbf{G}(j\omega)$ and its true eigenvalue matrix $\mathbf{\Omega}(j\omega)$ can be expressed by,

$$\mathbf{G}(j\omega)\mathbf{Q}(j\omega) = \mathbf{Q}(j\omega)\mathbf{\Omega}(j\omega) \tag{32}$$

where, $\mathbf{\Omega}(j\omega)$ is a diagonal matrix of the true eigenvalues λ_i, and $\mathbf{Q}(j\omega)$ is the matrix of the true eigenvectors of the plant response matrix $\mathbf{G}(j\omega)$ at the frequency ω. Therefore, the true eigenvalues are calculated in this case by,

$$\mathbf{\Omega}(j\omega) = \mathbf{Q}^{-1}(j\omega)\mathbf{G}(j\omega)\mathbf{Q}(j\omega) \tag{33}$$

For the four-mount flexible equipment structure, the plant response matrix $\mathbf{G}(j\omega)$ of size (4x4) has four frequency dependent true eigenvalues. Stability of the multichannel velocity feedback control of the mounted flexible equipment structure can thus be assessed on the corresponding Nyquist plots of the true eigenvalue loci. There is an inherent numerical difficulty in obtaining the true eigenvalue loci in order within MALAB, and a detailed description of an algorithm to solve this difficulty is given in Appendix A.

It is often convenient to judge the stability of the multichannel control system in the transformed coordinates [6] to prevent such an inherent numerical difficulty in obtaining the true eigenvalues of the plant response matrix $\mathbf{G}(j\omega)$. As a result, another approach is also investigated in which the mode shapes of the eigenvectors are assumed and the corresponding eigenvalues are calculated. The assumed eigenvectors correspond to the mode shapes of the heave, pitch, roll and torsion vibration modes and are given by,

$$\hat{\mathbf{Q}} = \begin{bmatrix} 1 & 1 & 1 & 1 \\ 1 & -1 & 1 & -1 \\ 1 & -1 & -1 & 1 \\ 1 & 1 & -1 & -1 \end{bmatrix} \tag{34}$$

The assumed eigenvalues are then calculated from the following equation,

$$\hat{\mathbf{\Omega}}(j\omega) = \hat{\mathbf{Q}}^{-1}\mathbf{G}(j\omega)\hat{\mathbf{Q}} \tag{35}$$

Although the matrix $\hat{\mathbf{\Omega}}(j\omega)$ calculated from the assumed mode approach is not completely diagonal in this case, the off-diagonal terms are rather small compared with the diagonal ones as demonstrated in Appendix B. Therefore, the use of a diagonal approximation to $\hat{\mathbf{\Omega}}(j\omega)$ to assess the stability of the multichannel feedback control system of the mounted flexible equipment structure appears to be a reasonable one.

Prior to implementing the four-channel control system in this research, it is useful to fully understand the behaviour of a single channel controller. When the mounted flexible equipment structure on a rigid base is excited by one of the four actuators, a single channel control can be implemented by feeding back the velocity at another mount position to the actuator there. Alternatively, single channel control can also be implemented in the same position using a summation box, which is specially designed to superpose the primary excitation and the feedback velocity control signal together. As pointed out earlier, stability of a single channel control system can be assessed by evaluating the Nyquist plot of the corresponding plant response term, $G_{ii}(j\omega)$.

Therefore, Nyquist plots of the diagonal terms in the plant response matrix, $G(j\omega)$, from both simulation and experiment are compared in Figure 23 to Figure 26.

For the single channel velocity feedback control, the mounted flexible equipment system exhibits very good stability properties from both simulation and experiment, since almost the whole Nyquist plot of the corresponding diagonal plant response term, $G_{ii}(j\omega)$, lies in the right real half plane. The big loop represents the rigid body modes, which are appeared in the Bode plots of plant responses in the previous section. The flexible modes of the mounted flexible equipment structure in the frequency range (0~200 Hz) is characterised by several small loops, whose radius decreases as the passive mounts become more efficient with the increasing frequency. The Nyquist plots of the diagonal plant response terms from simulation look very similar with each other, because the flexible equipment structure is symmetric and four identical mounts and actuators are assumed. Perfect operation of the electric equipment in the control loop is also assumed in the simulation. As a result, the Nyquist plots of the diagonal plant response terms from simulation are totally in the positive real half plane. In the experiment, the mounts are not exactly the same, which makes the Nyquist plots of the diagonal terms of the measured plant response from experiment a small discrepancy from one to another. Most of the Nyquist plots from experiment lies in the stable right half plane, except for a small region at very low frequencies suffered from the low sensitivities of the actuators and sensors. At low frequencies, the lowpass filter and integrator inside the charge amplifier may cause additional phase shift, which tends to be $\pi/2$. This is not expected to cause instability, but will give rise to vibration amplification at very low frequencies. The phase shift has to be added to the phase shift of the power amplifier at low frequencies. Theoretically, a phase advance of a little over 90° at low frequencies is sufficient for the Nyquist plot to cross the negative real axis. Thus, the phase shifts at very low frequencies are the causes of the small responses noticed on the upper left side of the origin in the Nyquist plots of the diagonal plant response terms from experiment. These effects are not large and are always associated with small amplitude vibrations as a result of passive mounts. However, some vibration amplification in the corresponding frequency band may be expected, which may then induce instability if the feedback control gain is very large.

It is also noted that, the actuators are not strictly collocated with the sensors for the installation of the mounted flexible equipment structure as shown in Figure 5, due to the flexibility of the isolated equipment. In practice, the diagonal plant elements are all almost entirely positive real above about 10 Hz, indicating that there is not a significantly different vibration response between the experimental actuators and sensor. Some additional phase shift is observed for at about 85 Hz in G_{33} as shown in Figure 16, but the amplitude is small at that frequency.

Stability of the multichannel control system of the mounted flexible equipment structure on a rigid base is also assessed using the true eigenvalue method as well as an assumed mode shape method described above. After the plant response matrix of the mounted flexible equipment structure is constructed both theoretically and experimentally, the amplitude and corresponding phase angle of the true eigenvalues are obtained as shown from Figure 27 to Figure 30. Again, the theoretical results match fairly well with those from experiment, which further validates the theoretical model developed for the four-mount flexible equipment structure. It is noted a special algorithm is designed to distinguish the true eigenvalues and their associated eigenvectors at different frequencies. Figure 31 to Figure 34 show the Nyquist plots of

the true eigenvalue loci of the mounted flexible equipment structure from simulation (dashed line) and experiment (solid line). It is noticed that each of the plots from both simulation and experiment only has one main loop for the configuration of the four-mount equipment structure, because each true eigenvalue is proportional to the amplitude of a certain mode. By assuming the appropriate mode shapes as described in equation (34), the stability of multichannel velocity feedback control of the mounted flexible equipment structure is further assessed as shown in Figure 35 to Figure 42. The Nyquist plots from the assumed mode shape method agree very well with those of the true eigenvalue loci, which shows that it is reasonable to assess the stability of the mounted equipment structure by the assumed mode shape method. Due to the imperfect operation of the electric equipment and low coherence suffered at low frequencies, the corresponding plots from experiment slightly cross the imaginary axis at very low frequencies, although its effect is very small. Smooth curves at low frequencies are observed in the simulation since perfect operation of the electric equipment is assumed. The loci predicted from the simulation lies wholly within the stable right half plane. However, for the experimental results there are relatively small loops in the middle of the frequency range as shown in the lower left half plane of the experimental Nyquist plots from both true eigenvalue method and assumed mode shape method. In general, they are associated with small amplitude vibration level as a result of increasing efficiency of the passive mount with the increasing frequency. The difference between the theory and experiment originates from the fact that the feedback control of the mounted equipment structure implemented in the experiment is not a collocated control strictly as pointed out previously. In the simulation, the actuator is simplified as a rigid mass point where the velocity is measured and fed back, whereas in the experiment the shape configuration of the actuator is comparable to that of the equipment. The distance between the actuator and the sensor in the experiment affects the measurement accuracy for a case of flexible equipment, which, probably, is the origin of the low coherence observed in the middle of the frequency band in the measured plant responses. As the velocity feedback control gain increases, the radii of the small loops in the left half plane of the Nyquist plots of the true eigenvalue loci will become greater and greater. Eventually the multichannel control system of the mounted equipment structure goes unstable when the true eigenvalue loci encircles the (-1,0) point for a large gain. In summary, as most of the true eigenvalue loci lies in the stable right half plane, good stable properties of the multichannel control system are expected for the four-mount equipment structure. The main threats to the control stability come from the phase shifts in the electronics of the control loop at low frequencies as similarly pointed out for the single channel control case and non-collocated installation of the sensor and actuator.

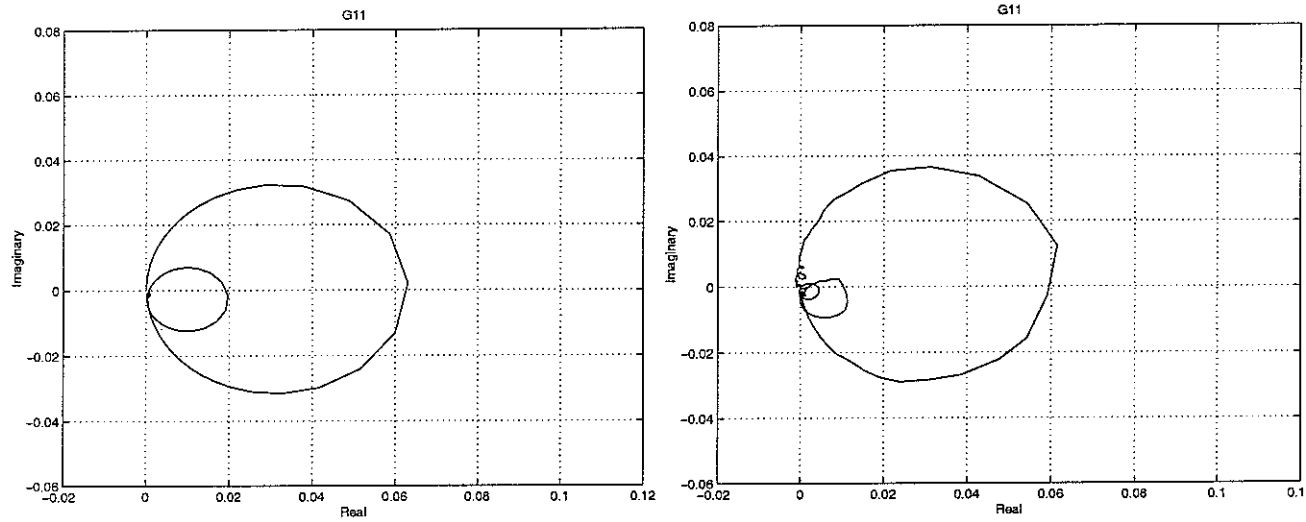

(a) Prediction (b) experiment

Figure 23 Nyquist plot of the plant response G_{11} for single channel control at node 1

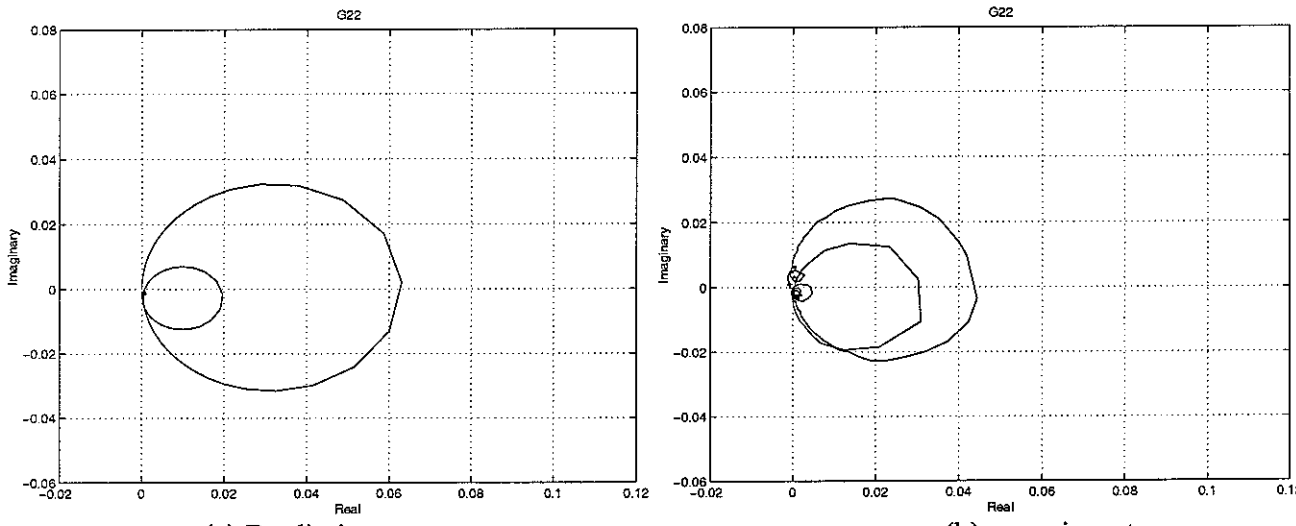

(a) Prediction (b) experiment

Figure 24 Nyquist plot of the plant response G_{22} for single channel control at node 2

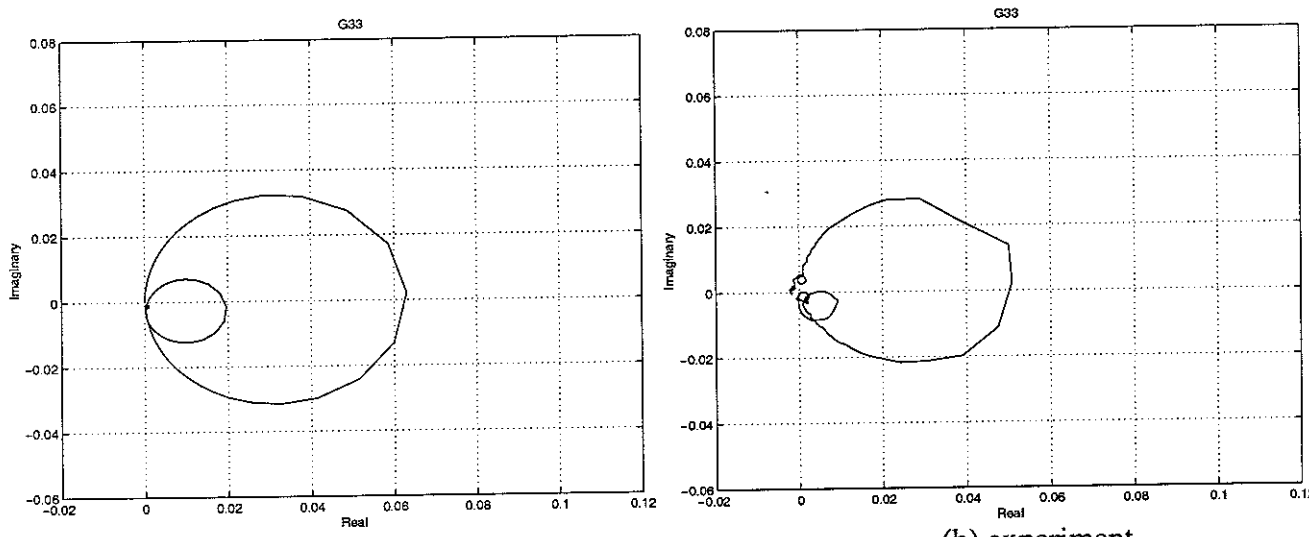

(a) Prediction (b) experiment

Figure 25 Nyquist plot of the plant response G_{33} for single channel control at node 3

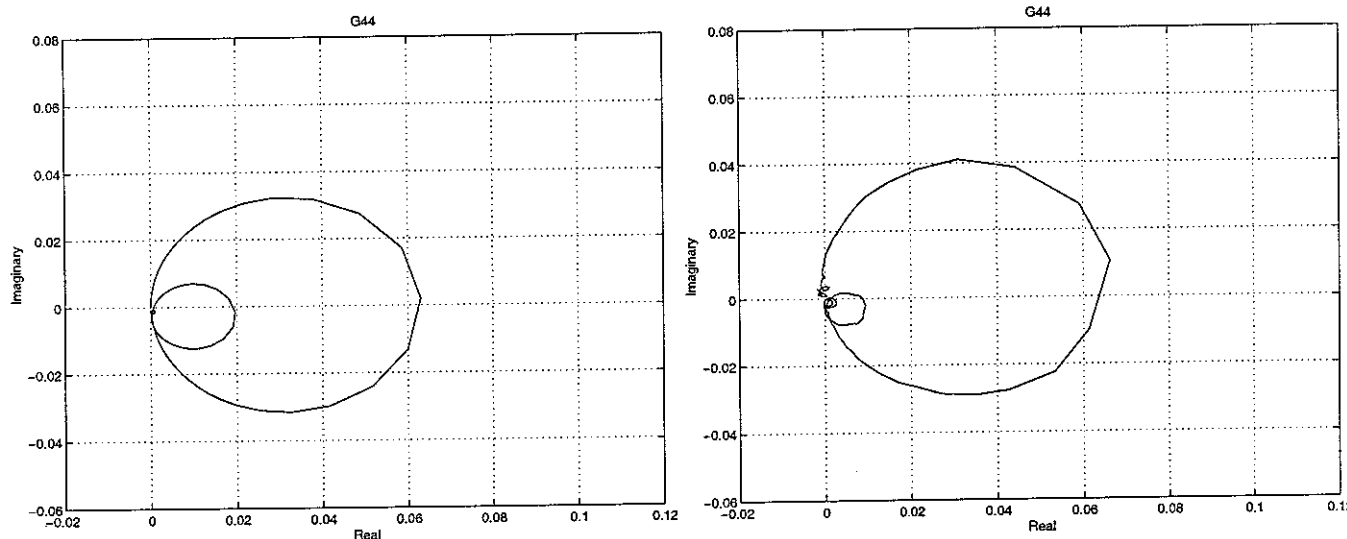

(a) Prediction (b) experiment

Figure 26 Nyquist plot of the plant response G_{44} for single channel control at node 4

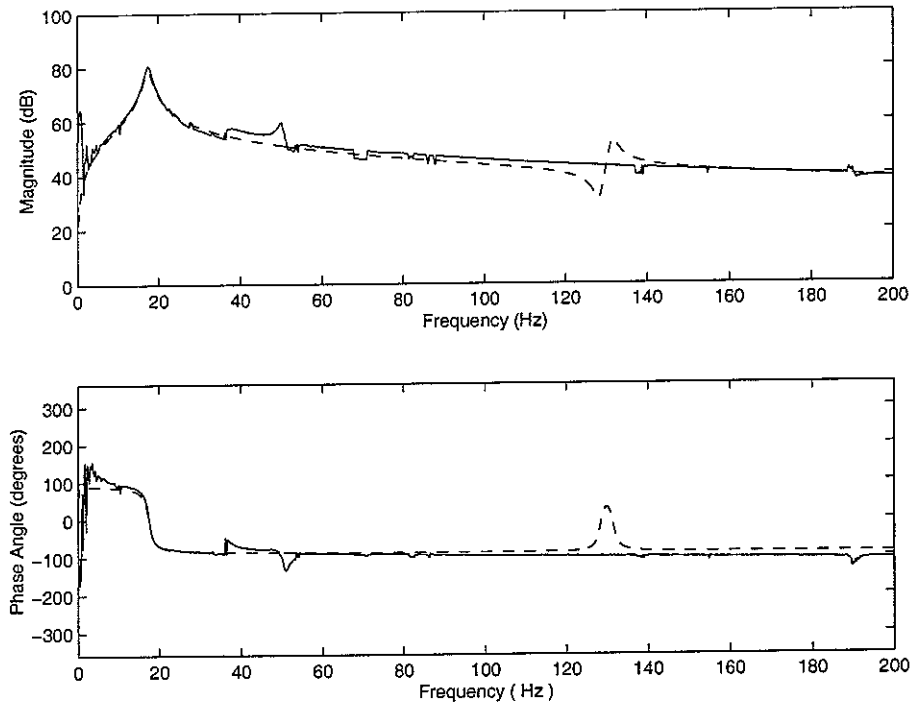

Figure 27 Bode plot of the true eigenvalue λ_1 of the mounted equipment structure (simulation: dashed line -- , experiment: solid line —)

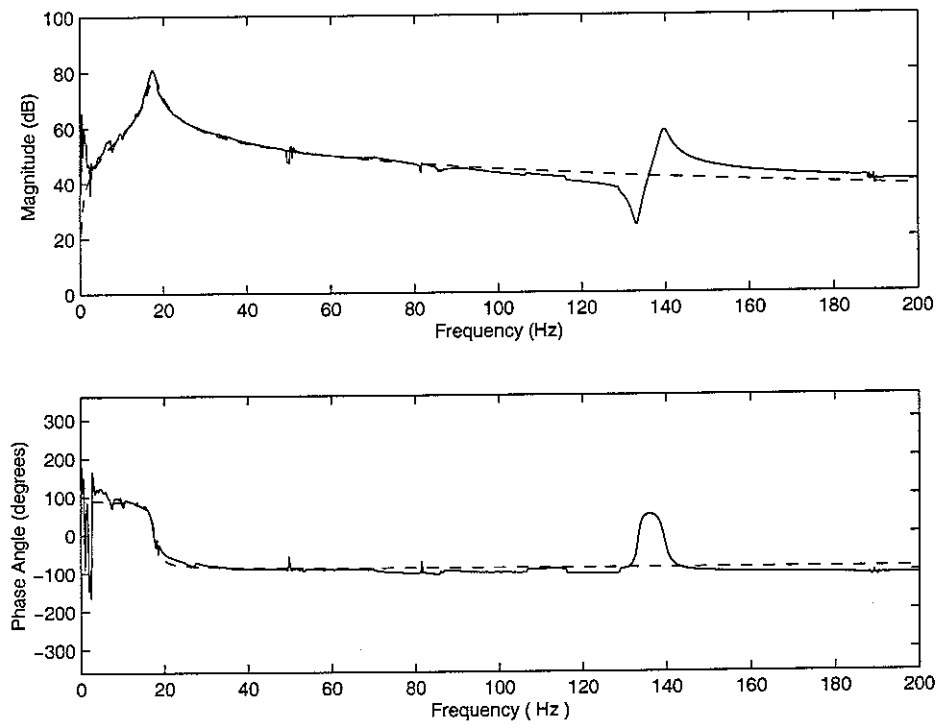

Figure 28 Bode plot of the true eigenvalue λ_2 of the mounted equipment structure (simulation: dashed line -- , experiment: solid line —)

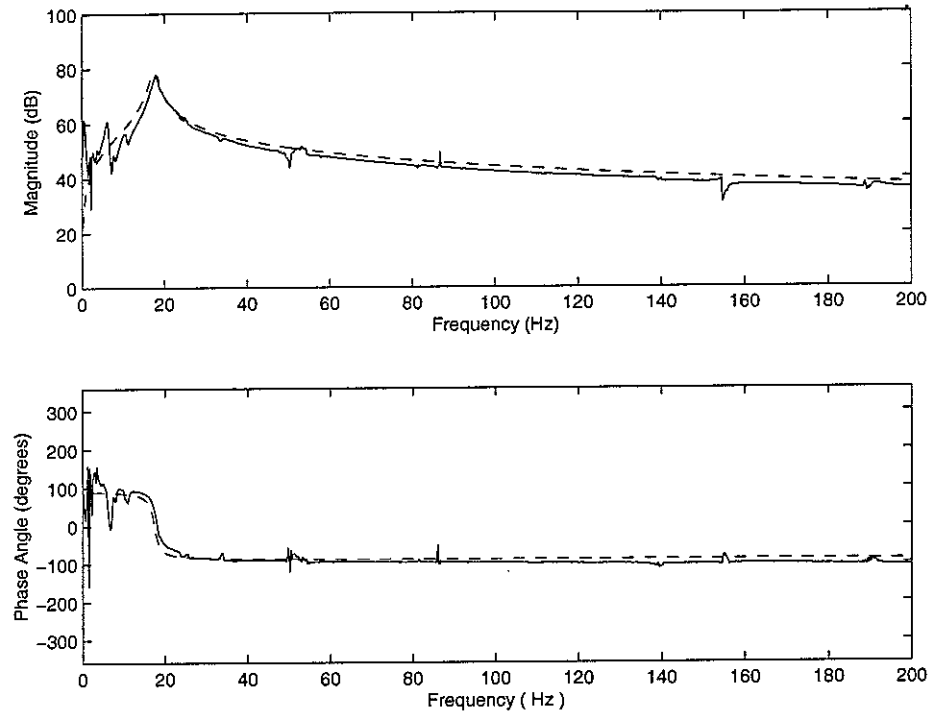

Figure 29 Bode plot of the true eigenvalue λ_3 of the mounted equipment structure (simulation: dashed line -- , experiment: solid line —)

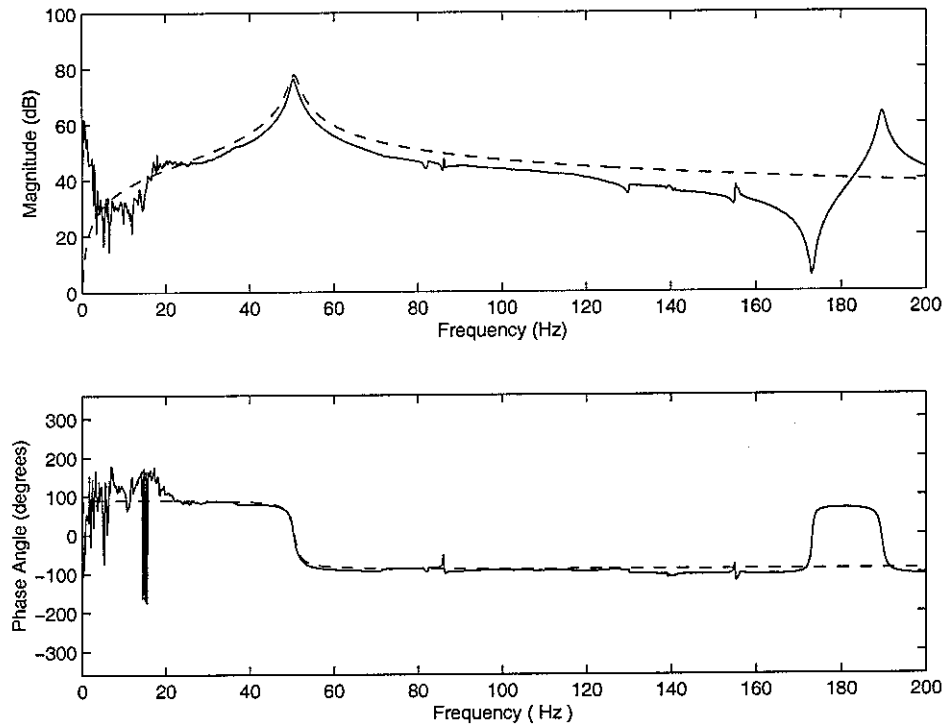

Figure 30 Bode plot of the true eigenvalue λ_4 of the mounted equipment structure (simulation: dashed line -- , experiment: solid line —)

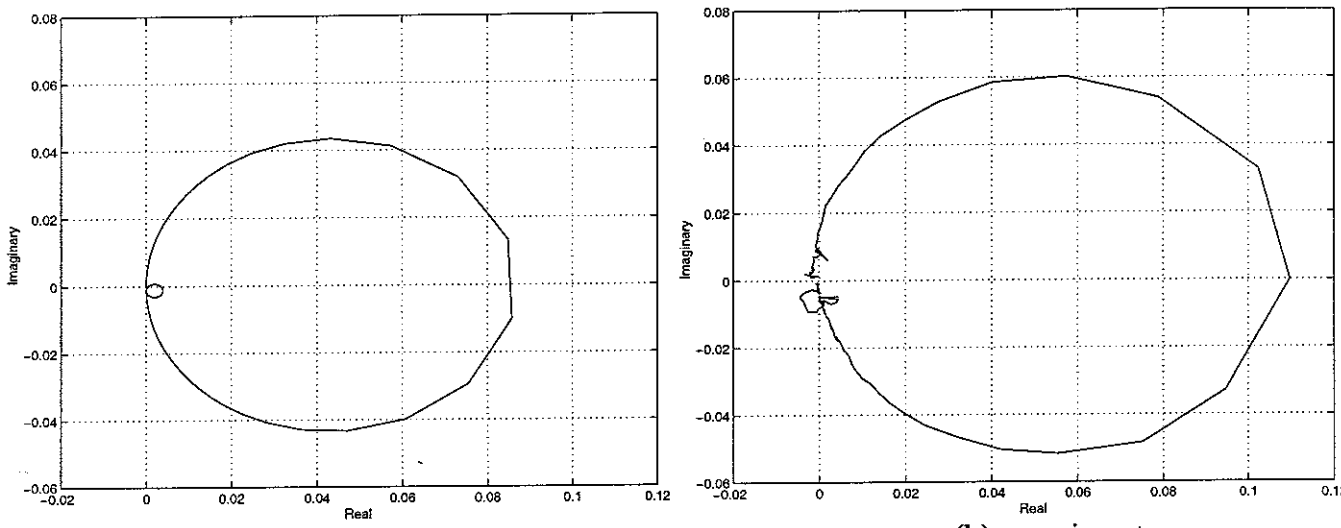

(a) Prediction (b) experiment

Figure 31 Nyquist representation of the true eigenvalue λ_1

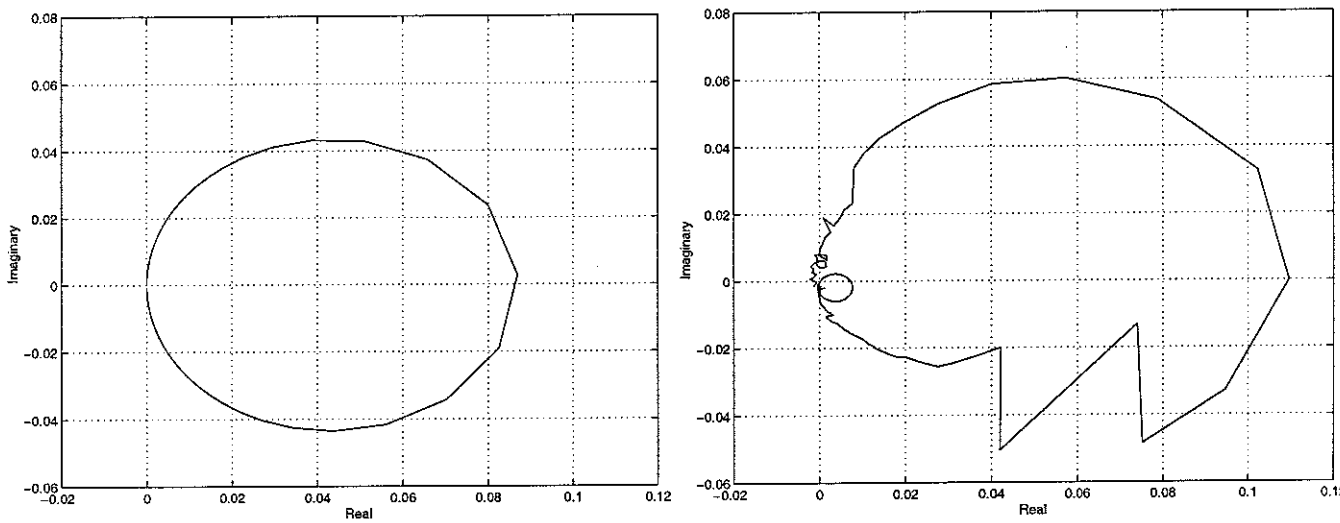

(a) Prediction (b) experiment

Figure 32 Nyquist representation of the true eigenvalue λ_2

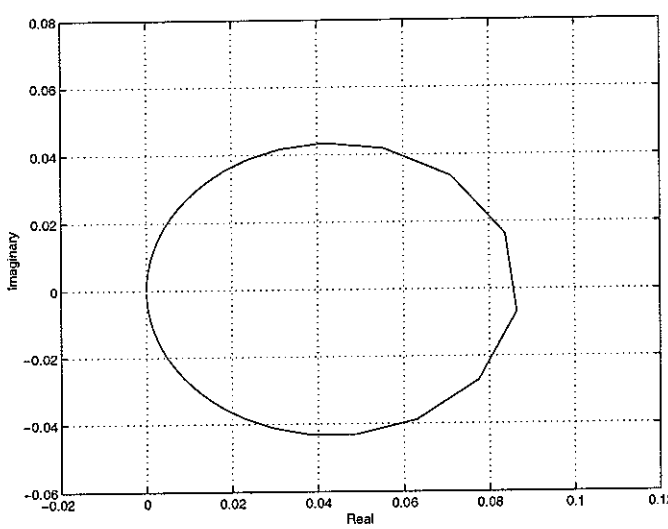

(a) Prediction

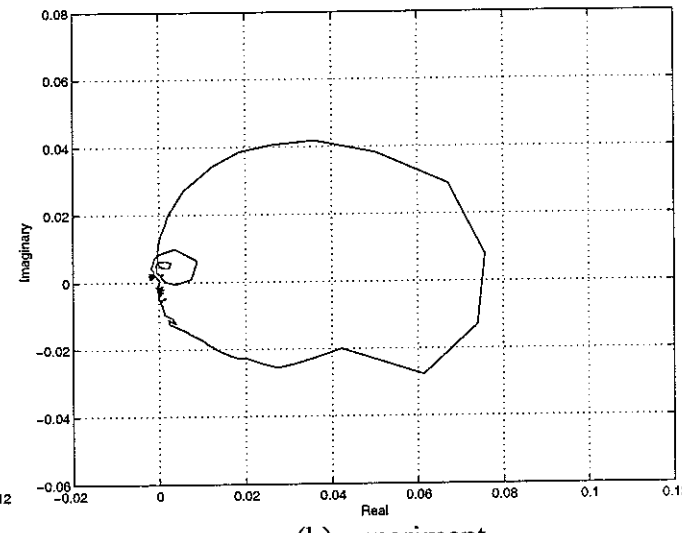

(b) experiment

Figure 33 Nyquist representation of the true eigenvalue λ_3

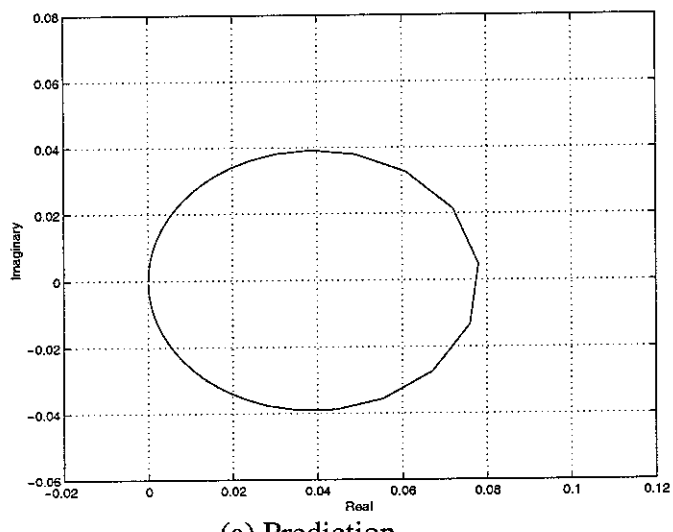

(a) Prediction

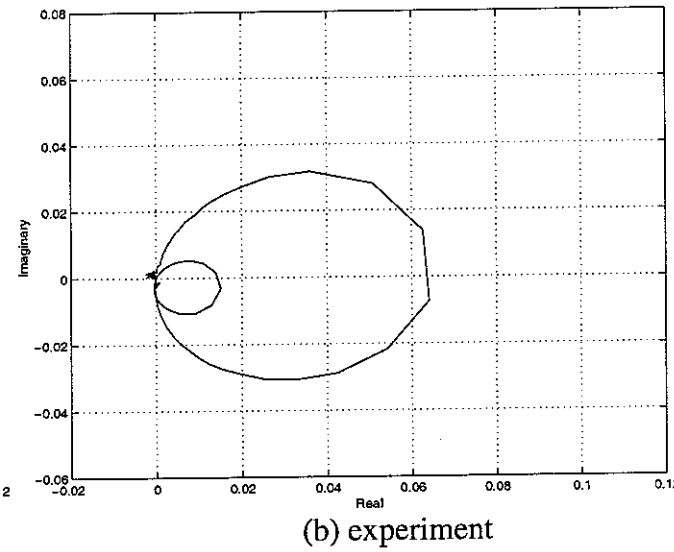

(b) experiment

Figure 34 Nyquist representation of the true eigenvalue λ_4

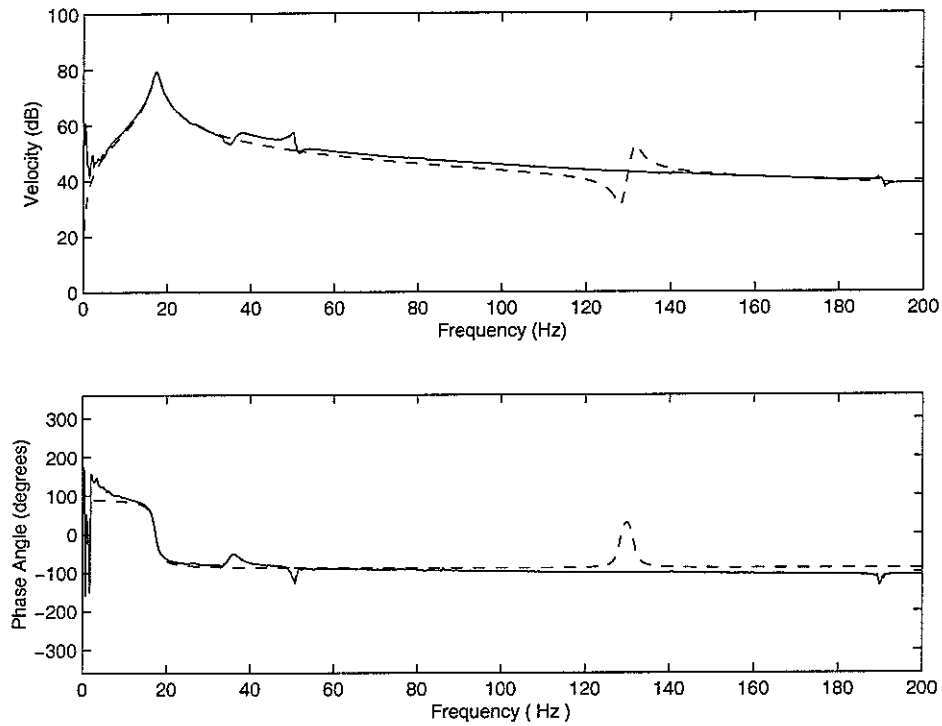

Figure 35 Bode plot of the assumed eigenvalue associated with the heave mode (simulation: dashed line -- , experiment: solid line —)

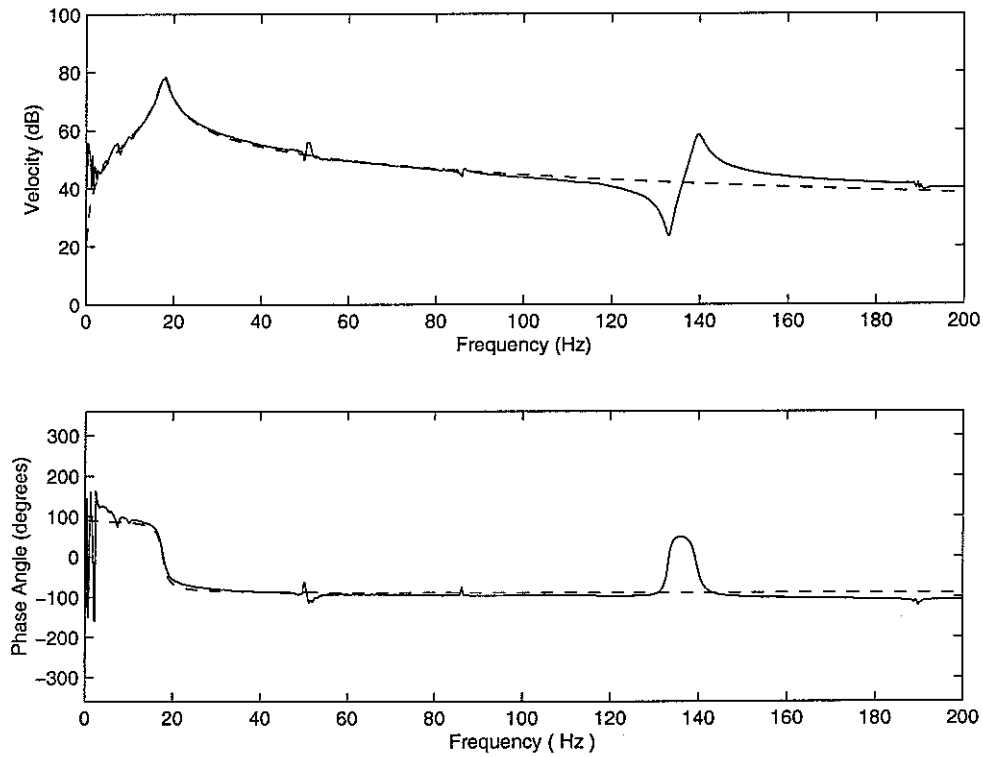

Figure 36 Bode plot of the assumed eigenvalue associated with the pitch mode (simulation: dashed line -- , experiment: solid line —)

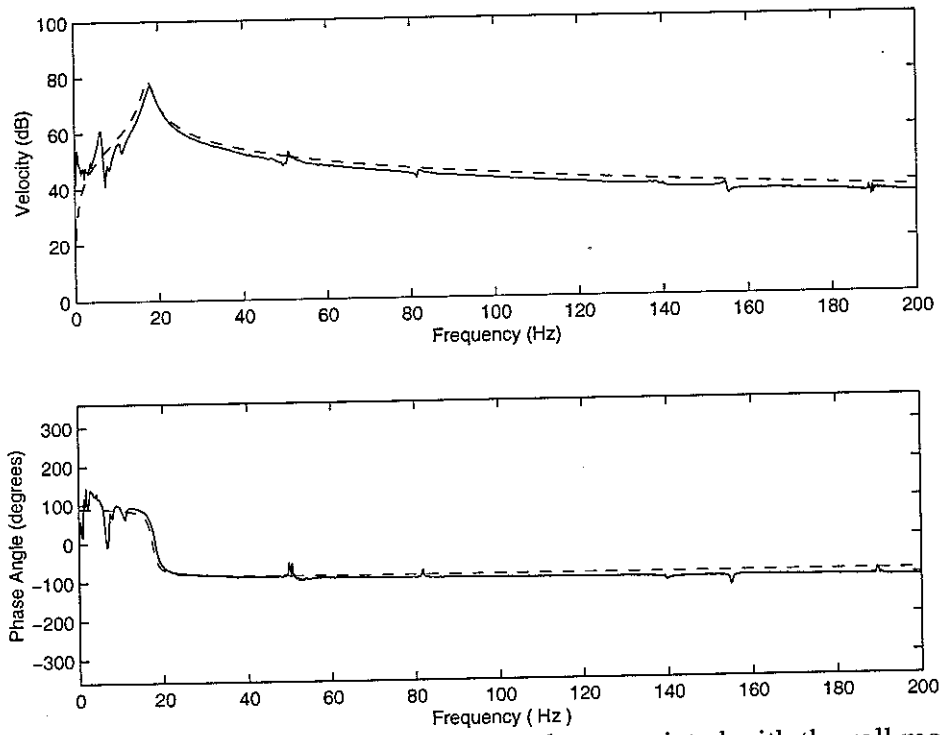

Figure 37 Bode plot of the assumed eigenvalue associated with the roll mode (simulation: dashed line -- , experiment: solid line —)

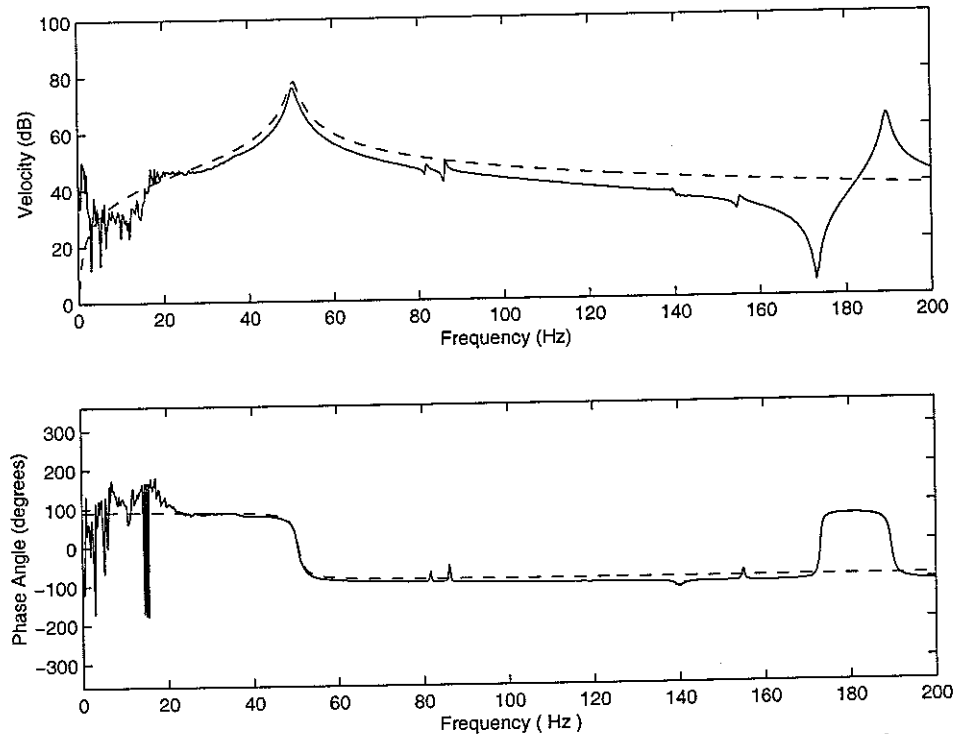

Figure 38 Bode plot of the assumed eigenvalue associated with the torsion mode (simulation: dashed line -- , experiment: solid line —)

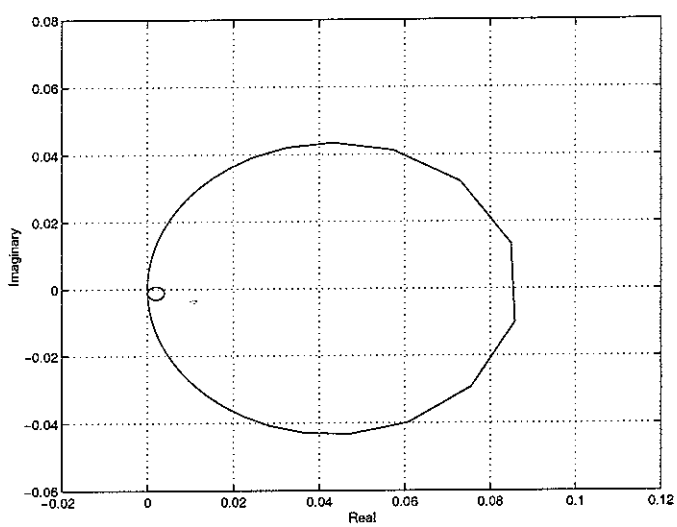

(a) Prediction

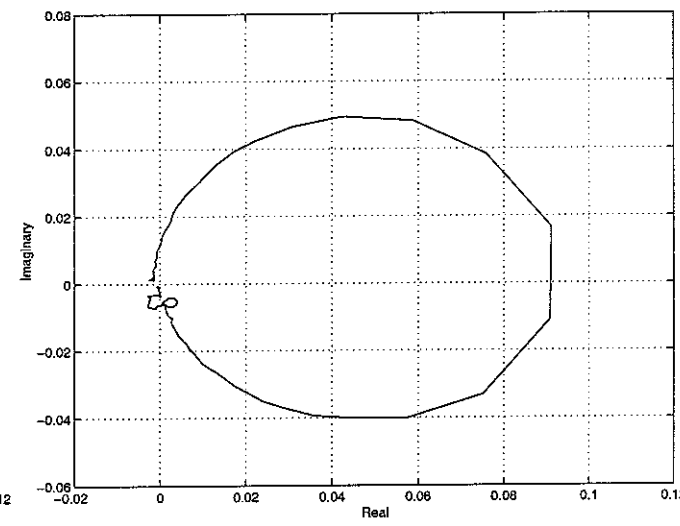

(b) experiment

Figure 39 Nyquist representation of the assumed eigenvalue loci associated with the heave motion

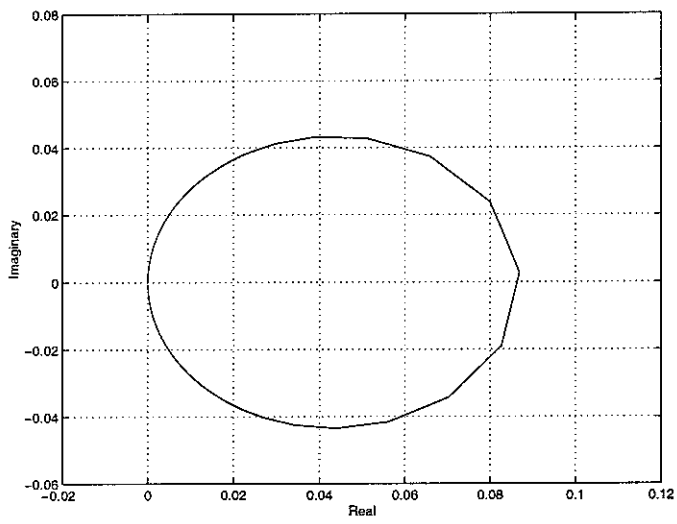

(a) Prediction

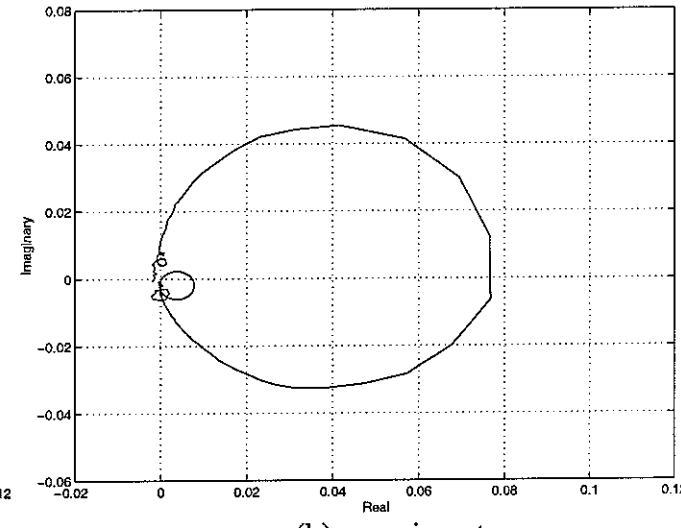

(b) experiment

Figure 40 Nyquist representation of the assumed eigenvalue loci associated with the pitch motion

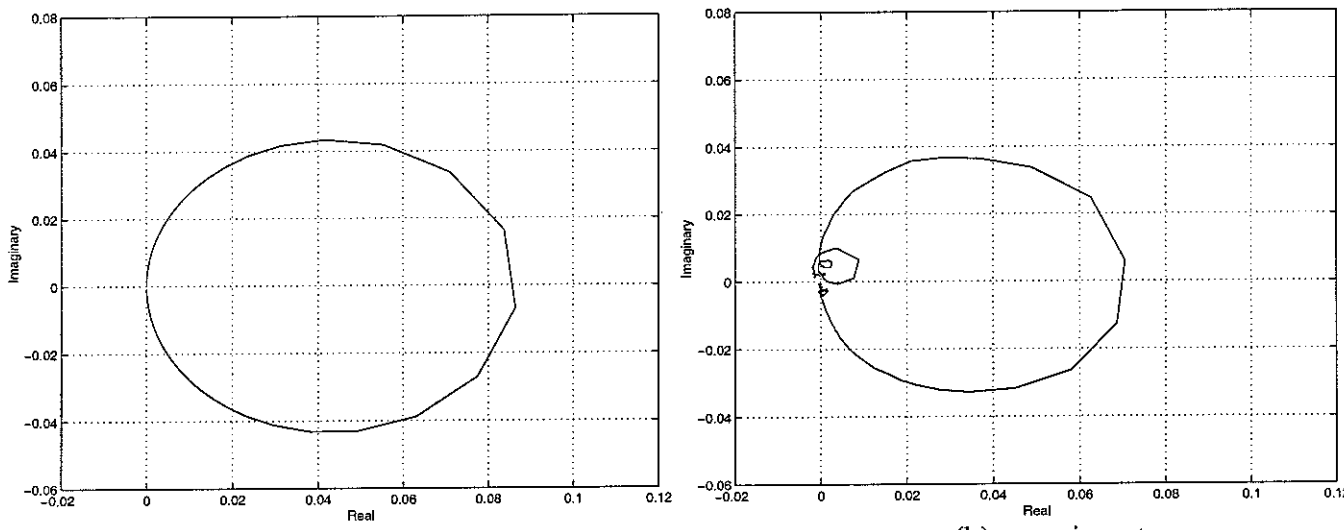

(a) Prediction (b) experiment

Figure 41 Nyquist representation of the assumed eigenvalue loci associated with the roll motion

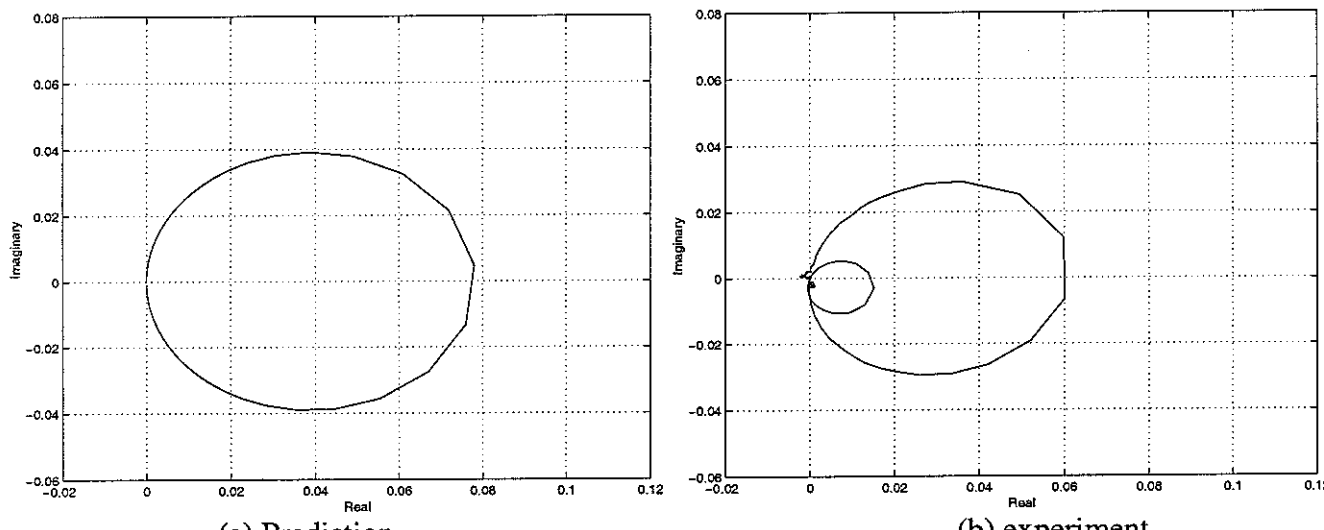

(a) Prediction (b) experiment

Figure 42 Nyquist representation of the assumed eigenvalue loci associated with the torsion motion

4.3 Control performance analysis and discussion

4.3.1 Single-channel control of the mounted equipment structure on a rigid base

In this section, various single-input-single-output (SISO) control systems are implemented for the four-mount flexible equipment structure. The acceleration signal obtained at the control location is integrated through a charge amplifier. The resulting velocity signal is amplified by a constant control gain using a power amplifier and fed back to the control shaker. Thus, activated by a velocity signal, the control shaker generates a control force at the corresponding control point. As mentioned in previous section, there are two possible ways to implement the single channel feedback control in the mounted flexible equipment structure as shown in Figure 43 and Figure 44. Due to a limitation in extending the first configuration of feedback control to the following four-channel active vibration control of the mounted flexible equipment structure on a rigid base, main efforts are placed on the implementation using the second method.

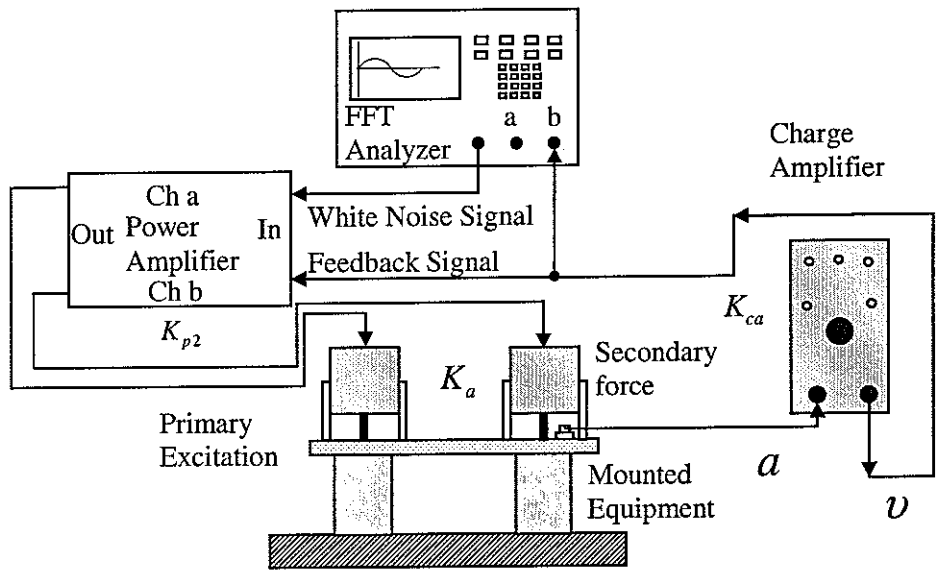

Figure 43. The first configuration of a single channel control system

Using the first configuration, the SISO velocity feedback control is implemented at one of the four actuators when the mounted flexible equipment structure is excited by another actuator. Considering the symmetry of the mounted equipment structure, typical velocity responses at the control position 2, 3 and 4 when the mounted flexible equipment structure is excited at node 1, are shown in Figure 45 to Figure 47 for simplicity. The velocity responses before control (dashed line) and after control (solid line) are compared to investigate the control performance. In the meantime, simulations have been performed for a comparison with the experiments in order to interpret the experimental results with a theoretical background. It is noted that the

physical control gain, (gain relating the secondary force to the control velocity in unit of Ns/m), used in the simulation must account for the different gains used in the feedback loop, which comprises the charge amplifier gain K_{ca}, the power amplifier gain K_{p2}, the sensitivity of the actuator K_a (equal to 0.91 Nv^{-1}). The sensitivity of the accelerometer is directly taken into account by the charge amplifier. Therefore, using the first single channel control configuration as shown in Figure 43, the physical control gain is expressed by,

$$H = K_a K_{p2} K_{ca} \tag{36}$$

When setting the sensor sensitivity properly, the integrator inside the charge amplifier is able to output 100 mv per ms^{-1} input. Multiple control gains are applied via the power amplifier in order to have a systematical control performance demonstration. Those values are measured and equal to 12.5, 24 and 40. Therefore, physical control gain values of 1.14, 2.18 and 3.64 Ns/m are calculated from equation (36) and modelled in the simulation for comparison purpose. The calculations are meaningful since the response of the actuator and sensors are reasonably independent of the frequency. Higher physical control gains can be applied, of up to 36.4 Ns/m for this configuration of single channel control in the experiment before instability occurs, which corresponds to a gain of 40 from the power amplifier and a gain of 1000 mv per ms^{-1} from the charge amplifier. Therefore, the gain margin of this configuration of SISO control system is approximately 20 dB for the maximum gain used in the comparison between simulation and experiment. Even for small physical gains as demonstrated from Figure 45 to Figure 47, the velocity feedback controller does effectively reduce the vibration levels at each resonance frequency as listed in Table 3 both from simulation and experiment. It is noted that, different degrees of attenuation of vibration amplitude are found at different control position in the experiment, which can be traced back to the differences in the four mounts. On the contrary, the attenuation predicted from simulations is much similar to each other as four identical mounts are assumed. Even for the single channel velocity feedback control implemented at node 2 as shown in Figure 45, up to 15 dB reductions in vibration level are obtained. Greater reductions in vibration level are obtained if the SISO control is implemented at node 3 or node 4. In particular, approximate up to 25 dB (30 dB) attenuation is observed at node 3 (node 4). Generally, the effect of the velocity feedback control gradually decreases with increasing frequency, since the control force is proportional to the control velocity which is strongly attenuated by the passive mount at high frequencies. In the experiment, the vibration level at very low frequencies is actually amplified due to the phase shift as discussed in the previous section. However, these amplifications are very small and are always associated with small amplitude of vibration. Similar control performances have been observed when the mounted flexible equipment structure is excited at nodes 2, 3 and 4, which are omitted here for brevity.

With the help of a specially designed summation box, a second configuration of the SISO control system is implemented as shown in Figure 44. The second configuration of SISO control system is different from the first configuration in that the control shakers act as both primary excitation sources and control actuators. The summation box superposes the primary excitation signal from the FFT analyzer and the velocity control signal from the sensor, which is placed before the power amplifier since the electromagnetic shakers need to be connected to a low output impedance device to be driven efficiently. Since the white noise signal generated by the FFT analyzer must be

amplified for the same reason, the control loop passes through both channels of the power amplifier consecutively. In this case, the physical control gain is expressed by,

$$H = K_a K_{p1} \alpha K_{p2} K_{ca} \tag{37}$$

where, K_{p1} and K_{p2} are the gains of the two-channel power amplifier respectively, α is the coefficient of the summation box, i.e., $\alpha = \sum output / (\sum input)$. In the experiment, α has been adjusted to a value of 1 for simplicity. K_{ca} and K_a represent the charge amplifier gain and the efficiency of the actuator respectively.

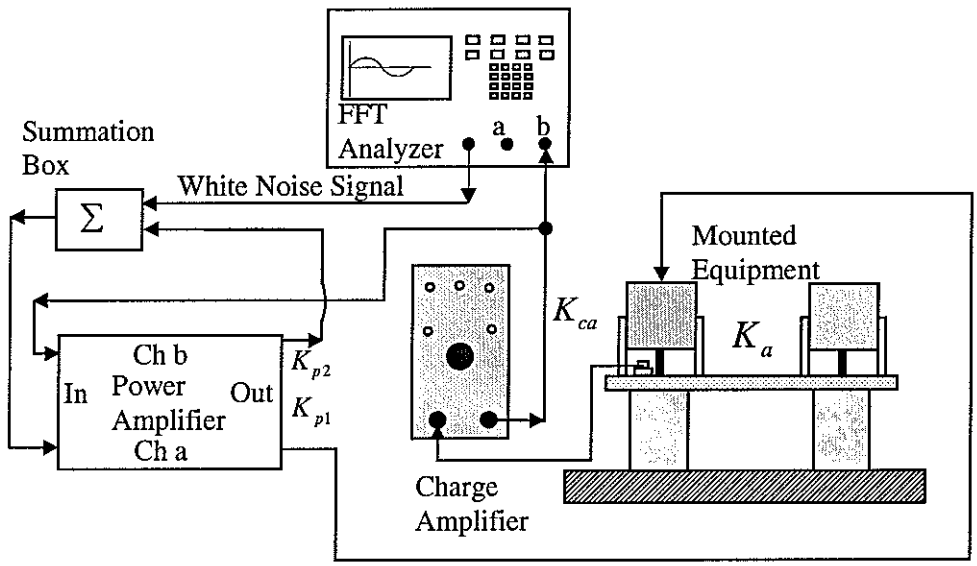

Figure 44 The second configuration of a single channel control system

Excited by the same white noise signal as used in the first configuration, the SISO control system as shown in Figure 44 has been investigated. In this case, the power amplifier and the charge amplifier have the same settings as those in the first implementation. It is noted that, K_{p1} is measured and equal to 1.6. Similar multiple control gains have been applied via the power amplifier as implemented in the first configuration. However, the overall physical control gains of the second configuration of the SISO velocity feedback control system are calculated from equation (37). The physical control gains are 1.82, 3.49 and 5.82, which are modelled in the simulation for a comparison with experiment. Typical velocity responses at each node when the system is excited by the shaker at node 1, are demonstrated in Figure 48 to Figure 51 both theoretically and experimentally. Again, the velocity responses before control are displayed in dashed lines and after control in solid lines respectively. Higher physical control gains can be applied by up to 58.2 Ns/m for the second configuration of SISO control system in the experiment before instability occurs, which corresponds to a gain of 40 from the power amplifier and a gain of 1000 mv per ms^{-1} from the charge amplifier. Therefore, gain margin of the second configuration of SISO control system is approximately 20 dB for the maximum gain used in the comparison between simulation and experiment. The predicted velocity responses before control and after control match well with those obtained from experiments. As demonstrated in Figure 48 to Figure 51, the vibration levels at each node are overall reduced at all the

resonance frequencies in the frequency band of analysis both theoretically and experimentally. In particular, approximately up to 30 dB attenuation is obtained from experiment at the rigid body frequencies around 17 Hz, up to 20 dB attenuation at the first flexible frequency of 50.6 Hz. Less than 10 dB attenuation at the second and third flexible frequencies are observed from experiment. The above observations hold true at the direct controlled node as well as in other nodes without direct control. Greater reductions in vibration level can be expected for a greater physical control gain within the gain margin reported previously. Again, small amplifications of vibration amplitude at very low frequencies are generally observed in the experiment due to the phase shifts in the electric equipment. Although their effects are generally small and always associated with small amplitudes of vibration level, they are the main threats to the stability if a large control gain is applied in the SISO control system. Similar vibration reductions have been obtained when the SISO control is implemented at nodes 2, 3 and 4, which are omitted in this report for brevity.

In summary, two configurations of SISO velocity feedback control of the four-mount flexible equipment structure have been investigated both theoretically and experimentally in this section. Considerable reductions in the vibration level at direct controlled positions as well as indirect controlled positions have been achieved at all resonance frequencies both in the experiments and simulations. In particular, up to 30 dB attenuation can be obtained in the experiments at the rigid body resonance frequencies around 17 Hz, up to 20 dB attenuation at the first flexible frequency of 50.6 Hz, if adopting the second configuration of SISO control system. Similar but a little lesser attenuation has been observed in the experiments using the first SISO control configuration. As the passive mount performance increases, the control effect decreases. As a result, less than 10 dB reductions in the vibration amplitude are achieved at the resonance frequencies of the second and third flexible modes. It is important to note that, the phase shifts due to the imperfect operation of the electrical equipment in the experiments, cause small amplifications of vibration level at very low frequencies (less than 5 Hz) in both configurations of the SISO velocity control system. These phase shifts are the main threats to the control stability in the experiments.

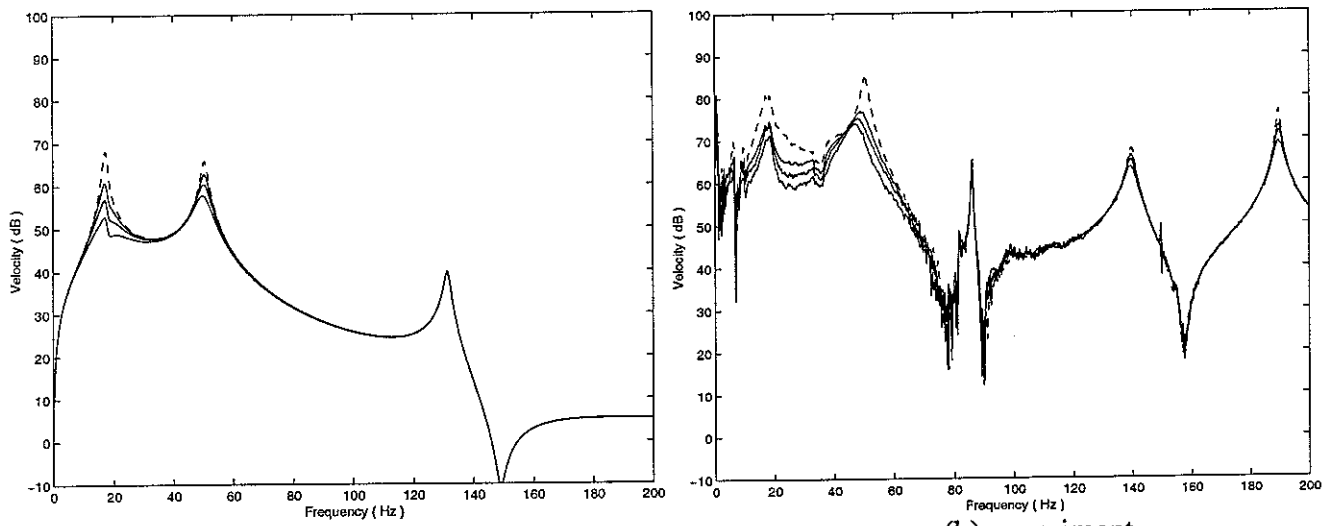

(a) Prediction (b) experiment

Figure 45 Velocity response at node 2 with single channel control implemented at node 2 when excited at node 1

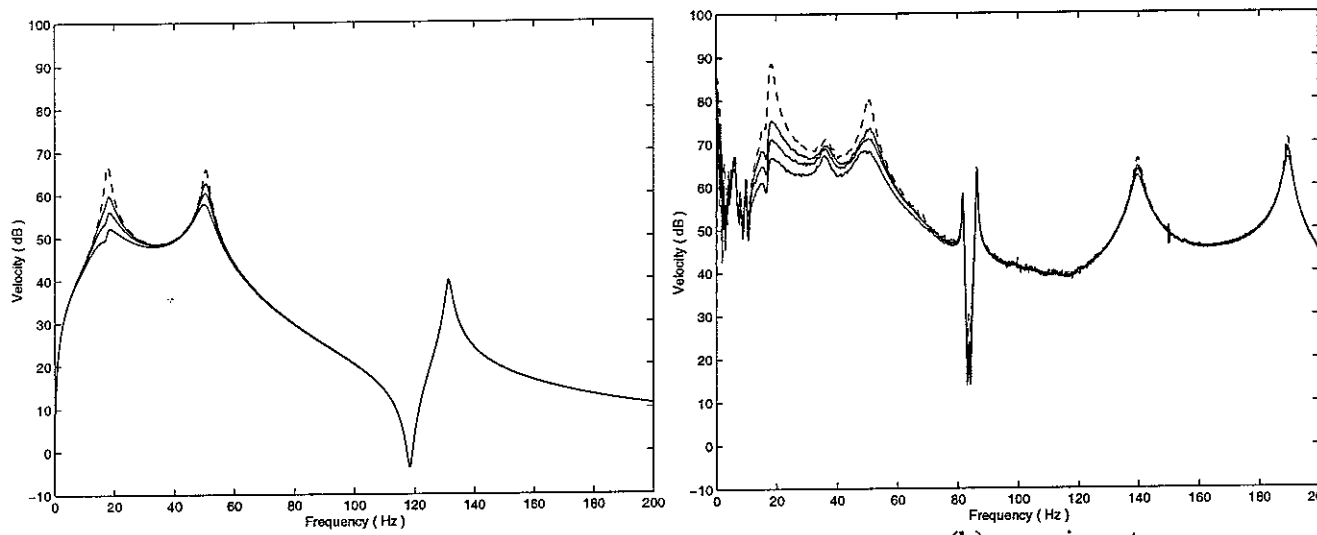

(a) Prediction (b) experiment

Figure 46 Velocity response at node 3 with single channel control implemented at node 3 when excited at node 1

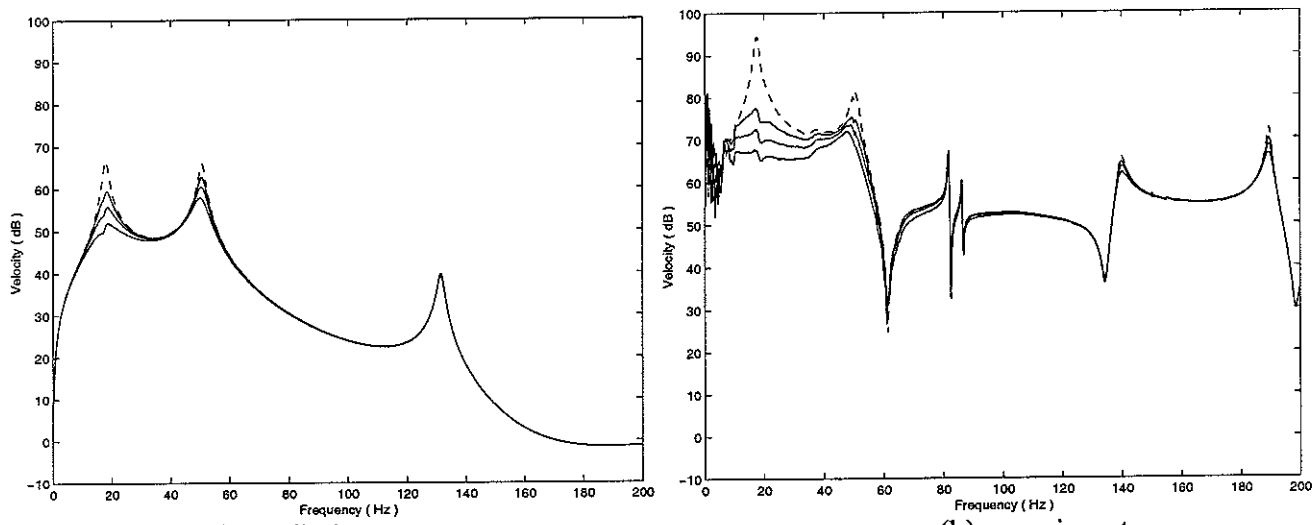

(a) Prediction (b) experiment

Figure 47 Velocity response at node 4 with single channel control implemented at node 4 when excited at node 1

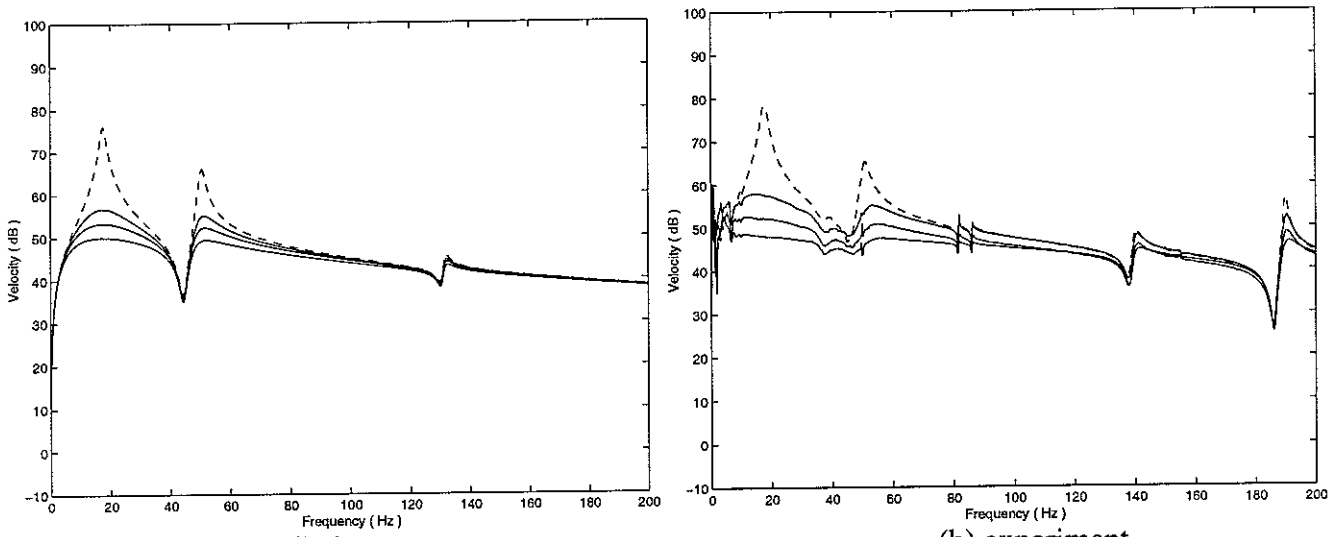

(a) Prediction (b) experiment

Figure 48 Velocity response at node 1 with single channel control implemented at node 1 when excited at node 1

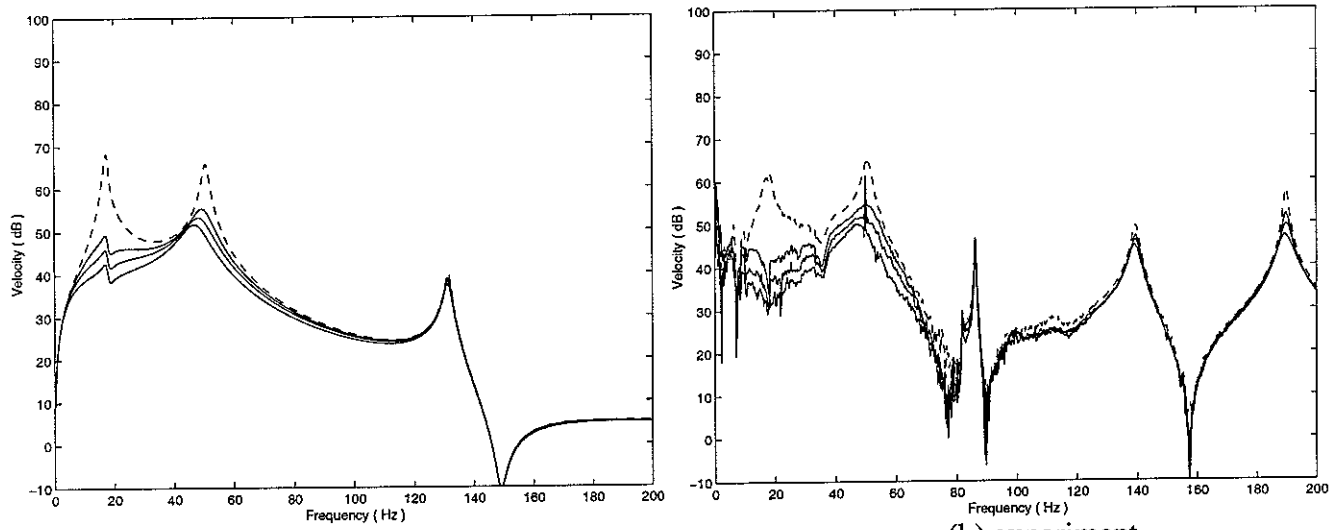

(a) Prediction (b) experiment

Figure 49 Velocity response at node 2 with single channel control implemented at node 1 when excited at node 1

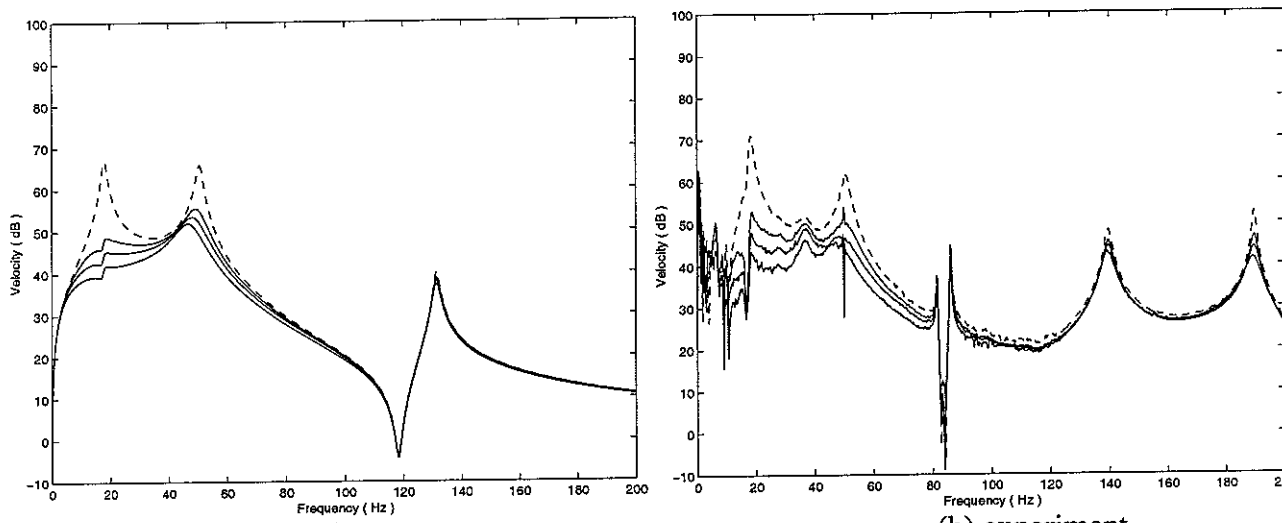

(a) Prediction (b) experiment

Figure 50 Velocity response at node 3 with single channel control implemented at node 1 when excited at node 1

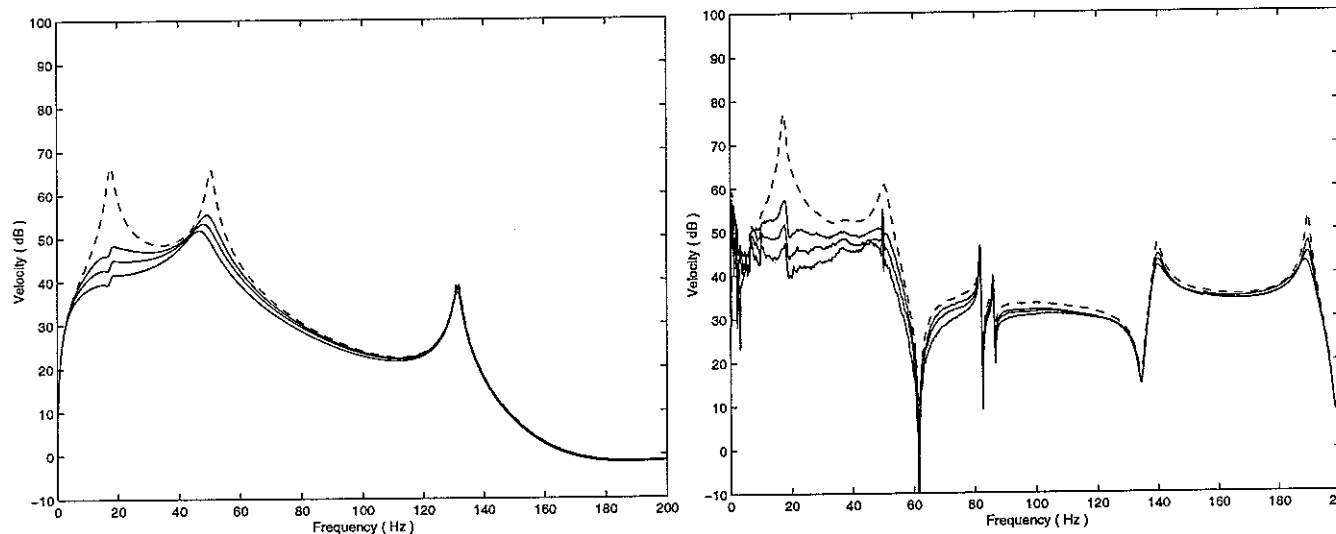

(a) Prediction (b) experiment

Figure 51 Velocity response at node 4 with single channel control implemented at node 1 when excited at node 1

4.3.2 Four-channel control of the mounted equipment structure on a rigid base

A four-channel velocity feedback control system of the mounted flexible equipment structure on a rigid base has been investigated which uses an independent SISO controller at each mount position. Using the summation box, one of the four shakers is also used to generate the primary excitation force as well as the control force. The induced velocity signals at each node are measured using accelerometers and directly fed back to the corresponding shakers after a charge amplifier and a power amplifier. The mounted flexible equipment structure is excited by a white noise signal from the FFT analyzer, and an equal gain of H is used to control each independent SISO controller. In this way, the control performance of an equi-gain decentralised multichannel control system of the mounted equipment structure on a rigid base has been investigated with multiple control gains.

Typical velocity responses at each node before control (in dashed lines) and after control (in solid lines) when the multichannel control system is excited by the shaker at node 1 are shown from simulation and experiment in Figure 52 to Figure 55. Similar results have been obtained for the four-channel velocity feedback control system when the mounted flexible equipment structure on a rigid base is excited by the shakers at nodes 2, 3 and 4, but they are omitted here for brevity. The three solid curves in these figures correspond to three different physical control gains of 0.18, 0.91 and 2.0 Ns/m respectively. The vibration amplitude is effectively reduced at all resonance frequencies within the frequency band of interest both theoretically and experimentally. The larger the physical control gain, the greater reduction in the vibration level. Stability of the four-channel control system is very good as the maximum physical control gain of 7.28 Ns/m can be applied before the control system goes unstable. In other words, the gain margin of the four-channel velocity feedback control system is about 14 dB. The control performance from simulation agrees well with those obtained from experiment except at very low frequency due to phase shifts. Both give a reduction in vibration level at the resonance frequencies of rigid body modes of up to 30 dB, and up to 20 dB at the first flexible frequency of 50.6 Hz. It is noted that, nearly 10 dB reductions in vibration level at the second and third flexible resonance frequencies are also obtained in the experiment, even though the simulation only predicts by 3-4 dB attenuation. However, the theoretical model developed in this research does interpret the experiment in a satisfactory degree of accuracy. The rigid body resonances as well as the first flexible resonance are no longer noticeable after control for the highest value of physical gain both theoretically and experimentally. Amplifications of the very low frequency response of the flexible equipment can be observed in the experiments due to the effect of phase shifts. Again, these effects are very small and no instability was encountered for the multiple feedback gains used in this investigation. However, instability occurs if the feedback gain is beyond the reported gain margin. In conclusion, the decentralised velocity feedback control implemented in the four-mount flexible equipment structure on a rigid base can significantly attenuate the vibration level at all resonance frequencies within 200 Hz.

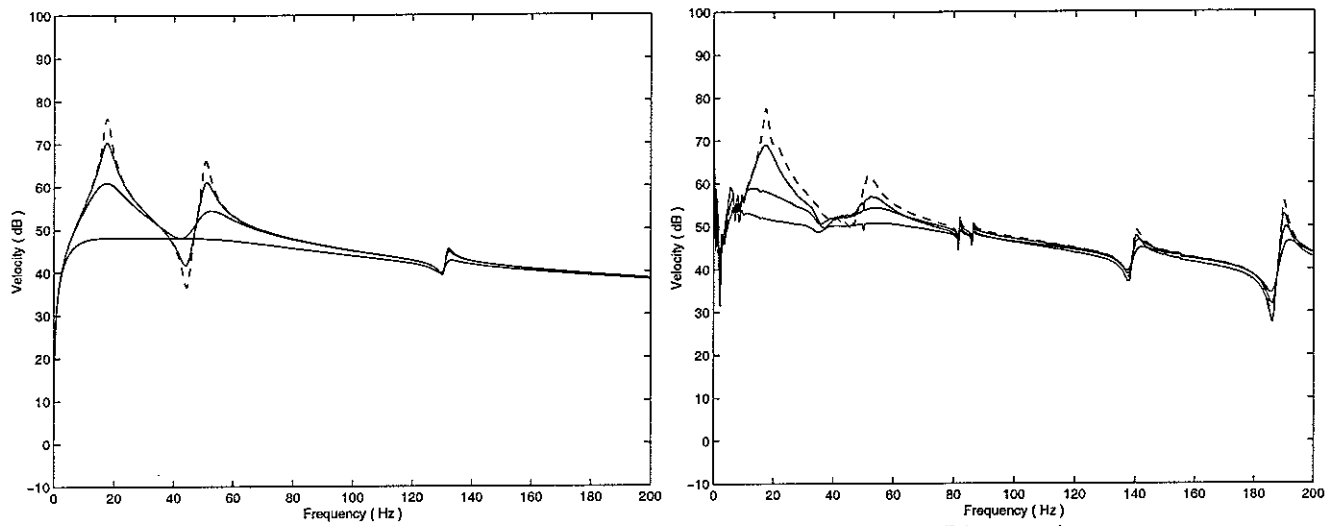

(a) Prediction (b) experiment

Figure 52 Velocity response at node 1 with four-channel control when excited at node 1

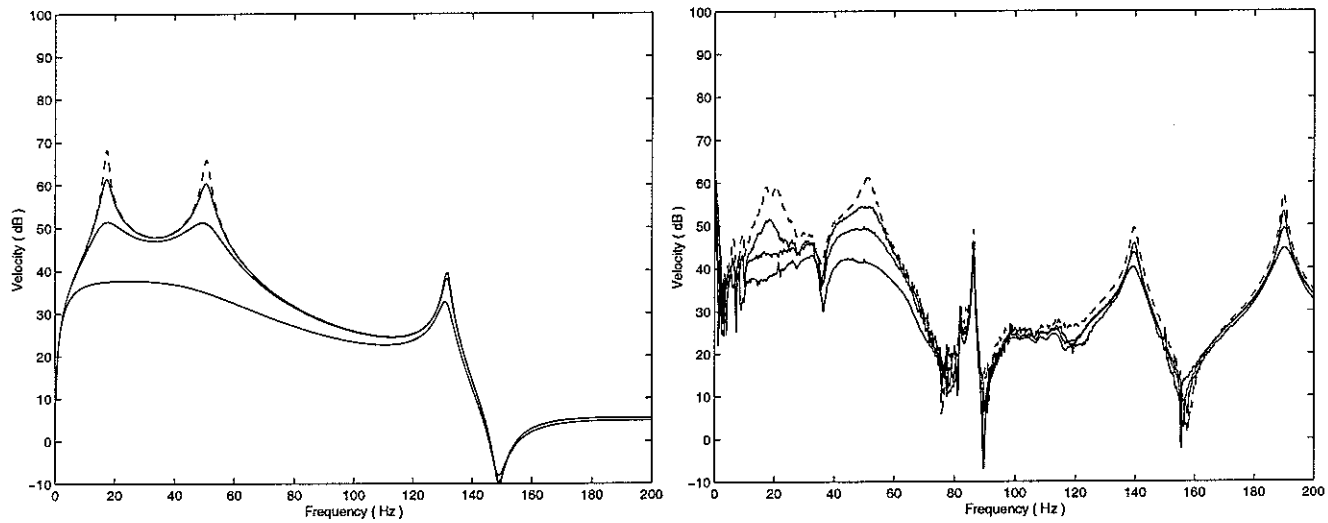

(a) Prediction (b) experiment

Figure 53 Velocity response at node 2 with four-channel control when excited at node 1

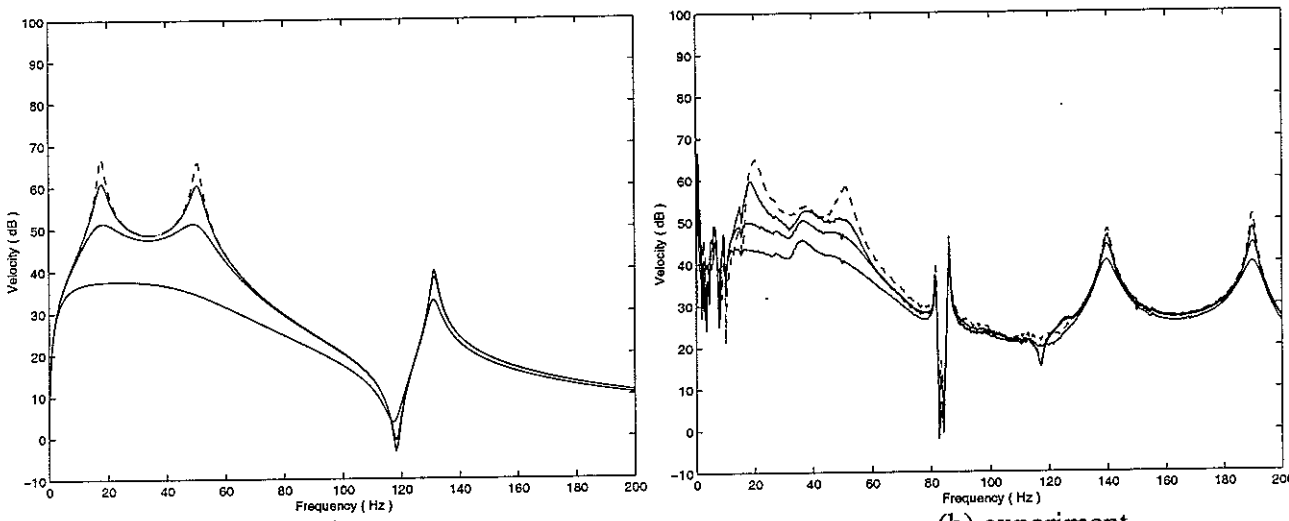

(a) Prediction (b) experiment

Figure 54 Velocity response at node 3 with four-channel control when excited at node 1

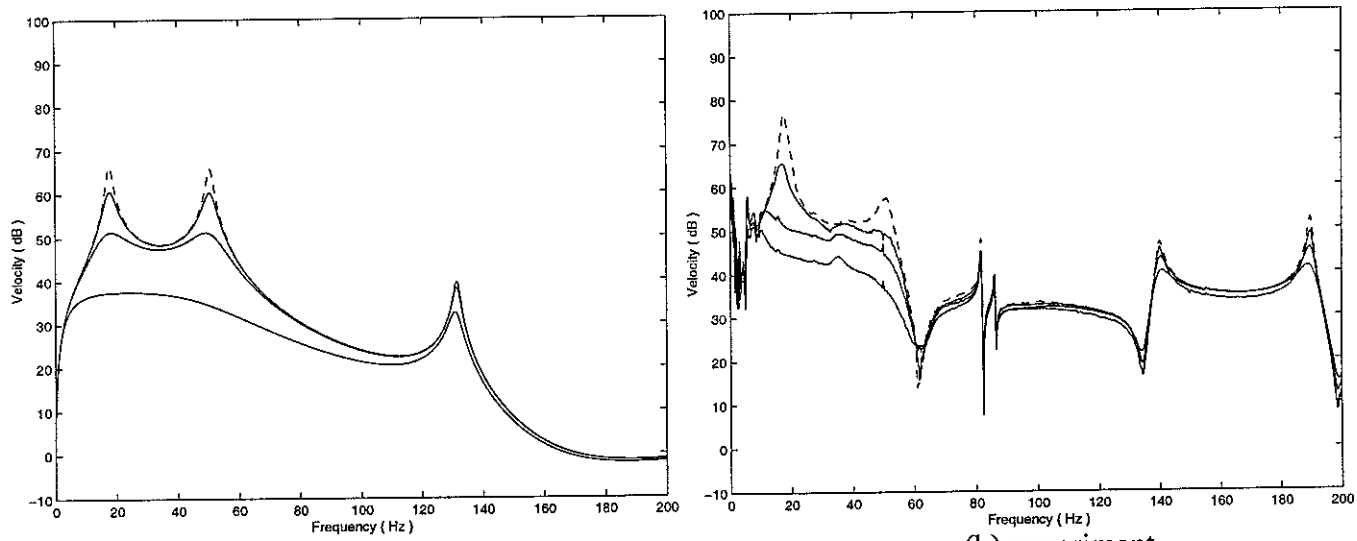

(a) Prediction (b) experiment

Figure 55 Velocity response at node 4 with four-channel control when excited at node 1

4.3.3 Kinetic energy analysis of the four-mount flexible equipment structure on a rigid base

The control performance of the single channel and multichannel velocity feedback control systems of the four-mount flexible equipment structure on a rigid base has been re-examined based on the kinetic energy. To calculate the true kinetic energy of the flexible equipment, the vibration of both the rigid body modes and the flexible body modes would have to be accounted for, as described in equation (20) in section 2.2. It is noted that, a transformation from the physical coordinates to the modal coordinates is necessary for the calculation of the true kinetic energy in the theory because of the flexibility of the equipment. In the experiments, however, only the vibration levels at the four corner positions of the flexible equipment were measured, and it is only possible to estimate the amplitudes of all the flexible modes with accurate models of all their mode shapes, which are not available. So in this section, the equipment has to be assumed to be rigid for the calculation of the experimental kinetic energy, which uses the kinetic energy contained in the rigid body modes to approximate the total kinetic energy of the flexible equipment. However, as most of the kinetic energy of the mounted flexible equipment structure is contained in the rigid actuators, such an assumption will not cause significant error in this research. In particular, the velocities of the equipment structure associated with the heave ($\dot{w}_a$), pitch ($\dot{\theta}_a$) and roll ($\dot{\varphi}_a$) motions, are determined from the velocities at four mount positions,

$$\dot{w}_a = \frac{(v_1 + v_2 + v_3 + v_4)}{4} \tag{38}$$

$$\dot{\theta}_a = \frac{[(v_1 + v_4)/2 - (v_2 + v_3)/2]}{l_\theta} \tag{39}$$

$$\dot{\varphi}_a = \frac{[(v_1 + v_2)/2 - (v_3 + v_4)/2]}{l_\vartheta} \tag{40}$$

where, v_1, v_2, v_3, v_4 are the velocities at the mount positions in the physical coordinates. Therefore, the total kinetic energy of the mounted equipment structure, as well as the kinetic energy associated with the heave, pitch and roll motions, have been calculated and compared between simulations and experiments.

Multiple feedback gains has been applied for the single channel and multichannel velocity feedback control systems of the mounted equipment structure both in the simulation and experiment, which are described in sections 4.3.1 and 4.3.2. Therefore, the total kinetic energy as well as the decomposed kinetic energy associated with the rigid body modes has been calculated and shown in Figure 56 to Figure. It is noted that, a direct comparison between the kinetic energies from the single channel control and the corresponding ones from multichannel control is not possible because of different feedback control gains used in the different control systems. The kinetic energies of the mounted flexible equipment structure on a rigid base before control are displayed in dashed lines and those after control in solid lines respectively.

The total kinetic energy is effectively reduced at all resonance frequencies within the frequency band of interest both theoretically and experimentally. The larger the physical feedback control gain, the greater reduction in the total kinetic energy. The calculated kinetic energy from simulations agrees reasonably well with those obtained

from experiments. For the single channel control system, both theory and experiment give a reduction of up to 60 dB in the kinetic energy at the resonance frequencies of rigid body modes, and up to 40 dB at the first flexible frequency of 50.6 Hz. It is interesting to note that, nearly 10 dB and 20 dB reductions in the kinetic energy at the second and the third flexible resonance frequencies are obtained in the experiment, although the simulation only predicts by 3-4 dB attenuation. Similar conclusions can also be made for the multichannel control system. In particular, the rigid body resonances as well as the first flexible resonance are no longer noticeable after control for the highest value of physical feedback gain used in the multichannel control system both theoretically and experimentally. Small amplification in the experimental kinetic energy is generally observed at very low frequencies due to phase shifts of the electric equipment. However, their effects are very small and always associated with small amplitude of vibration. Although no instability occurs in the experiments under steady control conditions, instability will occur if the feedback control gain is beyond the safe gain margin reported in the previous sections.

To remedy the assumption made in the calculation of the experimental kinetic energy, the sum of the velocity squares at each mount position is proposed to further evaluate the control performance of the single channel and multichannel control experiments. The results are shown in Figure 60 to Figure 61. It is evident from both figures that both single channel and multichannel control strategies are effective in reducing the vibration level at all resonance frequencies of interest. Similar conclusions can be still made.

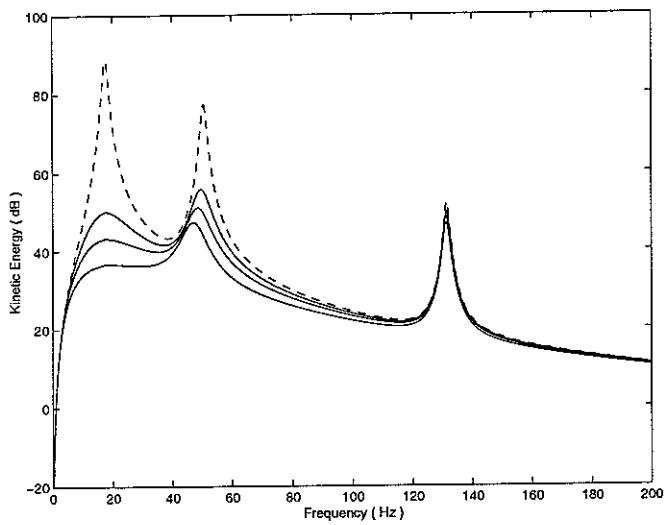

(a) Total kinetic energy

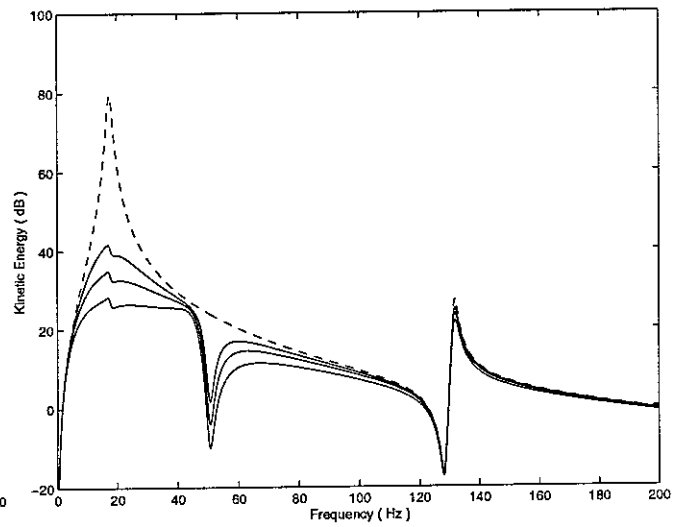

(b) Kinetic energy in heave motion

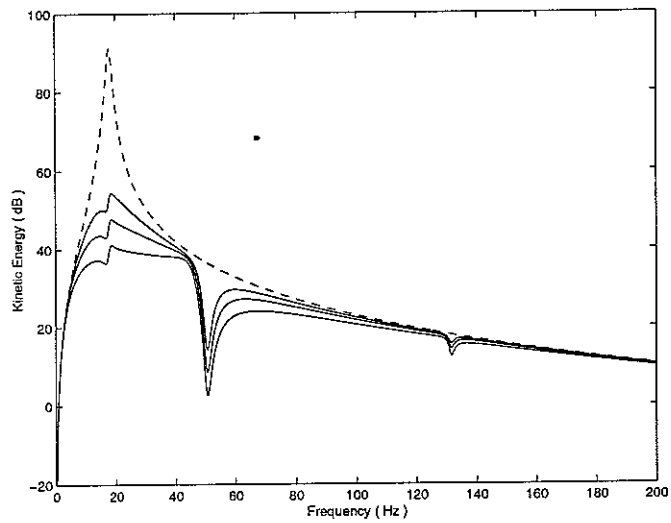

(a) Kinetic energy in pitch motion

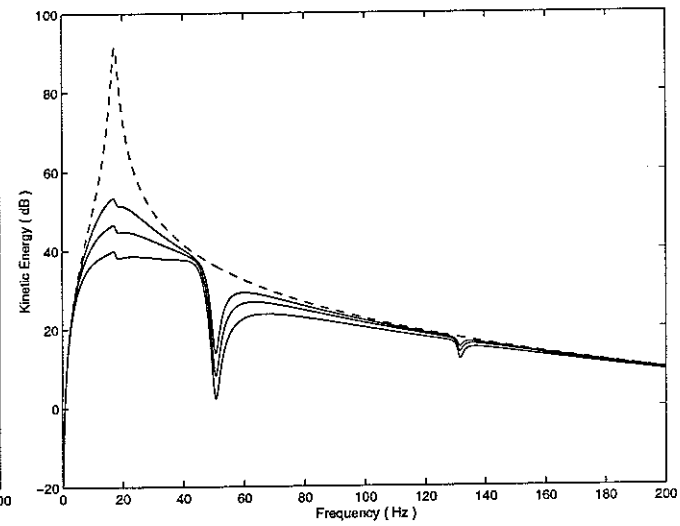

(b) Kinetic energy in roll motion

Figure 56 Simulation with single channel control implemented at node 1 when excited at node 1

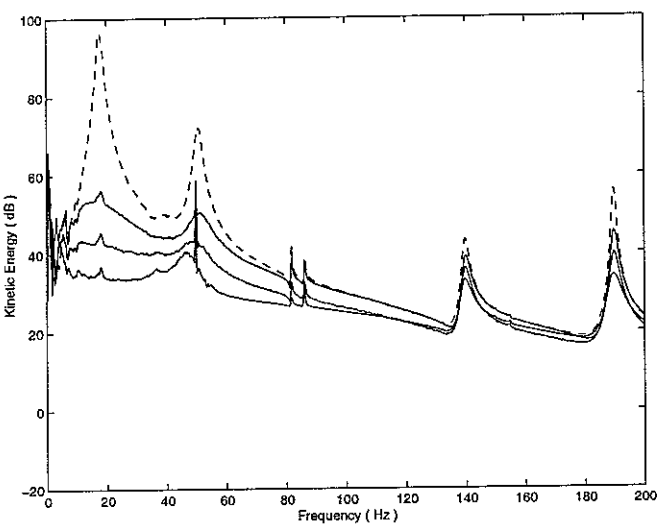

(a) Total kinetic energy

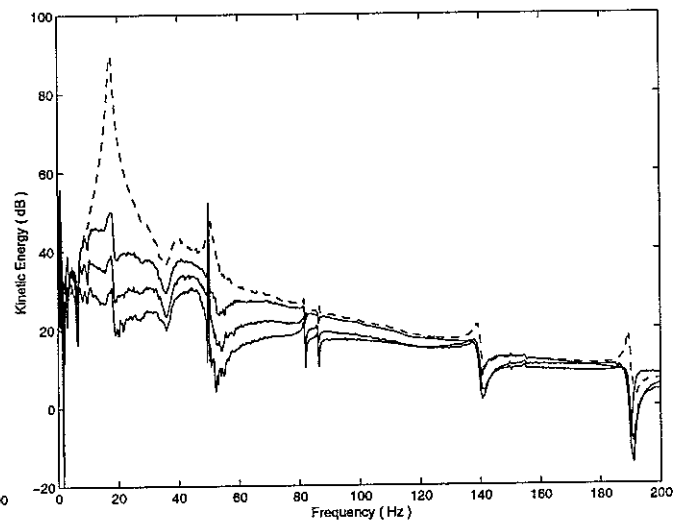

(b) Kinetic energy in heave motion

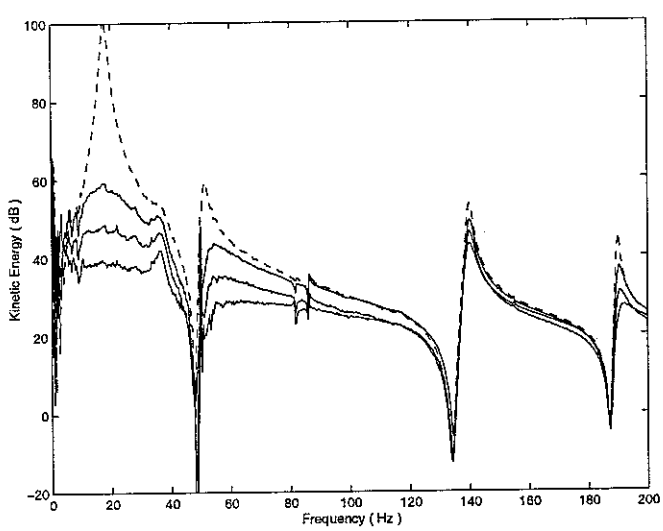

(a) Kinetic energy in pitch motion

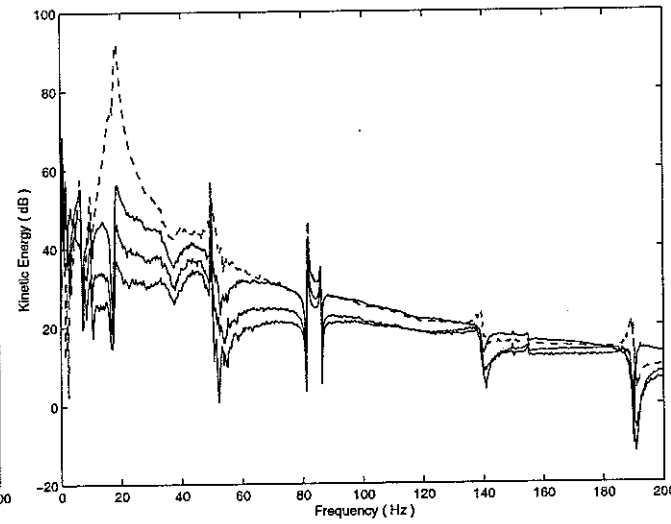

(b) Kinetic energy in roll motion

Figure 57 Experiment with single channel control implemented at node 1 when excited at node 1

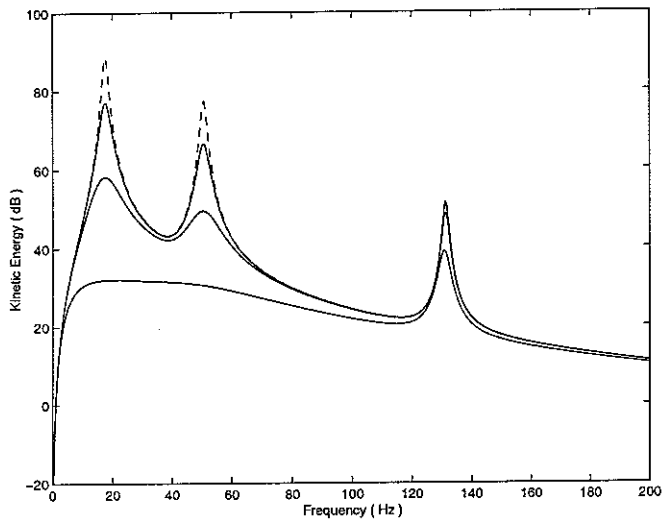

(a) Total kinetic energy

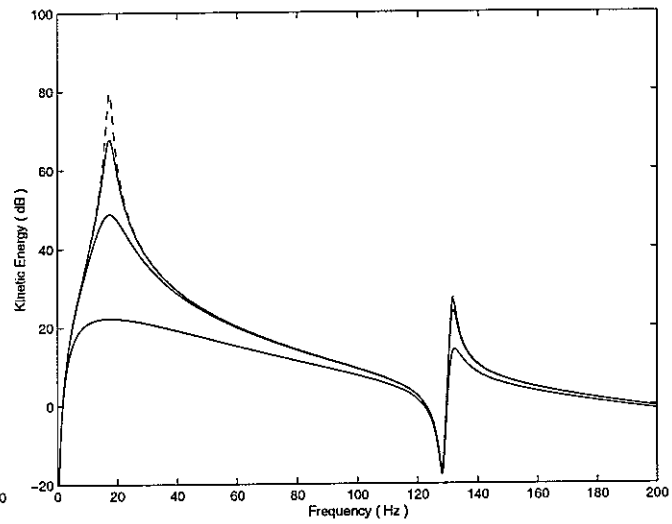

(b) Kinetic energy in heave motion

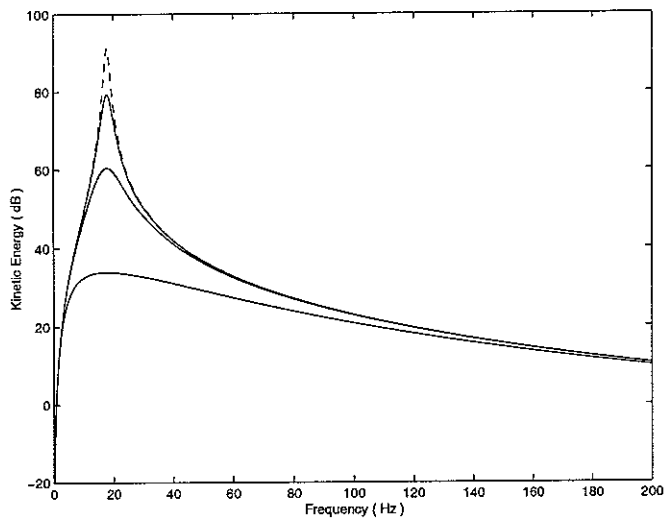

(a) Kinetic energy in pitch motion

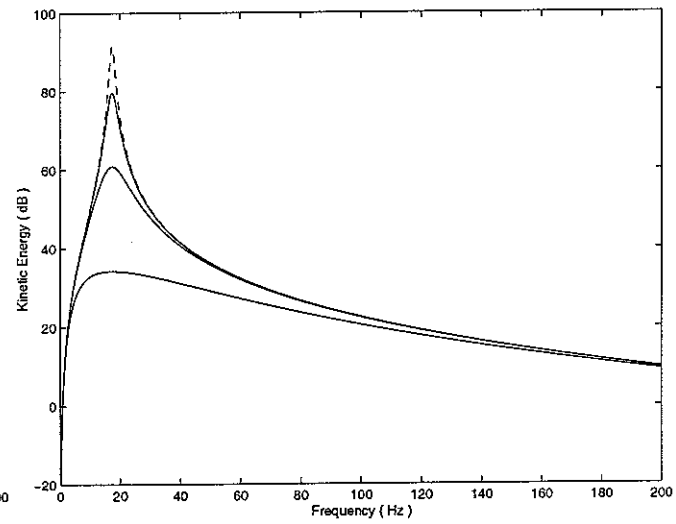

(b) Kinetic energy in roll motion

Figure 58 Simulation with multichannel control implemented when excited at node 1

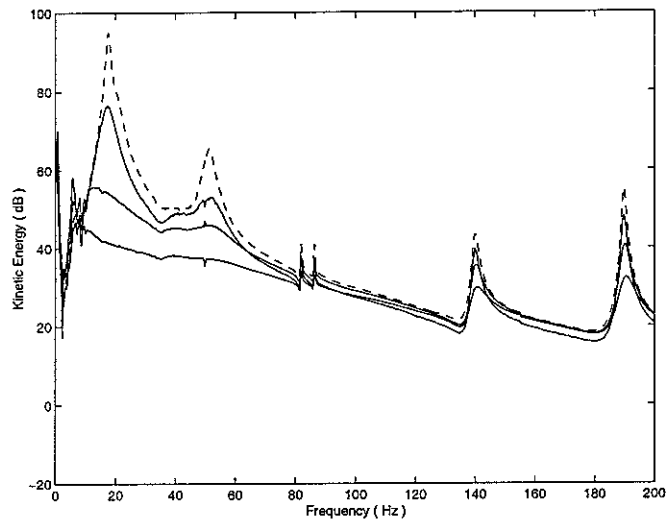

(a) Total kinetic energy

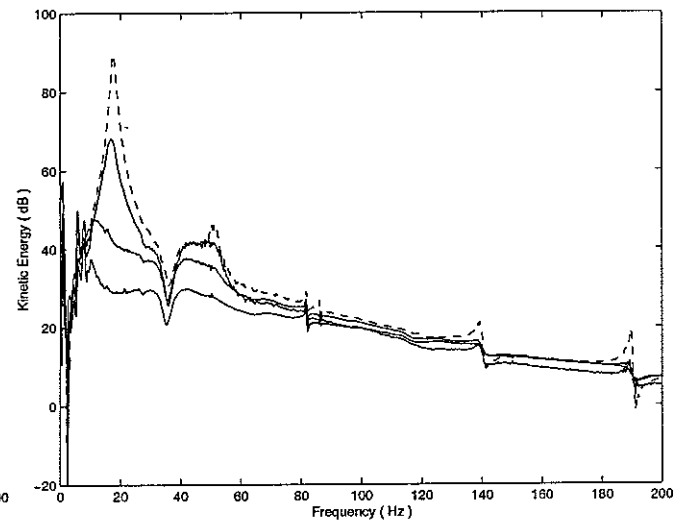

(b) Kinetic energy in heave motion

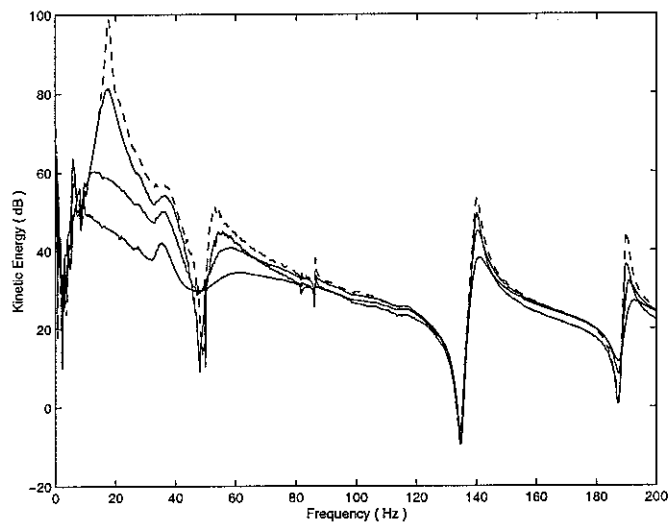

(a) Kinetic energy in pitch motion

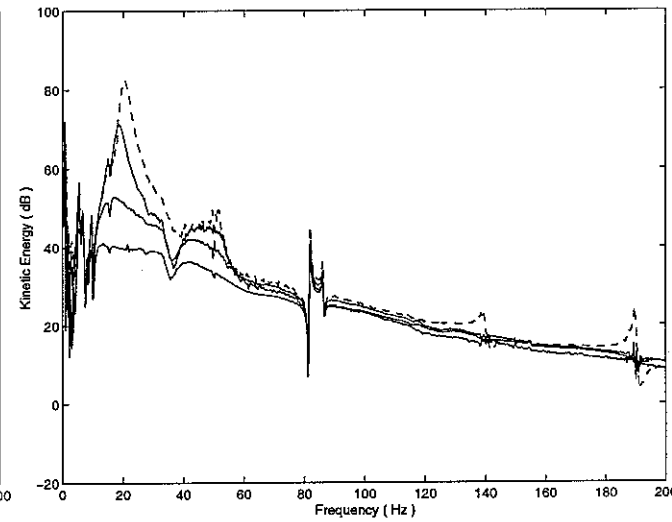

(b) Kinetic energy in roll motion

Figure 59 Experiment with multichannel control implemented when excited at node 1

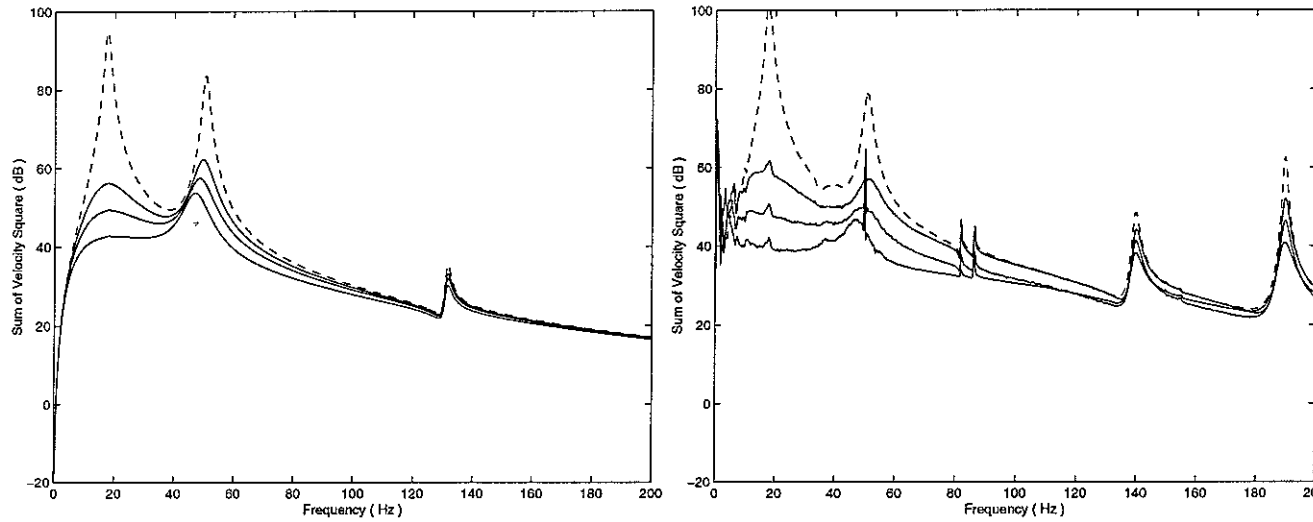

(a) Prediction (b) experiment

Figure 60 Sum of velocity squares with single channel control implemented at node 1 when excited at node 1

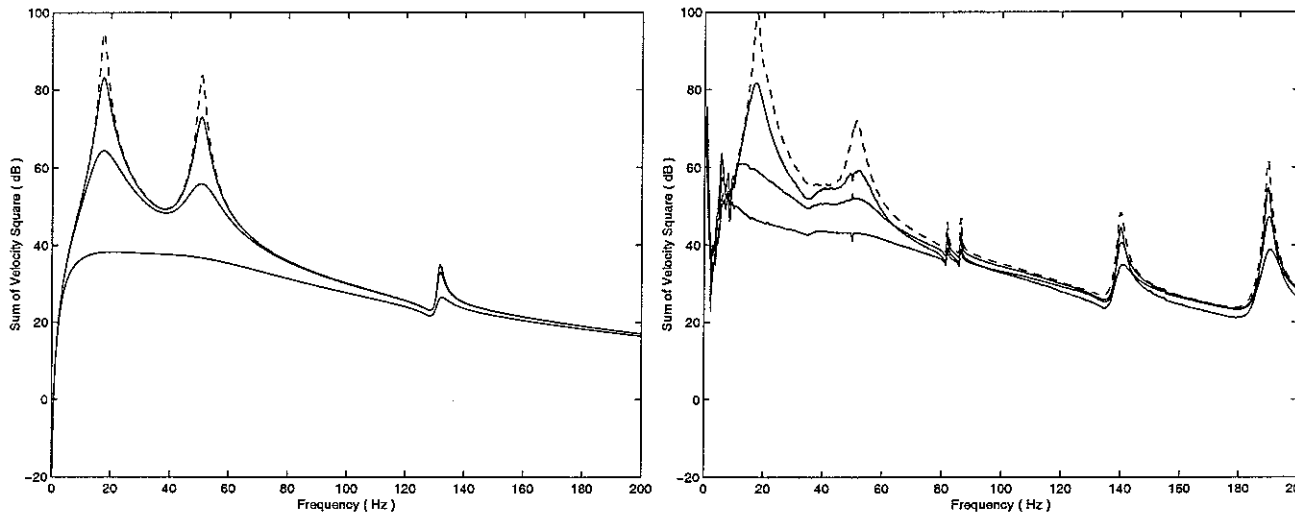

(a) Prediction (b) experiment

Figure 61 Sum of velocity squares with multichannel control implemented when excited at node 1

5 Conclusions

The objective of this research was to investigate the active vibration isolation of a four-mount flexible equipment structure from a flexible base. This report has described the mechanical analysis of a single-mount and multiple-mount vibration isolation systems using the impedance method. In particular, the dynamics and control mechanisms of a four-mount flexible equipment structure on a rigid base as well as on a flexible, where the actuators are installed in parallel with each mount, have been studied theoretically, by assuming the massless mounts as a combination of springs and dampers. As an initial study, single channel and multichannel control systems of the mounted flexible equipment structure on a rigid base have been investigated in this report. The plant responses measured in the experiments agree very well with those from simulation, which validates that the theoretical model developed in this report can be used to understand the dynamics and the active vibration control of the mounted flexible equipment structure. Stability of the single channel velocity feedback control of the mounted flexible equipment structure has been studied based on the Nyquist plots of the diagonal terms in the plant response matrixes from theory and experiment, and good stability properties are assured. For the multiple channel control system, the stability has been assessed using the Nyquist plots of the true eigenvalue loci of the plant response matrixes as well as using an assumed mode shape method. The implementation of four-channel decentralised velocity feedback control strategy has been proved to have good stability properties from both methods.
Various single channel velocity feedback control systems using a constant gain have been implemented experimentally. Furthermore, multiple feedback gains have been applied in the four-channel equi-decentralised velocity feedback control of the mounted flexible equipment structure on a rigid base. Both single channel and multichannel control systems present good control performance theoretically and experimentally, where the vibration levels of the mounted flexible equipment structure are effectively reduced at all resonance frequencies of analysis. In particular, up to 30 dB reductions in vibration levels at the rigid body modes at around 17 Hz, up to 20 dB at the first flexible frequency of 50.6 Hz, up to 10 dB at the second and third flexible resonance frequencies, have been achieved experimentally from both single channel and four-channel velocity feedback control implementations in the mounted flexible equipment structure on a rigid base. The control performances of both single channel and multichannel control systems have been re-assessed in terms of kinetic energy. Again, the total kinetic energy of the mounted flexible equipment structure has been reduced globally all over the frequency band of analysis for both single channel and multichannel control implementations theoretically and experimentally. As the initial control results on a rigid base from simulation and experiment are very promising, following investigation will be performed on the active vibration control of the mounted flexible equipment structure on a flexible base.

References

1. C.E. Crede and J.E. Ruzicka,1996, Shock and Vibration Handbook (C.M. Harris, editor) New York: McGraw-Hill. Ch.30 Theory of vibration isolation.
2. M.J. Beard, A. H. Von Flotow and D.W. Schubert, 1994, Proceedings of IUTAM Symposium on the Active Control of Vibration, University of Bath, UK. A Practical product implementation of an active/passive vibration isolation system.
3. M. Serrand and S.J. Elliott, 2000,Journal of Sound and Vibration, Vol. 234(4), 681-704, Multichannel feedback control for the isolation of base-excited vibration.
4. M.J. Balas, 1979, Journal of Guidance and Control, Vol. 2, 252-253, Direct velocity feedback control of large space structures
5. S.M. Joshi, 1986, Journal of Guidance and Control, Vol.9, pp.85-91, Robustness properties of collocated controllers for flexible spacecraft
6. S.M Kim, S.J. Elliott and M.J. Brennan, 1999, Institute of Sound and Vibration Research Technical Memorandum No 845, University of Southampton. Active Vibration Isolation of 3-Dimentional Structure Using Velocity Feedback Control.
7. S. Skogestad and I. Postlethwaite, 1996, Multivariable feedback control; Analysis and design, John Wiley & Sons, Inc.
8. M. Morari and E. Zafiriou, 1989, Robust process control, Prentice-Hall, Inc.
9. J. Pan and C.H. Hansen, 1993, Journal of the Acoustical society of American, 93(4), 1947-1953. Active control of power flow from a vibrating rigid body to a flexible panel through two active isolators.
10. S.M. Kim 1998, PhD Thesis, University of Southampton, Active control of sound in structural-acoustic coupled systems
11. B. Noble and J.W. Daniel, 1988, Applied Linear Algebra, Prentice-Hall Inc.
12. S. Skogestad and I. Postlethwaite, 1996, Multivariable feedback control. Analysis and design, John Wiley & Sons, Inc.
13 P. Gardonio, S.J. Elliott and R.J. Pinnington, Sep. 1995, Institute of Sound and Vibration Research Technical Memorandum No 765, University of Southampton. Active Isolation of Multiple-Degree-of-Freedom Vibrations Transmission between a Source and a Receiver.
14 F. B. Hildebrand, 1965, Methods of Applied Mathematics, Second Edition, Prentice-Hall Inc.

Appendix A: An algorithm to obtain the true eigenvalues in order

There is an inherent numerical difficult in obtaining the true eigenvalues of the plant response matrix in the right order within MATLAB, because the built-in functions automatically output the calculated eigenvalues in a specific order. For example, the eigenvalues of a real symmetric matrix are output in an ascending order. Generally, the built-in output order causes a significant problem in the stability assessment. A typical plot of the calculated true eigenvalues of the plant response matrix before data treatment is shown in Figure A1, which makes it very difficult to evaluate the stability of the multichannel control system. An algorithm is therefore proposed in this report to distinguish the corresponding eigenvalues from one to another using the corresponding true eigenvectors.

The relationship between the plant response $\mathbf{G}(j\omega)$ and its true eigenvalue matrix $\mathbf{\Omega}(j\omega)$ can be expressed by,

$$\mathbf{G}(j\omega)\mathbf{Q}(j\omega) = \mathbf{Q}(j\omega)\mathbf{\Omega}(j\omega) \tag{A1}$$

where, $\mathbf{\Omega}(j\omega)$ is a diagonal matrix of the true eigenvalues λ_i, and $\mathbf{Q}(j\omega)$ is the matrix of the true eigenvectors of the plant response matrix $\mathbf{G}(j\omega)$ at the frequency ω, whose columns are the corresponding true eigenvectors. The plant response matrix $\mathbf{G}(j\omega)$ is obtained by,

$$\mathbf{G} = (\mathbf{Z}_e + \mathbf{Z}_a + \mathbf{Z}_m)^{-1} \tag{A2}$$

where, $\mathbf{Z}_a$, and $\mathbf{Z}_m$ are the impedance matrixes of the actuators, flexible equipment and mounts, respectively. In particular, $\mathbf{Z}_e = \mathbf{Y}_e^{-1}$, provided the mobility matrix $\mathbf{Y}_e$ of the flexible equipment is invertible. Impedance matrixes $\mathbf{Z}_a$ and $\mathbf{Z}_m$ are ($M\times M$) diagonal matrixes (thus symmetry), whose diagonal terms are the impedances due to the mass of each actuator, the stiffness and damping of the corresponding mount, respectively. Because of the uniformity of the flexible equipment plate and the symmetry of the mount locations, $\mathbf{Z}_e$ is symmetry. Therefore, the summation of symmetric matrixes is symmetric. Moreover, any integral power of a symmetric matrix is also symmetric [14]. The inverse of a symmetric matrix can be numerically treated as a power of (-1) of the symmetric matrix and thus is symmetric. This is proved from the Bode plots of each term in the theoretical plant response matrix as seen in Figure 6 to Figure 21 in dashed lines. Although two eigenvectors of a symmetric real matrix corresponding to different eigenvalues are orthogonal [14], the preceding statement is not necessary true for a symmetric complex matrix. However, if the true eigenvectors are denoted by q_1, q_2, $\cdots$, q_n (in this case, $n = 4$), which have been normalized by $q_i^T q_i$ ($i = 1,\ 2,\ \cdots,\ n$), then,

$$q_i^T q_k = \begin{cases} a & i = k \\ b & i \neq k \end{cases} \tag{A3}$$

where, a and b are generally non-zero complex and $1 \geq |a| > |b|$. The matrix of $|Q(j\omega)^T Q(j\omega)|$ is diagonal dominant.

In the experiments, the measured plant response matrix is not strictly symmetric due to some differences in the mounts and actuators as well as imperfect operation of the electric equipment. However, the measured plant response matrix is nearly symmetric

as demonstrated in solid lines in Figure 6 to Figure 21. Equation (A3) still holds true for the experimental plant response matrix. Therefore, the property of true eigenvectors described by equation (A3) can be used to distinguish the true eigenvalues in a right order and the algorithm is described as follows.

Without lost generality, assuming that the eigenvectors corresponding to the i_{th} frequency step have been distinguished in the computation loop, so a set of eigenvectors denoted as q_{i1}, q_{i2}, $\cdots$, q_{in} in the right order has been obtained. For the next $(i+1)_{th}$ step, using MATLAB built-in function (eig.m) to calculate the eigenvalues and corresponding eigenvactors,

[VGs, EGs]=eig(Gs); [VGe, EGe]=eig(Ge);

where, VGs and VGe are the eigenvectors corresponding to the true eigenvalues EGs and EGe of the plant response matrixes of Gs and Ge, the suffix s and e denote for the simulated and experimental results.

For ij = iteration ($ij = 1, 2, \cdots, n$, where n is the rank of the plant response matrix),

a) Initialize:

bigs=0; bige=0;

for the theoretical and experimental plant response matrix respectively, and

bigsnumber=ij; bigenumber=ij;

which are used to recorder the series numbers of the true eigenvectors. Remember the true eigenvectors obtained from last step using MATLAB script,

eval(['Sv=Svector' int2str(ij) ';']); eval(['Ev=Evector' int2str(ij) ';']);

b) Calculate the scalar product between the eigenvectors from last step and these from current step according to equation (A3), for $jj = 1, 2, \cdots, n$,

judges=Sv'*VGs(:,jj); judgee=Ev'*VGe(:,jj);

c) Find out the biggest calculated value of the scalar product

if abs(judges)>bigs {bigs=abs(judges); bigsnumber=jj;} end

if abs(judgee)>bige {bige=abs(judgee); bigenumber=jj;} end

d) If the iteration variable jj is less than n, then go back to b) until the biggest value of the scalar product of the eigenvectors is found and the associated series number is recorded.

e) Therefore, save the corresponding true eigenvalues into the series in a right order.

eval(['Lambdas' int2str(ii) '(' int2str(i) ')=EGs(' int2str(bigsnumber) ','...
int2str(bigsnumber) ');']);

eval(['Lambdae' int2str(ii) '(' int2str(i) ')=EGe(' int2str(bigenumber) ','...
int2str(bigenumber) ');']);

The above algorithm can sort the true eigenvalues associated with a specified eigenvector (a vibration mode). After this algorithm, the true eigenvalues are much clear as demonstrated from Figure A2. Therefore, the stability analysis can be evaluated.

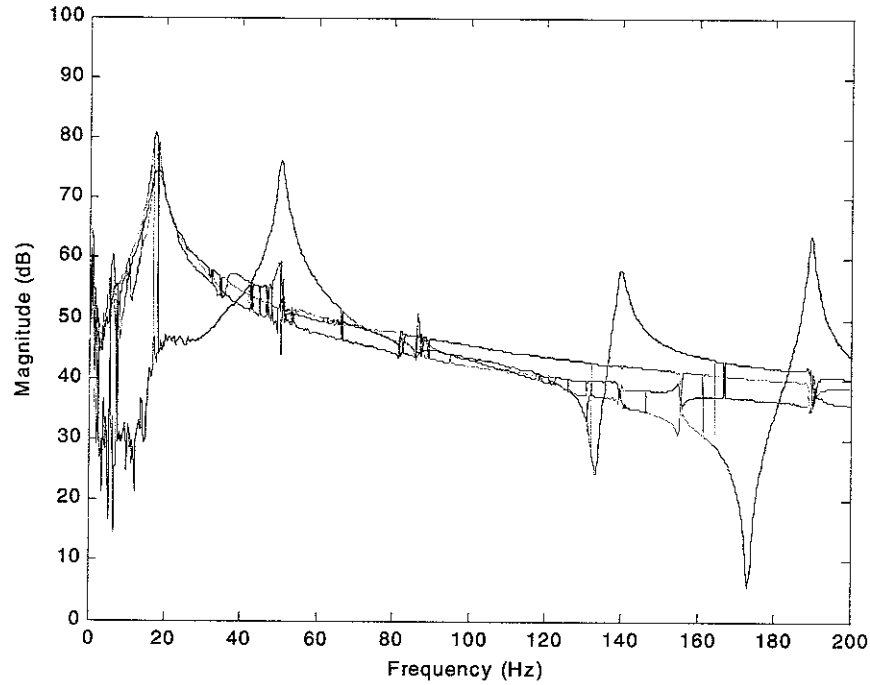

Figure A1 Magnitude of the experimental true eigenvalues before data treatment

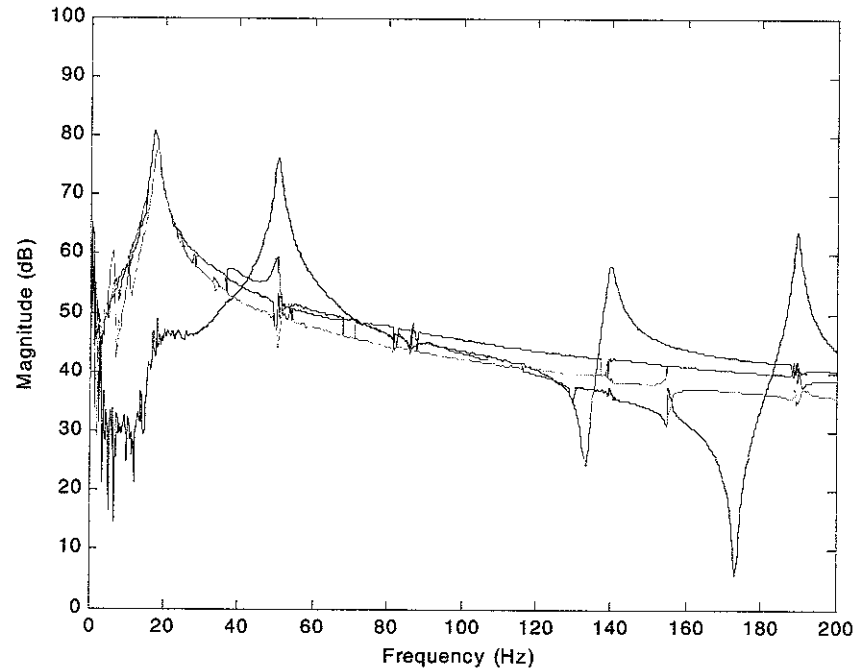

Figure A2 Magnitude of the experimental true eigenvalues after data treatment

Appendix B: Assumed mode approximation for stability analysis

When assessing the stability of multichannel feedback control of the mounted equipment structure, an assumed mode shape method is used to calculate the eigenvalues to avoid the numerical difficulty in obtaining the true eigenvalues. Therefore, assuming the mode shapes as in equation (30), the corresponding matrix, whose diagonal terms are the eigenvalues, can be calculated conveniently according to equation (31). Such an assumed mode shape method is valid as long as the corresponding eigenvalue matrix is a diagonal dominant matrix, i.e., the magnitudes of the diagonal terms are relatively bigger than those off-diagonal terms. If ideal condition is assumed, (i.e., all four mounts are identical and massless, which can be modelled as springs and dampers; all electrical equipments work perfectly.) the eigenvalue matrix obtained from simulation is completely diagonal, as demonstrated in Figure B1. In the experiment, the four mounts are not exactly the same as well as

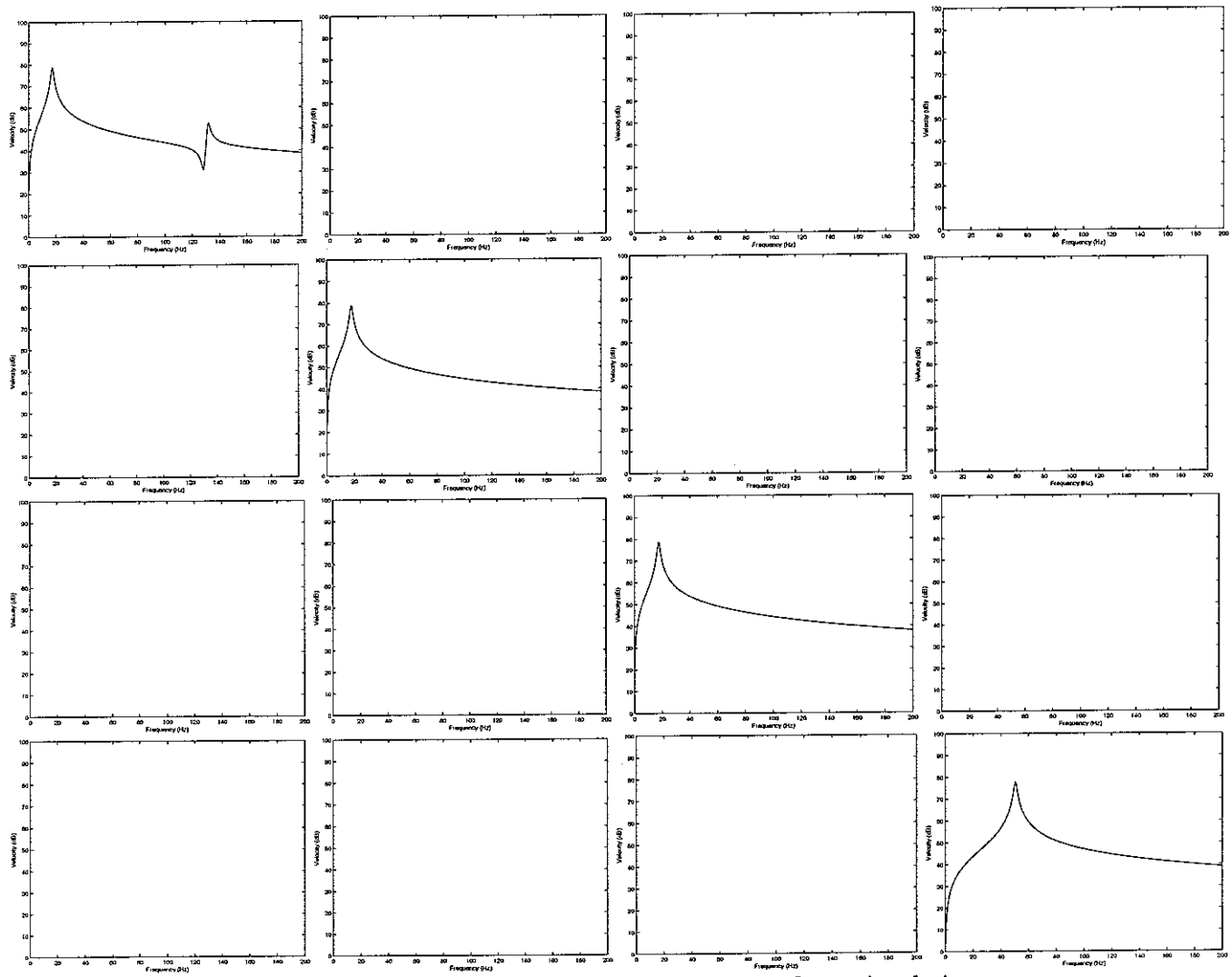

Figure B1 Magnitude plots of plant response from simulation

the imperfect operation of the electronic equipment. Therefore, the corresponding eigenvalue matrix is not completely diagonal as shown in Figure B2. However, it is clearly shown that the matrix is diagonal dominant, with the magnitude of these diagonal terms larger than those off-diagonal terms by about 15 dB. As the off-diagonal terms are small compared with those diagonal terms, the use of the diagonal approximation to the eigenvalue matrix is reasonable to assess the stability of the multichannel control of the mounted equipment structure.

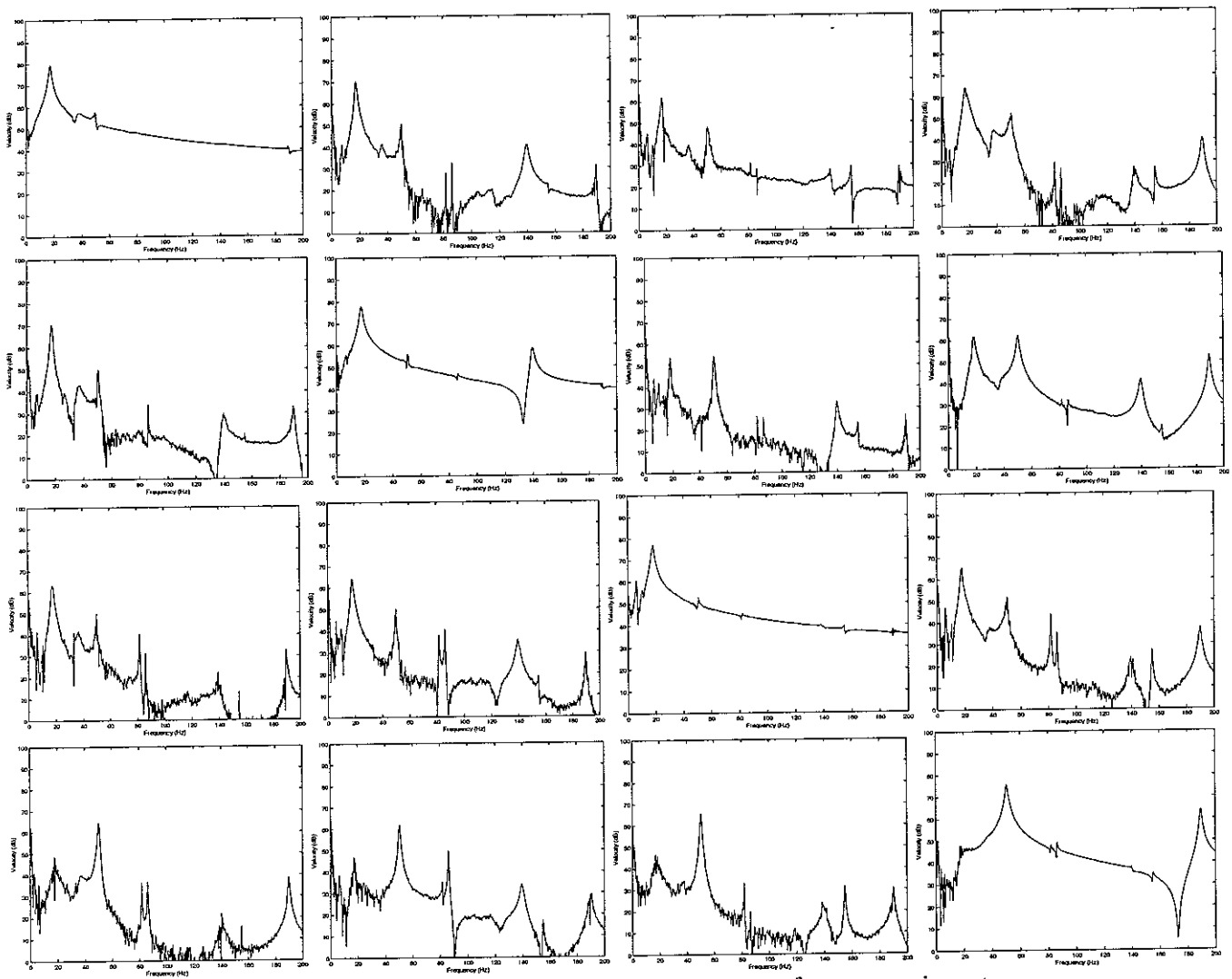

Figure B2 Magnitude plots of plant response from experiment